Report # N00014-94-C-0046
Data Item No. A002

The Production of Distorted 3-3 Hydrophone Composites from Reticulated Ceramics -Final Report

Prepared by:
Douglas Karst
Andy Norris
Truett Sweeting

Hi-Tech Ceramics
Box 788
Alfred, NY 14802

December 30, 1997

Contract # N00014-94-C-0046

Prepared for
ONR
Office of Naval Research
Washington, DC

ABSTRACT

Reticulated ceramics have been in production for over 20 years, primarily for molten metal filter applications. Annually, hundreds of thousands of square feet are produced with prices ranging down to twenty cents per cubic inch for some materials. This work was undertaken to apply reticulated ceramic processing techniques to piezoelectric ceramic-composite production and the subsequent production, testing, and evaluation of six hydrophone arrays. This first generation composite material is a rugged, distorted 3-3 piezoelectric ceramic composite with appreciable acoustical properties. Modeling results suggest that simple modifications will bring about enhanced sensitivities and acoustics. Sensitivity limits are imposed by the need to maintain strength at high pressures. Processing details are given in the Manufacturing Report, also delivered as part of this contract. Suggestions for an improved second generation material are presented. Composite costs are projected to be under $10/square inch in moderate volumes.

CONTENTS

LIST OF FIGURES

LIST OF TABLES

SUMMARY

Vesuvius Hi-Tech Ceramics was sponsored by the Office of Naval Research to adapt technology developed for reticulated ceramic production to the production of piezoelectric ceramic composites for hydrophone and similar applications. This work was in collaboration with the New York State College of Ceramics, Matt Creedon, then Ph. D. student, and his advisor, Dr. Walter A. Schulze at the New York State College of Ceramics.

Polyurethane foam was stretched at elevated temperatures and cooled in place. This foam was then cut into pieces ~ 1" x 1" x 6 (or 8) mm with the stretching direction parallel to the 6 mm dimension. After stretching, the foam was coated with piezoelectric ceramic. Much developmental effort went into the foam selection process and the stretching of the foam to the optimal aspect ratio. A 15 ppi foam with a 3:1 cell aspect ratio and 15 volume percent ceramic was ultimately chosen. The ceramic coated foam was dried and placed in a high temperature furnace to "burn off" the foam and sinter the ceramic. Next, the fired ceramic reticulate was filled with epoxy, surface ground, cut, electroded, and poled in the 6 mm direction. The result is a distorted 3-3 piezoelectric composite with properties similar to 1-3 piezoelectric composites. Under contract, Vesuvius Hi-Tech Ceramics delivered six 4" x 4" arrays. The arrays were each composed of sixteen ~ 1" square PZT composite coupons. The first array was 4 mm thick and the last five were made 6 mm thick (to increase the sensitivity). The arrays were tested acoustically by Fred Geil and John McMaster at Northrup Grumman in Annapolis, MD.

Though the sensitivities are modest, -192 dB re 1 Volt/ μPa at 50 kHz (-189 dB subtracting out losses from the wire), the composite material is highly robust. It is believed that the sensitivity can be appreciably enhanced by modifying the epoxy filler. Both a thickness resonance and a lateral resonance were evident from the acoustic and electronic testing. The lateral resonance causes some acoustical nonlinearity. It is felt that a much higher degree of consistency from coupon to coupon

can be expected with scale-up and specialized equipment for manufacturing, as well as the tightening of certain production tolerances.

Research is underway at the New York State College of Ceramics to modify the epoxy filler portion of the ceramic composite. It appears that the current epoxy is more stiff than desired for this application, and does not allow the impinging acoustic sound waves to apply their load to the piezoelectric ceramic portion of the composite. As much as 90 percent of the acoustic sound pressure is not being "felt" by the piezoelectric ceramic because of the excessive stiffness of the epoxy (Ref. #1, p 132). This is discussed in the following paragraph and later in relation to finite element modeling results.

Modifications to lower the stiffness of the epoxy by varying the mix ratios of the components, results in the Poisson's ratio increasing. If Poisson's ratio increases, d_{31} (the lateral strain coefficient) becomes more negative. since Poisson's Ratio is the lateral strain divided by the axial strain (applied force direction). The hydrostatic coefficient, d_h, is given by $d_h = d_{33} + 2d_{31}$ (d_{31} is negative). If the d_{31} component were to go toward zero, d_h could approach the d_{33} of the piezoelectric ceramic material; this would happen if Poisson's ratio were to decrease toward zero. For example, $d_{33} = 593$ for PZT5, but for the reticulated piezoelectric ceramic composite, d_h was only 50. Thus d_h could potentially reach more than ten times the present composite value. Fairly large benefits are expected by modifying the epoxy such that the stiffness and Poisson's ratio both decrease. Of course, a trade-off is made in that as the epoxy stiffness is lowered, the composite becomes less robust.

A search is underway to utilize negative Poisson's ratio polymers and/or modify the precursor foam to have a negative Poisson's ratio (positive d_{31}). Potentially, d_h could exceed d_{33} of the pure ceramic.

It is believed that a highly sensitive composite with a fairly linear acoustic response as a hydrophone and output as a transmitter can be realized with only minor modifications. Vesuvius Hi-Tech Ceramics, is anxious to produce and evaluate this second generation of reticulated piezoelectric ceramic composite.

It was concluded that reticulated ceramic processing is adaptable to hydrophone production. Moreover, the processing adapts well to low volume, custom shapes and high volume repetitive shapes. A wide range of shapes are readily fabricated with low tooling costs (plates, donuts, cylinders, tubes, ...). Furthermore, the low tooling costs allow for fast prototyping.

INTRODUCTION

Vesuvius Hi-Tech Ceramics produces several hundred thousand cubic inches per week of reticulated ceramics. The Office of Naval Research, Vesuvius Hi-Tech Ceramics and the NYS College of Ceramics joined forces to apply the established process of reticulated ceramic production used for making molten metal filters, kiln furniture, ceramic burners, ... to the production of reticulated piezoelectric ceramic composites for hydrophone and transmitter applications. Also, under contract with the ONR, Vesuvius Hi-Tech Ceramics agreed to fabricate and deliver for testing six hydrophone arrays. The phase I, Performance Optimization Section, focuses on production of the piezoelectric ceramic composite material, the processing of that material into electroded and poled one inch square by four or six mm thick coupons and the testing of the coupons at the NYS College of Ceramics. Phase II describes the assembly of the coupons into hydrophone arrays as well as the electrical and acoustical test results of the arrays. Phase III, The Manufacturing Assessment, discusses variability and process control as well as scale-up considerations. The conclusions include suggestions and follow up efforts to improve the composite material as well as improvements to the hydrophone arrays.

PHASE I, PERFORMANCE OPTIMIZATION

Composite Production and Testing

A flow chart for processing piezoelectric ceramic reticulate composite arrays is shown in Figure 1. A special lab was established to separate the processing of the piezoelectric ceramic (PZT5H from Morgan Matroc) from the main Vesuvius Hi-Tech Ceramics manufacturing facility to prevent contamination of the standard ceramic products. This area was set up and furnished with the appropriate processing equipment. The lab included jar mills and a mixer dedicated to PZT slurry preparation, a hood and exhaust with HEPA filtration to capture any fine airborne PZT powder which may result from batching, a portable HEPA vacuum for spot clean up and a sink equipped with a settling tank to prevent the release of contaminated wash water. Also included in the lab, were a small dryer and a high temperature electric furnace for firing the ceramic.

A great deal of effort went into optimizing the foam stretching process, aspect ratio, pore size and ceramic volume percent of the composite. Special equipment was built at Vesuvius Hi-Tech Ceramics to perform the foam stretching repeatably. Figure 2 shows the general isotropic nature of unstretched foam. Enhanced piezoelectric properties were obtained by stretching the foam in one direction under heat and then cooling the foam in this stretched state. The stretched direction later becomes the poled direction. Stretching of the foam creates a distorted 3-3 structure with properties similar to the desirable properties known to exist for 1-3 piezoelectric composites. Figure 3 shows polyurethane foam stretched to an aspect ratio of 2:1, and Figure 4 shows foam stretched to an aspect ratio of 3:1.

Cut Foam

Stretch Foam

Cut Foam

Batch and Ball Mill PZT Slurry

Coat Foam with Slurry

Fire

Impregnate Reticulate with Epoxy

Surface Grind

Cut

Electrode Composites

Pole

Test Composite Segments

Assemble Array with Conductive Interconnects

Attach Wires

Encapsulate with Urethane

Test Array

Figure 1. Flow chart for processing piezoelectric ceramic reticulate composite arrays.

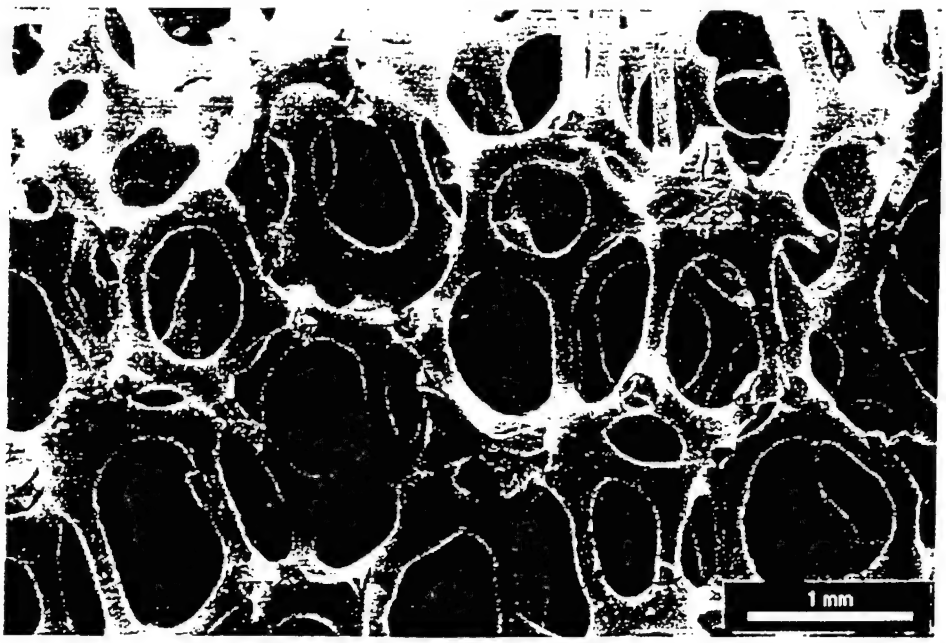

Figure 2. Unstretched foam showing its isotropic nature (Ref. 1, p 90).

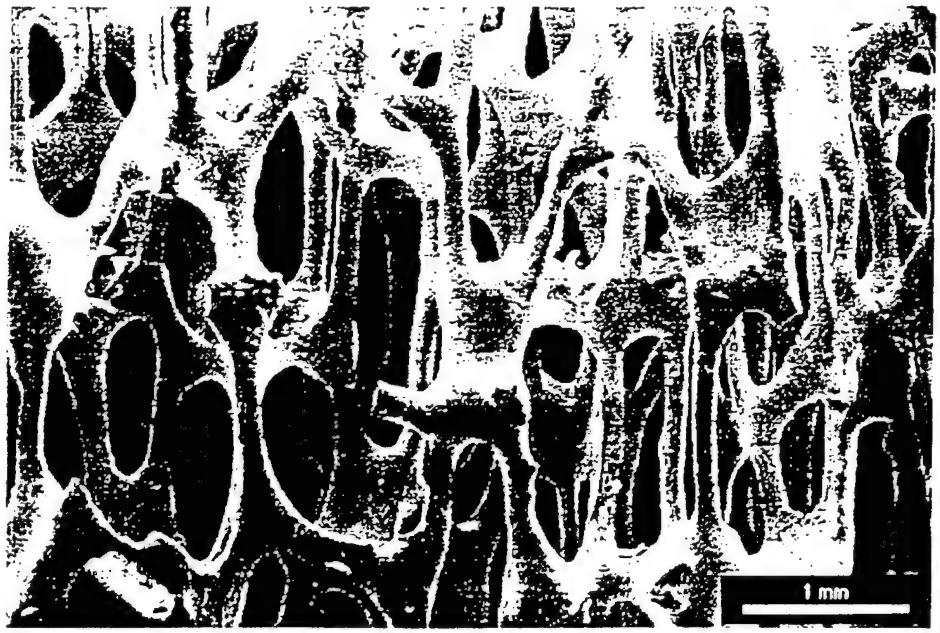

Figure 3. Distorted reticulated ceramic with a 2:1 cell aspect ratio (Ref. 1, p 91).

Figure 4. Distorted reticulated ceramic with a ~ 3:1 cell aspect ratio (Ref. 1, p 91).

The effects of foam distortion level, pore size, volume percent ceramic and polymer matrix type on composite performance were investigated.. Degree of distortion, pore size and densities were all varied as described in Table I. The Spurr epoxy matrix was held constant for these comparisons. The effects of distortion of the ceramic structure on the uniaxial charge coefficient d_{33} can be seen in Figures 5 and 6. It was found that distortion of the structure did improve d_{33} with the greatest improvement observed for the higher density composites with the largest pore sizes. Distorting the structure also yielded considerable improvements in d_h and the figure of merit, $d_h g_h$, at both density levels and most pore sizes. In general, as the level of distortion increases, the strain and voltage coefficients increase as well. This can be seen in Figures 7, 8, 9, and 10.

Table I Factors Varied in Ceramic Configuration Effect Experiments

Factor	Levels
Distortion	1:1, 2:1, 3:1*
Pore Size (PPI)	15, 30, 45, 65
Density	10, 15 vol % PZT

* Only tested at 15 vol. % PZT

The effects of the aspect ratio can best be seen in Figures 11 and 12 where 15 ppi, 15 ceramic volume percent samples are compared. The charge coefficients, both d_{33} and d_h , and the figure of merit $d_h g_h$(corrected for density), increase linearly with cell aspect ratio. The increase in d_h with aspect ratio is indicative of continued alignment of the ceramic ligaments parallel to the direction of polarization. The improved alignment allows more effective stress transfer to the ceramic. It also allows a more thorough poling of the PZT material which may account for at least a small part of the observed improvement.

The change in voltage coefficient with respect to aspect ratio is not quite as linear as for the charge coefficients. The reason may be that g_h includes the effects of both the dielectric constant and density which are not necessarily linearly related in these composites. For example, the dielectric constant of the 2:1 cell aspect ratio composites was approximately 140 compared to 200 for the 3:1 composites. The increase is expected since the volume percent of ceramic that is continuous from one electrode to the other electrode increases.

Processing of distorted foam with greater than a 3:1 cell aspect ratio presented processing challenges which could not be solved in the time frame of this contract. The difficulties arise in that the distortion process greatly increases the bulk foam density and limits slurry penetration and uniform web formation. In general the best results were obtained for the high density more open foams. The large pore size allowed good slurry penetration into the foam and uniform web

formation. The higher density foams have more ceramic material in contact with the electrode producing a greater charge for a given area.

The best overall hydrostatic charge coefficient, d_h, and figure of merit, $d_h g_h$, were obtained for composites consisting of a 3:1 cell aspect ratio, 15 ppi pore size, and 15 volume percent PZT in a Spurrs epoxy polymer matrix. For this reason the cell aspect ratio, ppi, and ceramic volume percent were standardized to these values for manufacturing the arrays. Having a common composite unit allowed variations to be compared in the assembly methods, array fabrication and encapsulation of the multi-composite assemblies.

Matt Creedon looked at different epoxies to compare the effects of stiffness of the epoxy on the piezoelectric and other properties of the final composite. A four part "soft" Spurr epoxy formula was chosen, since it has a very low room temperature viscosity before cure, and since the final stiffness can be easily varied by changing the mix ratios of the four parts (see Manufacturing Report for mix ratios). The low viscosity was important in that it allowed the epoxy to easily penetrate the fired reticulated piezoelectric ceramic, and for entrapped air bubbles to be easily removed in a bell jar under a vacuum. The webs of the reticulated ceramic are hollow as seen in Figures 13, 14, and 15. Some webs are filled with the epoxy and others are not.

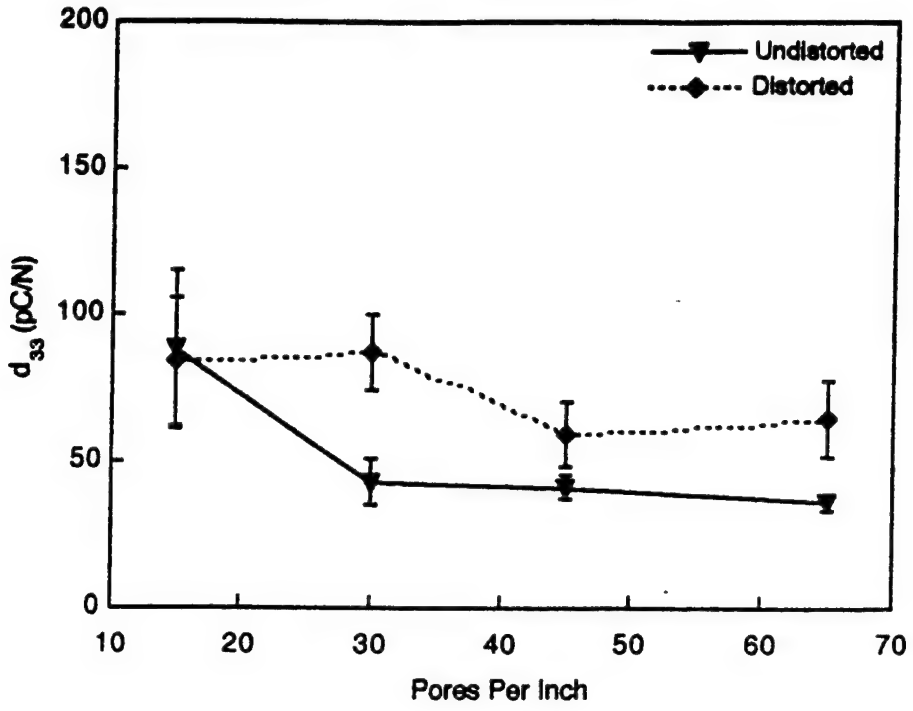

Figure 5 d_{33} as a function of foam pores per inch for 10 volume % composites. Error bars indicate one standard deviation above and below average.

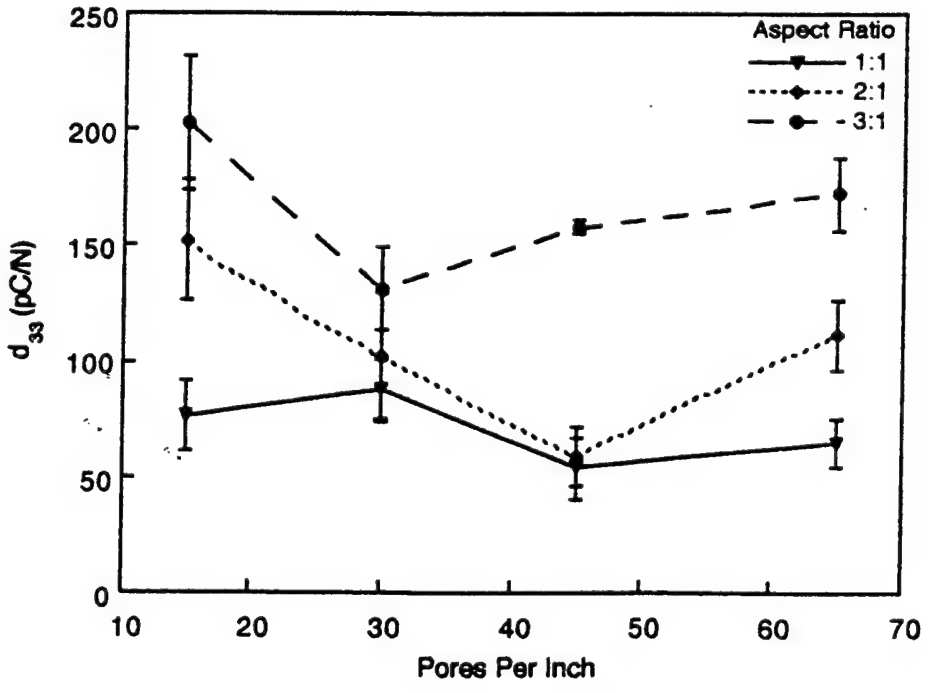

Figure 6 d_{33} as a function of foam pores per inch for 15 volume % composites.

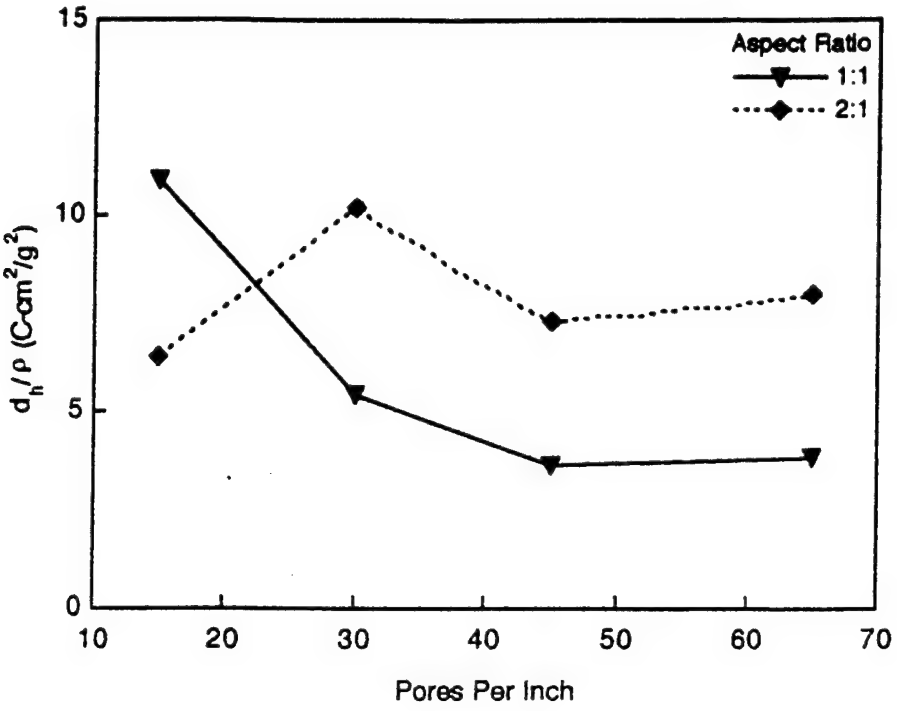

Figure 7 d_h as a function of foam pores per inch for 10 vol. % composites.

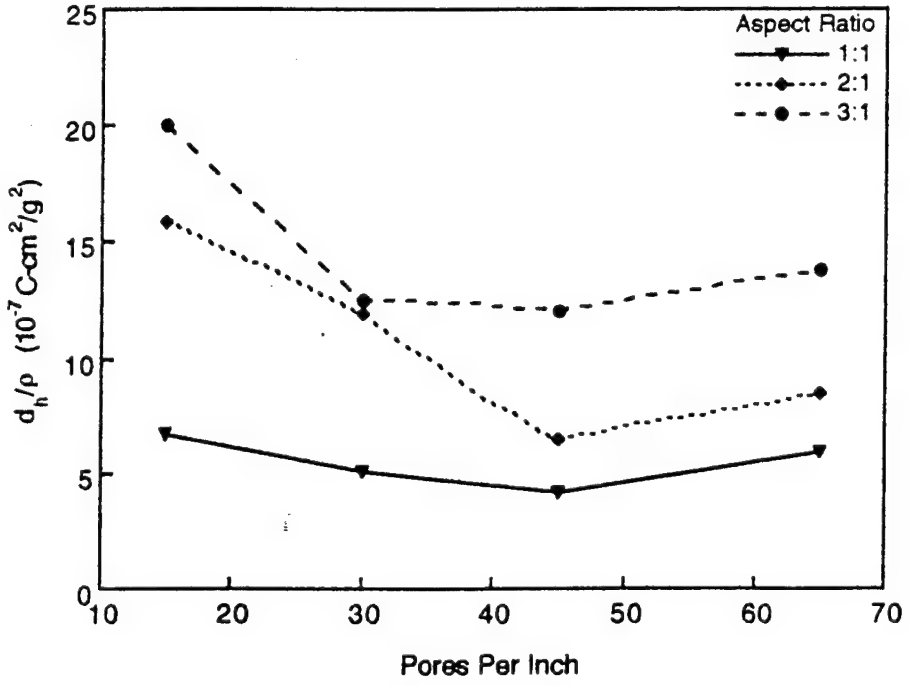

Figure 8 d_h/ρ as a function of foam pores per inch for 15 vol. % composites.

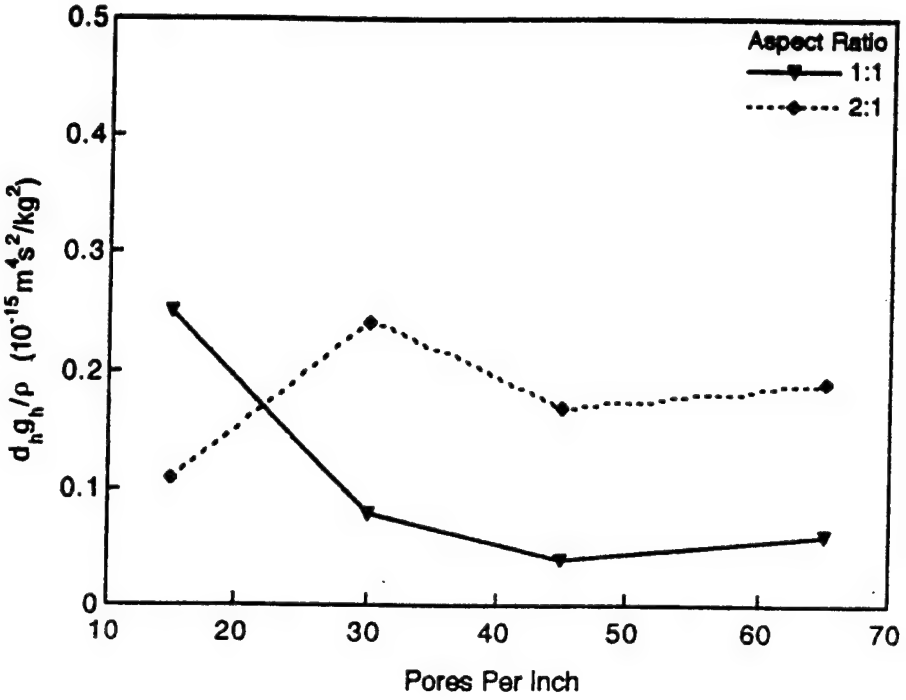

Figure 9 $d_h g_h/\rho$ as a function of foam pores per inch for 10 vol. % composites.

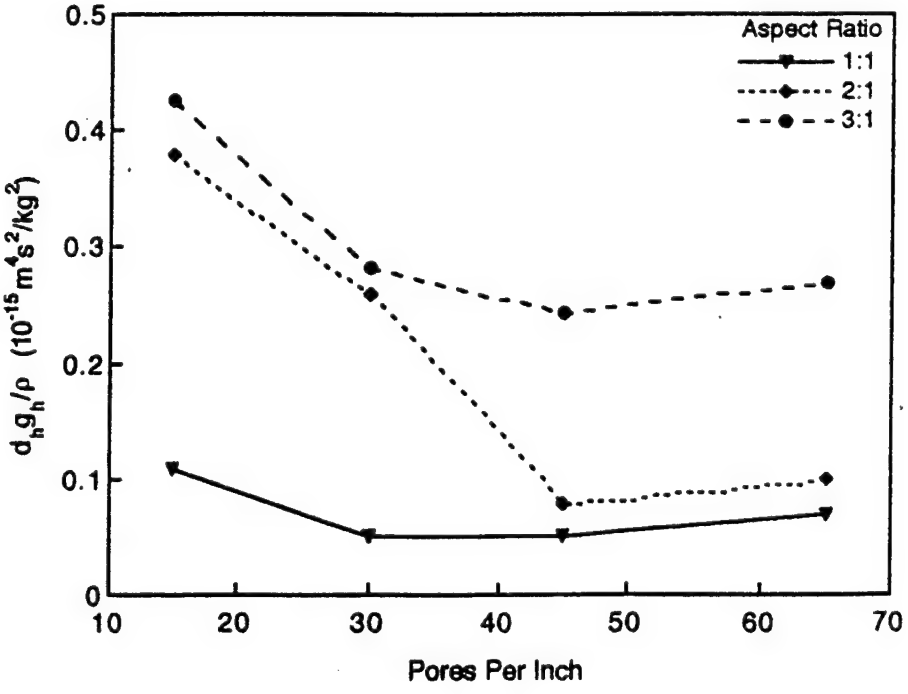

Figure 10 $d_h g_h/\rho$ as a function of foam pores per inch for 15 vol. % composites.

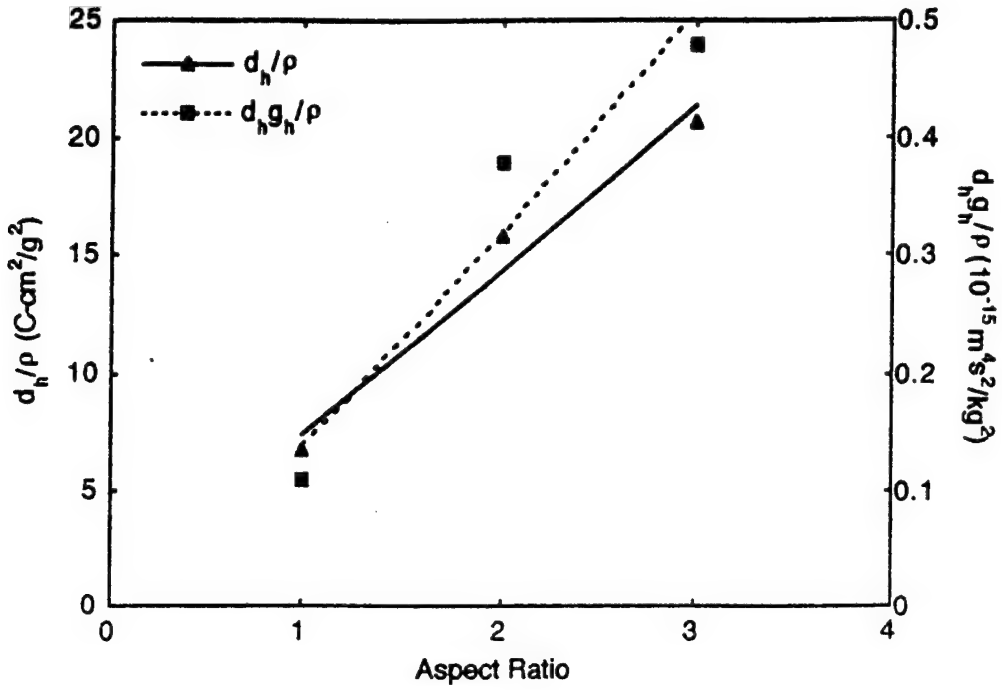

Figure 11 d_h and $d_h g_h$ as a function of cell aspect ratio for 15 vol %, 15 ppi composites for actual composite density, ρ.

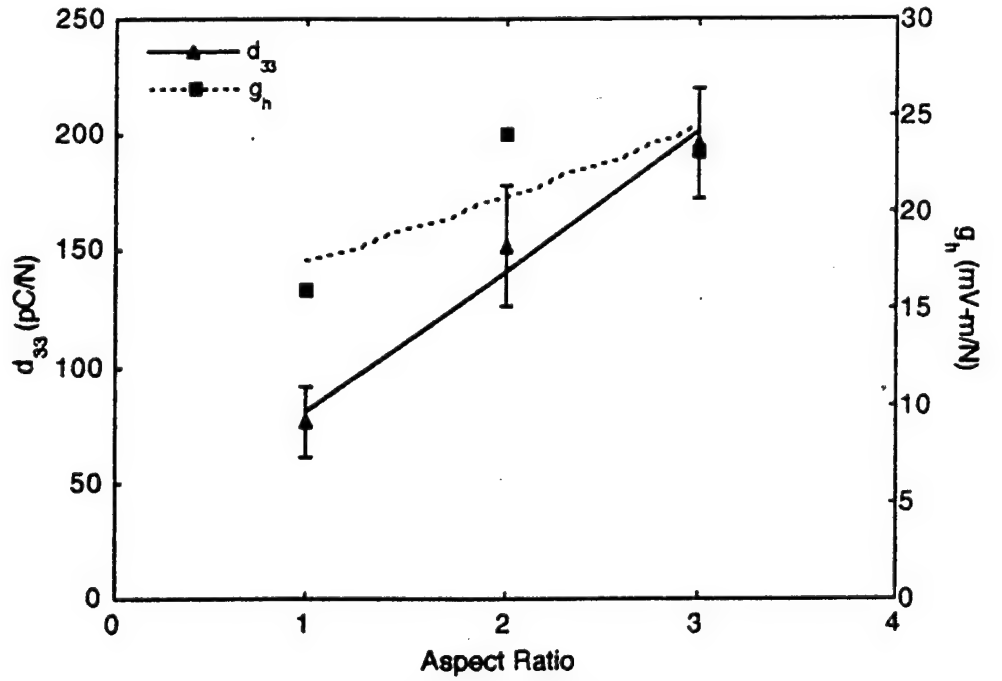

Figure 12 d_{33} and g_h as a function of cell aspect ratio for 15 vol. % composites.

Figure 13 Fractured surface of a piezoelectric ceramic exposes the hollow webs (Ref. 1, p 101).

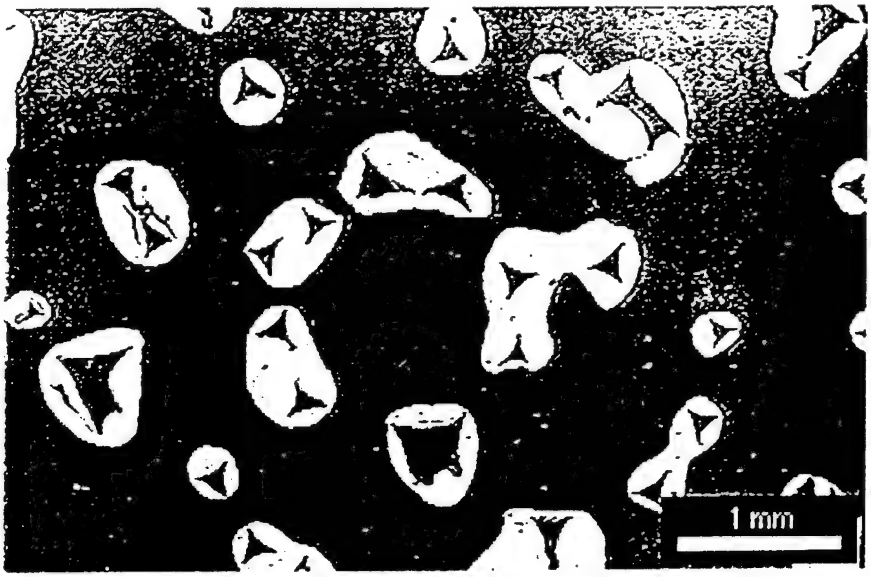

Figure 14 Polished section of PZT/Spurr epoxy composite surface (Ref. 1, p 101).

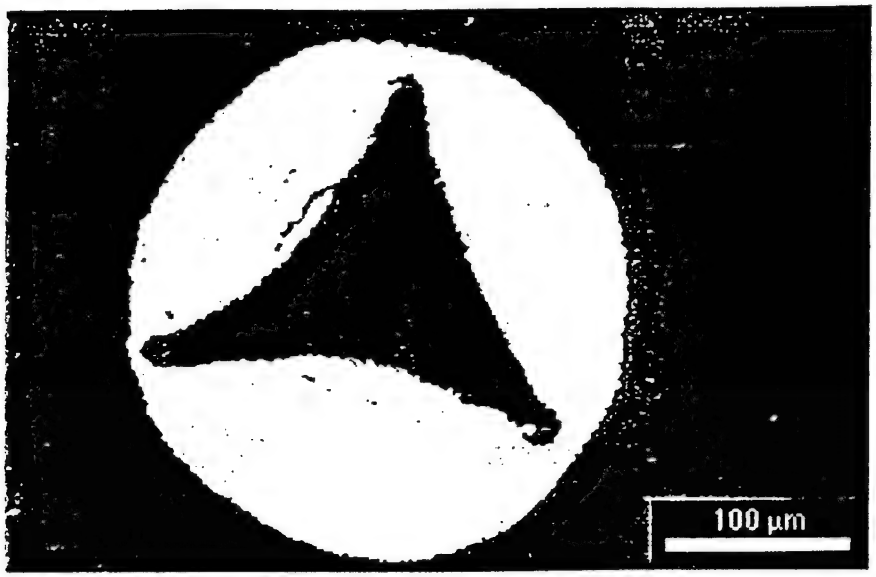

Figure 15 Enlarged view of polished section of PZT/Spurr epoxy composite surface (Ref. 1, p 101).

A lower modulus polymer than Spurr epoxy was found to have a higher d_h . Restrictions on the softness of the polymer exists in that a soft polymer presents machining challenges. Some samples experienced changes in the hydrostatic strain coefficient upon repeated cycling between high and low pressures. It was suggested that this might be due to damage imposed during machining, i.e. broken webs. Therefore, the depths of cut during machining were minimized and the premachining sizes were held as closely as possible to the finished sizes. Finite element modeling results indicate that 90 percent of the acoustic load is supported by the epoxy and only 10 % by the ceramic, resulting in a very strong shock resistant composite with sensitivities significantly suppressed from those that could be realized (Ref. # 1, p 132). Figure 16 shows the reticulated piezoelectric ceramic filled with the clear Spurr epoxy.

Figure 17 shows the relation between poling voltages applied and d_h of the poled composite. The highest d_h's are at 10 kV/cm and decrease with increased voltages. This may be due to the poling process. It was proposed in Matt Creedon's thesis that with higher voltages that the poling is able to follow the webs even where the webs are not parallel to the poling axis (Ref. 1, p 133). After removing the polarizing voltage, if some of the dipoles have been rotated to follow the webs to become less parallel to the poling axis, then the overall average polarization is diminished.

Figure 16 Reticulated piezoelectric ceramic impregnated with clear Spurr epoxy.

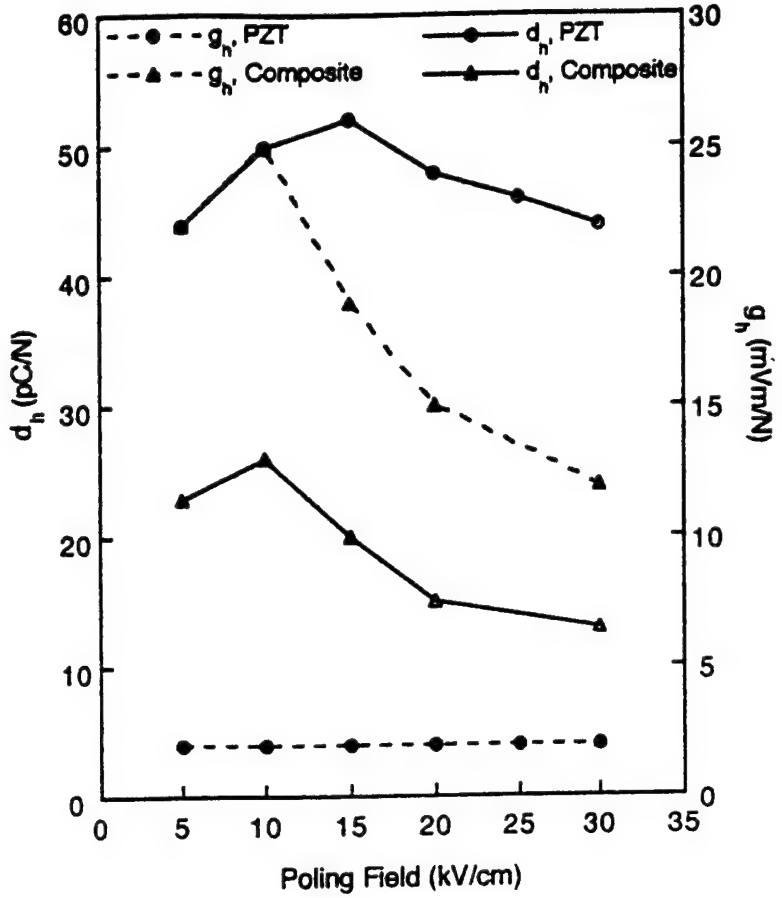

Figure 17 The hydrostatic strain coefficient, d_h, vs poling voltage for 15 ppi foam, 15 volume % PZT, 2:1 distorted PZT/Spurr composites. (Ref. 1, p 133).

The voltage output from the material is given by V= (g_h) (thickness)(acoustic pressure). The initial composite material was ~ 4 mm thick (Array #1) but was increased to 6 mm, in order to enhance the overall voltage output and sensitivity.

The composite material was characterized by density, volume percent ceramic, ppi, aspect ratio, d_h, d_{33}, dielectric constant, and g_h. In order to measure d_h and to arrive at g_h a special apparatus was set up at the NYS College of Ceramics at Alfred University. A schematic is shown in Figure 18. The chamber was set up to hold two samples and a Navy standard, however, with samples 1" square, only one sample and the Navy standard would fit. The hydrostatic voltage coefficient of the composite was found from the following formula by measuring the voltages across the Navy standard and across the composite. Knowing the hydrostatic coefficient of the Navy standard to be 47 pC/N,

$$d_{comp} = d_{std} \frac{V_{comp}}{V_{std}} \frac{A_{std}}{A_{comp}} \quad ,$$

where d_{comp} is the hydrostatic charge coefficient being determined for the composite. The hydrostatic charge coefficient for the Navy standard is d_{std}. A_{std} is the area of the standard, A_{comp} is the area of the composite being tested, V_{comp} is the voltage measured across the composite, and A_{std} is the area of the Navy standard.

A temperature controlled oil heater was incorporated as a means of affecting the stiffness of the epoxy of the composites. The initial thought was that if the hydraulic oil was heated, that the stiffness of the epoxy would drop and the hydrostatic voltage coefficient would increase. From Figure 19 there seems to be a very slight if any increase in d_h when the oil temperature is increased and then it drops off. It was hypothesized that Poisson's ratio of the Spurr epoxy increases with temperature, making the d_{31} component more negative and thus making the g_{31} component more negative, dropping g_h, since $g_{31} = d_{31} / \varepsilon_o \varepsilon_r$, and $g_h = g_{33} + 2\, g_{31}$ where ε_r is the relative permittivity and ε_o is the permittivity of free space.

The sound velocity derived from the thickness resonance was determined to be ~ 1.88 mm/ μsec. The acoustical impedance of the composite was ~ 4.2 MRayl compared to ~ 35 MRayl for pure dense PZT. This low value allows the sound energy to be coupled much more easily into and out of water with an acoustical impedance of 1.5 MRayl. The g_{33} component was calculated to be 97 mVm/N, five times that of the pure PZT. The physical and electrical properties of the composites are shown in Table II.

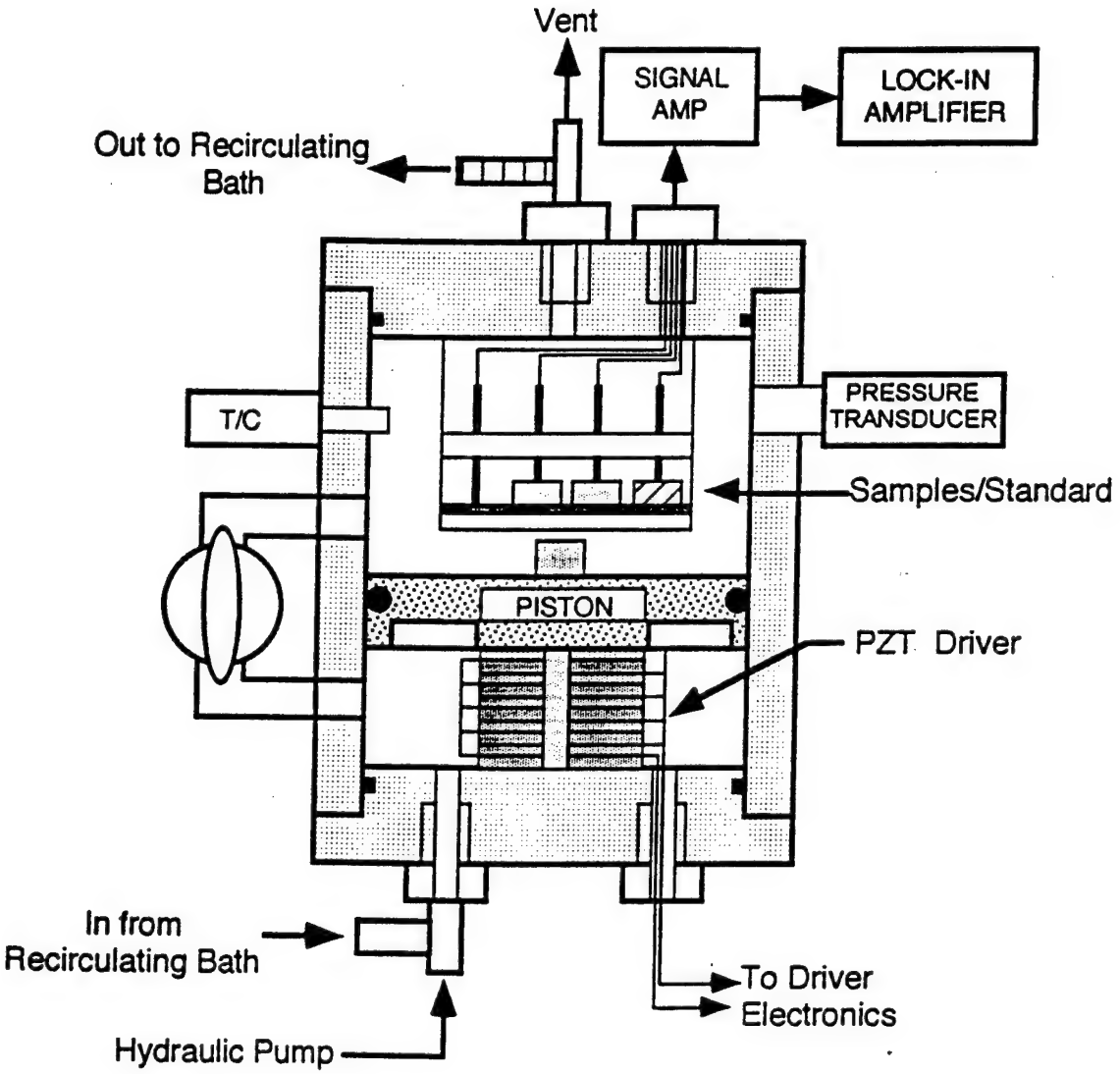

Figure 18 Schematic of the chamber used to measure d_h (Ref. 1, p 52).

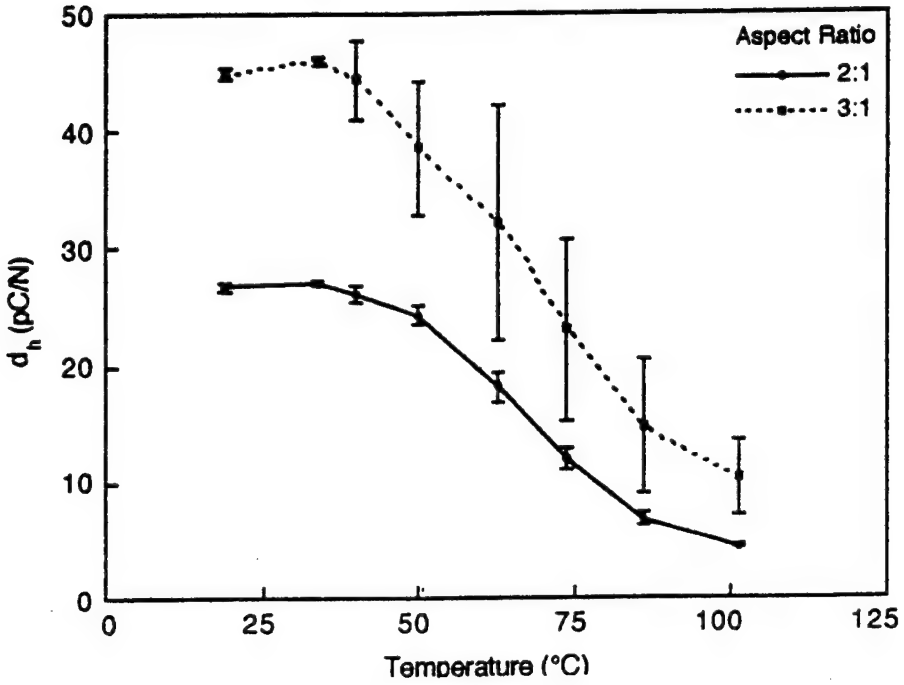

Figure 19 d_h vs. the temperature of the hydraulic oil that the composite is immersed in. (Ref. 1, p 130)

Table II Typical Properties of 1:3 Cell Aspect Ratio Distorted Reticulate Ceramic Composite Coupons

Characteristic/Property	Average	Std. Dev.	Units
Fired Bulk Density of PZT5H Reticulate	1.24	(0.10)	g/cm^3
Apparent Density of PZT5H Reticulate	7.57	(0.03)	g/cm^3
Composite Density	2.22	(0.09)	g/cm^3
Volume % PZT	15.86%	(1.13)	
Dielectric Constant	224	(25)	
Average d_{33}	196	(24)	pC/N
Average d_h	46	(4.2)	pC/N
Average g_h	23	(0.16)	mVm/N
Average $d_h g_h$	1067	(149)	10^{-15} m^2/N

Note (above): Total 25 coupons, approximately 25 x 25 x 4 mm

Longitudinal Sound Velocity	~ 1.88	mm/μsec
Acoustical Impedance	~ 4.2	MRayl
g_{33}	~ 97	mVm/N

Some of the reticulated ceramics were fabricated without impregnating them with epoxy, that is they were filled with air. These had a high sensitivity but low strength. The "PZT/air" composites with silicone side enclosures indicate the potential for high sensitivity (see Figure 20) as does the d_{33} component of PZT5H, 593 x 10^{-12} m/V, since $d_h = d_{33} + 2\, d_{31}$ if d_{31} is made to approach zero.

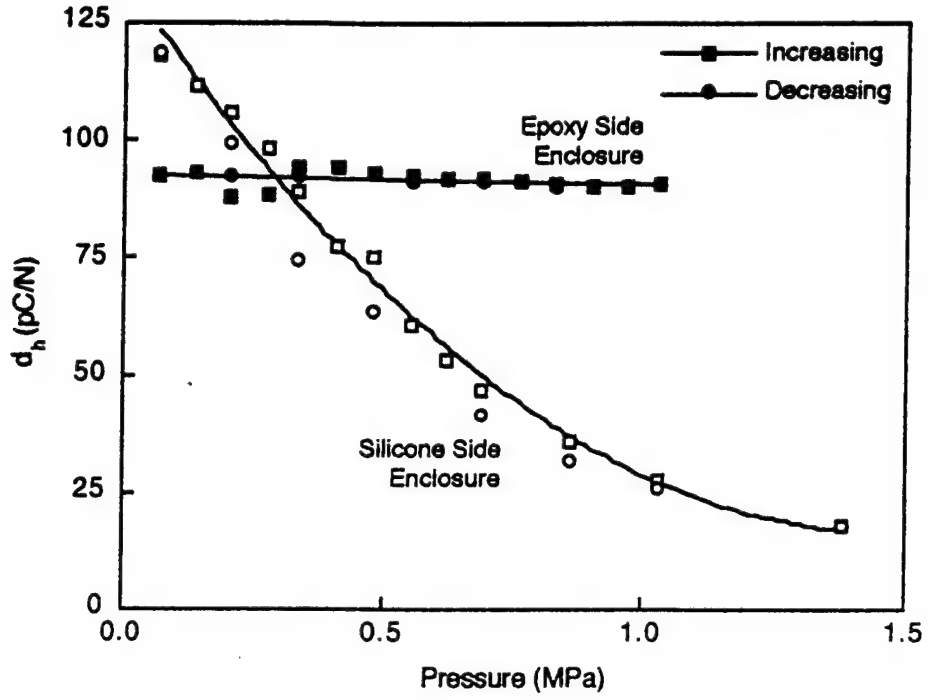

Figure 20 d_h of "PZT/ air" composites as a function of pressure. (Ref. 1, p 132)

PHASE II, PANEL ASSEMBLY

Array Production and Testing

Sixteen 1" x 1" coupons were used to make one 4" by 4" flexible array. The assembly details are given in the manufacturing report. Six arrays were included as deliverables of this contract. The first array was 4 mm thick and the last 5 were made 6 mm thick to increase the sensitivity. The first array had all 16 coupons in parallel as one set with the positive polarity all facing the same direction. The last 5 arrays had two sets of 8 coupons, separating the array into two halves for testing. Each set of 8 coupons were electrically in parallel with the positive polarity all facing the same direction as with the first array. These last five arrays each had two coaxial wires, one for each side of the array (referred to as Side A and Side B).

Tables III, IV, and V (page 38) show the properties of the coupons used in the arrays. The variability is discussed in more detail in the Phase III Manufacturing Assessment section of this report and is of concern in relation to the acoustical properties of the final arrays.

Table III Coupon Dimensions and Average d_{33}.

SAMPLE #	THICKNESS	LENGTH	WIDTH	AVE d_{33}
	(mm)	(mm)	(mm)	
54b	6.06	22.18	21.8	299
55	6.01	22.53	21.81	272
56	6.02	21.8	22.01	285
57	6.02	22.25	22.79	245
58	6.04	21.75	22.33	270
59	6.01	22.44	22.33	281
60	6.05	22.39	22.14	271
61	6.08	22.44	22.57	337
62	5.77	22.35	22.52	224
63	5.73	22.76	22.09	254
64	6.22	22.07	22	234
65	5.88	21.36	21.78	277
66	6.04	22.45	22.3	296
67	6.21	21.85	22.33	277
68	6.07	22.62	22.38	250
69	6.13	21.88	22.38	301
70	6.19	22.75	22.36	288
71	6.22	21.75	22.29	341
72	6.14	22.66	22.55	238
73	6.17	21.96	22.03	296
74	5.9	22.51	22.67	217
75	6.21	22.6	22.58	351
76	6.05	22.48	22.62	239
77	6.11	22.16	22.47	378
78	5.87	22.15	22.13	316
79	6.05	22.45	22.71	302
80	5.87	21.86	21.79	325
81	5.74	22.23	21.63	214
82	6.17	22.11	22.26	259
83	5.99	22.6	22.34	287
84	6.15	22.3	21.1	277
AVERAGE	6.0	22.2	22.2	281
STD. DEV.	0.1	0.3	0.4	39.7

Table IV **Capacitance of Coupons used for Arrays 4, 5, and 6.**

sample #	capacitance (pF)
64	193
76	198
82	205
48	205
62	206
74	207
68	209
49	211
65	212
80	213
57	214
58	216
50	217
51	217
73	221
55	223
52	223
59	224
84	224
88	225
56	228
54b	229
67	230
60	231
63	231
81	234
44	234
86	235
53	235
70	236
83	240
71	249
85	253
90	253
66	254
78	255
89	256
69	258
92	260
45	264
79	267
61	269
77	278
93	278
54	282
75	283
91	285
94	285

ARRAY # 4

Mean	**210**
Median	212
Standard Deviation	8
Sample Variance	64
Range	**30**
Minimum	193
Maximum	223

ARRAY # 5

Mean	**232**
Median	231
Standard Deviation	7
Sample Variance	46
Range	**26**
Minimum	223
Maximum	249

ARRAY # 6

Mean	**268**
Median	266
Standard Deviation	12
Sample Variance	156
Range	**32**
Minimum	253
Maximum	285

In order to connect the coupons electrically, conductive copper adhesive tape was used. The tape was precut and bent in such a way as to allow the coupons to flex without pulling the conductive tape loose. This resulted in a highly flexible composite, moldable to curved surfaces. The interconnects are illustrated in Figure 21. See the Manufacturing Report for more details.

An aluminum mold was made for encapsulating the coupons in urethane. See Figure 22. Modifications made to the mold during the contract period included adding "ears" so that the arrays could be more easily handled and a protrusion about the exiting coaxial cables to prevent the wires from being torn from the array during handling. Other molds were made to produce urethane sheets that were used to make discs of urethane, 1 or 2 mm in thickness. These discs were superglued to the coupons as spacers in the mold to keep the separation between the coupons and one another, and between the coupons and the mold. Figure 23 shows the spacers attached to the composites before the array has been placed in the aluminum mold for encapsulation with urethane. This technique was quite effective, yielding a uniform thickness, bubble free coat of urethane, covering the face of the arrays and separating the coupons. Figure 24 shows the array placed in the aluminum mold with cabling attached prior to urethane encapsulation and Figure 25 shows Array # 4 finished.

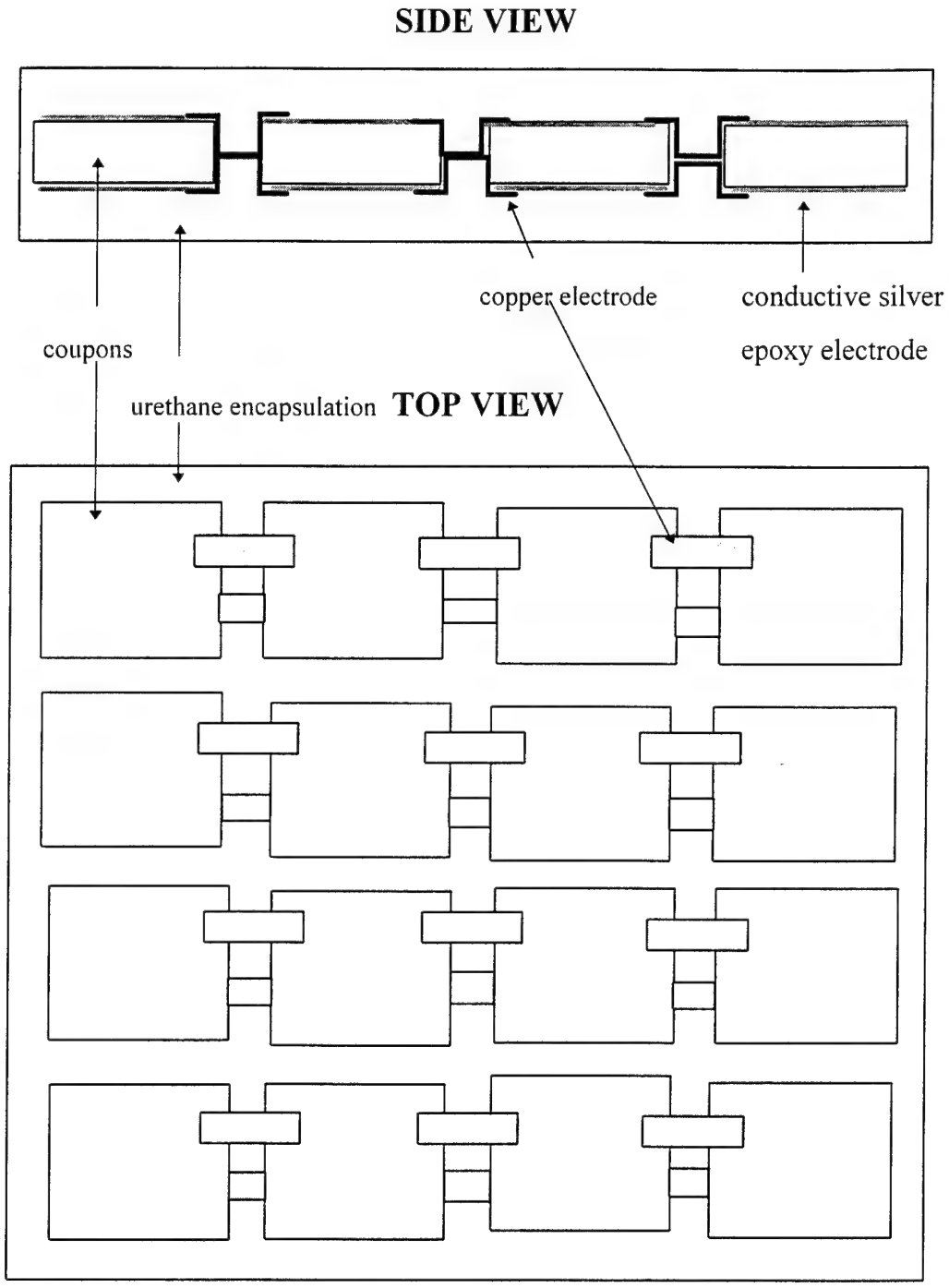

Figure 21 Side view and top view of array assembly showing the copper electrode arrangement.

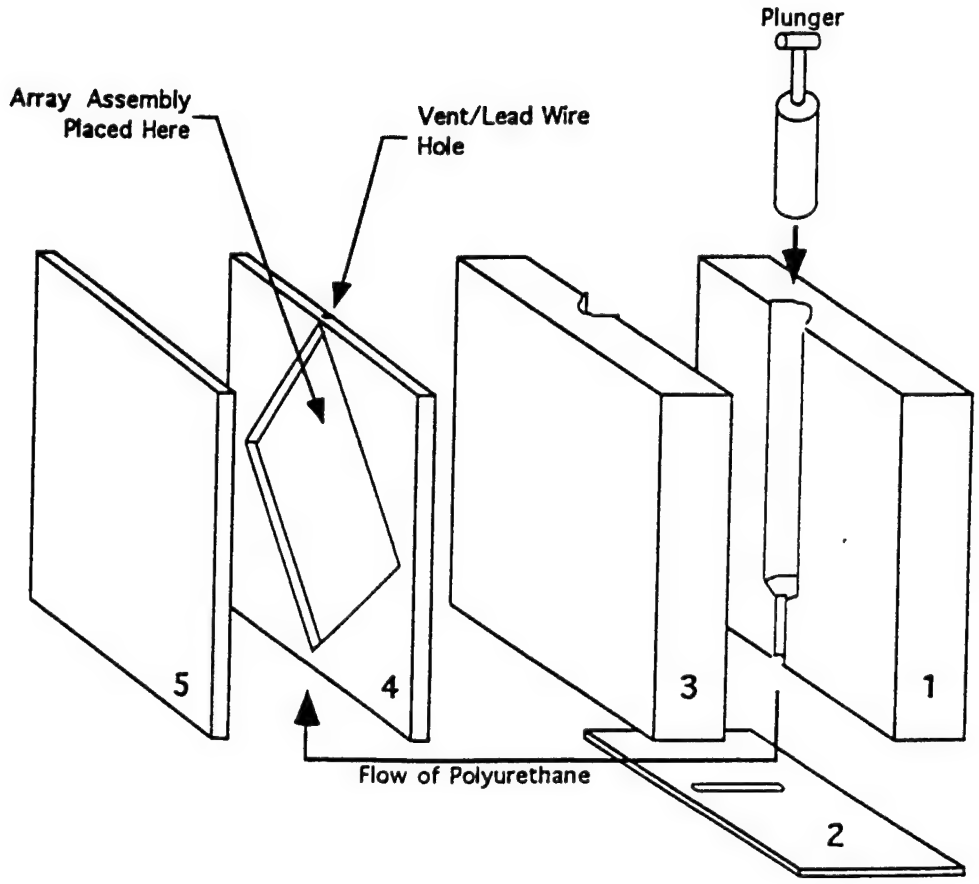

Figure 22 Aluminum mold for encapsulating the arrays in urethane. (Ref. 1, p 60)

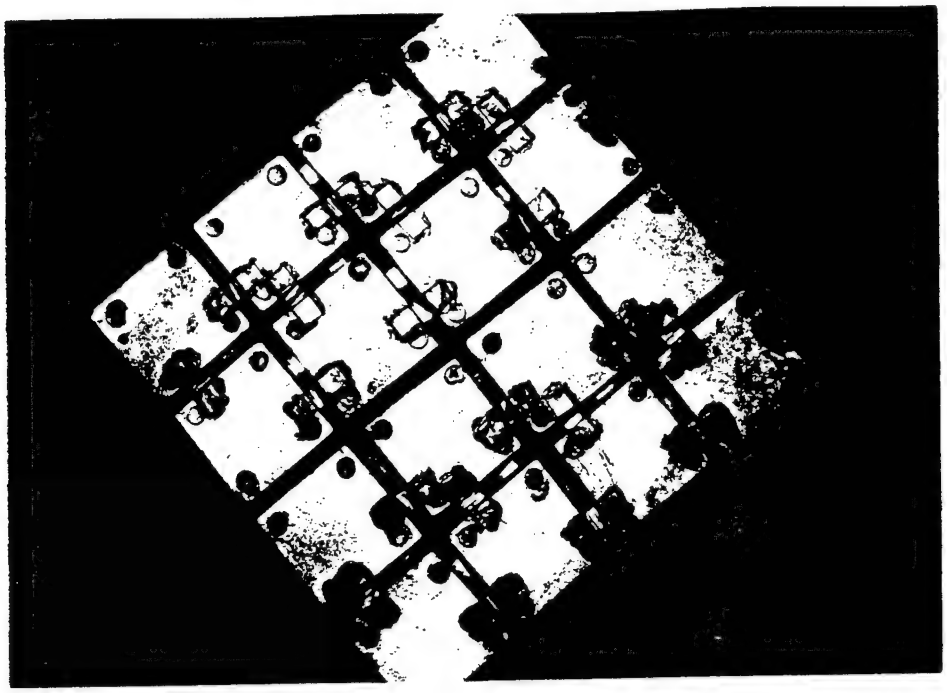

Figure 23 Array with urethane spacers bonded to the faces of the coupons and between the coupons prior to encapsulation in urethane.

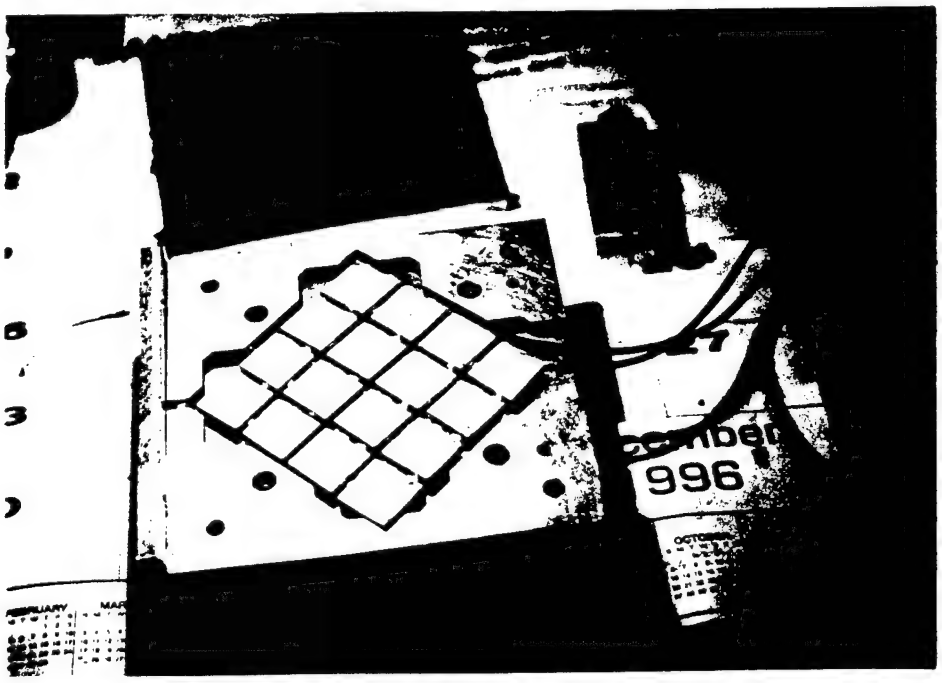

Figure 24 Array with spacers and cables attached placed inside the aluminum mold ready for urethane encapsulation.

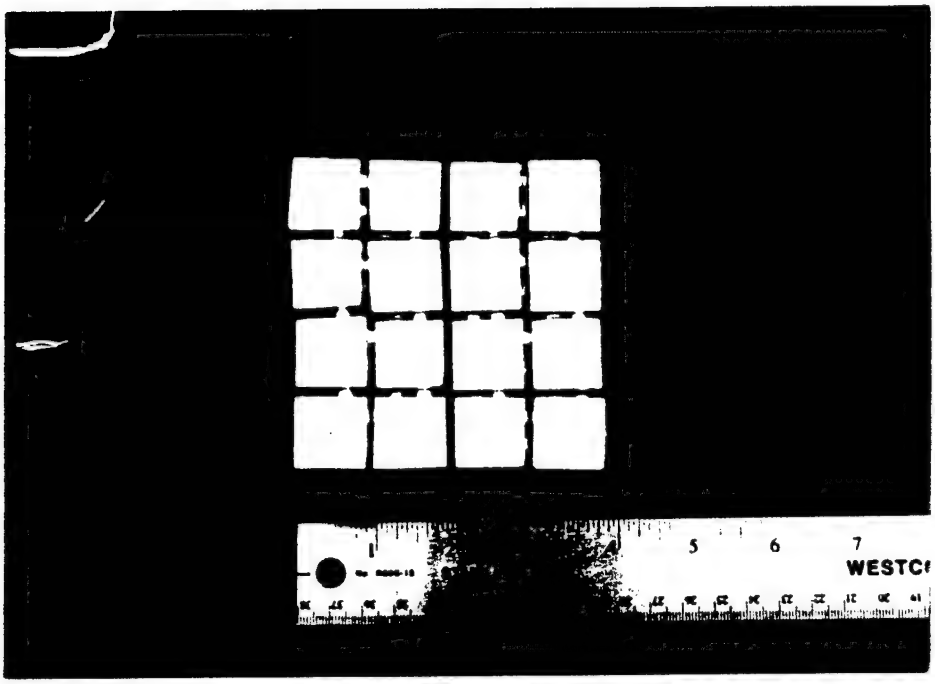

Figure 25 Photograph of Array # 4 with pure urethane between the coupons.

Figures 27a, b, and c show the electrical impedance of Array # 3 as a function of frequency, using an HP 4192A impedance analyzer. The thickness resonance (162 kHz) shown here is also evident from the acoustic data from Northrup-Grumman (Figure 54). A lateral resonance, not so pronounced in the electrical impedance plots, appears pronounced in the acoustical plot of Figure 54.

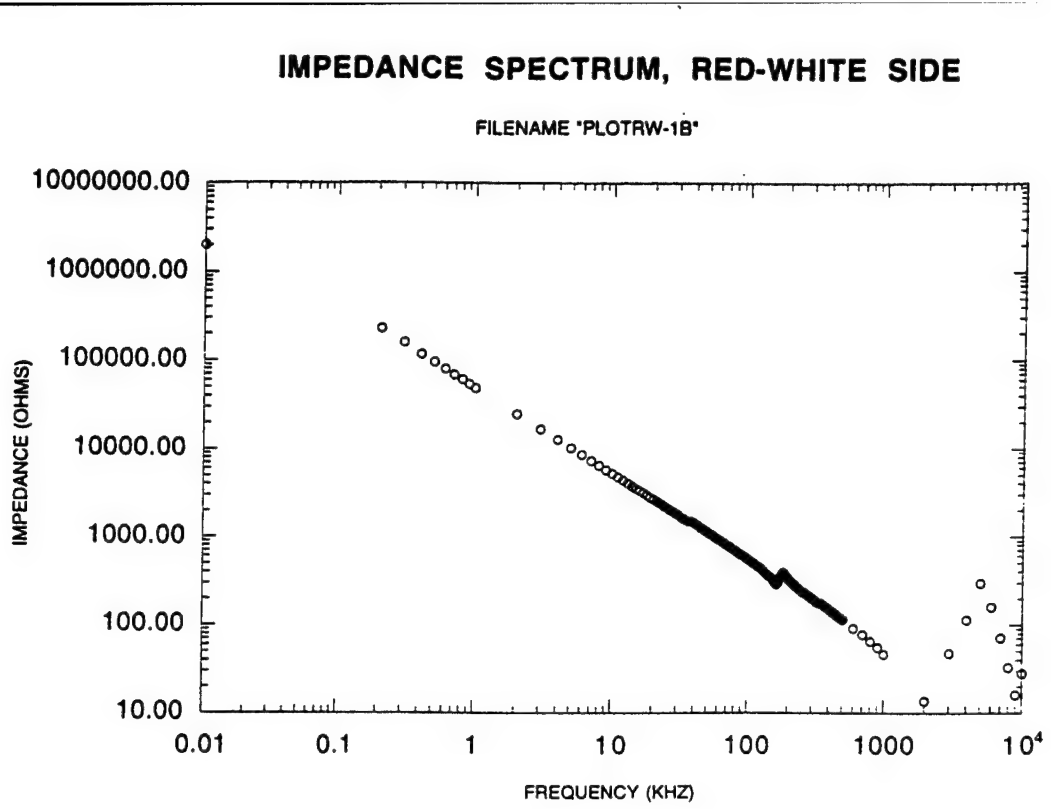

Figure 26a Electrical impedance of 8 coupons in parallel as a function of frequency, "Red-White" side of Array # 3.

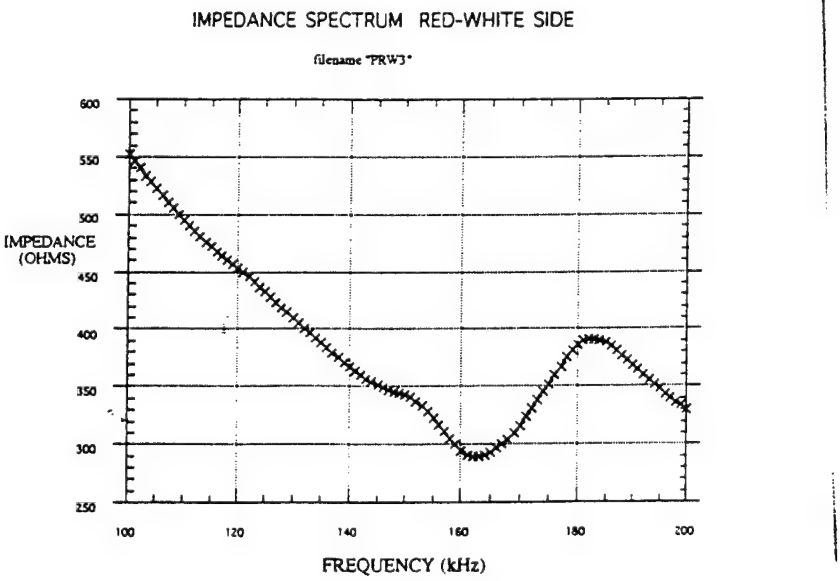

Figure 26b Electrical impedance of 8 coupons in parallel as a function of frequency, "Red-White" side of Array # 3 (thickness resonance).

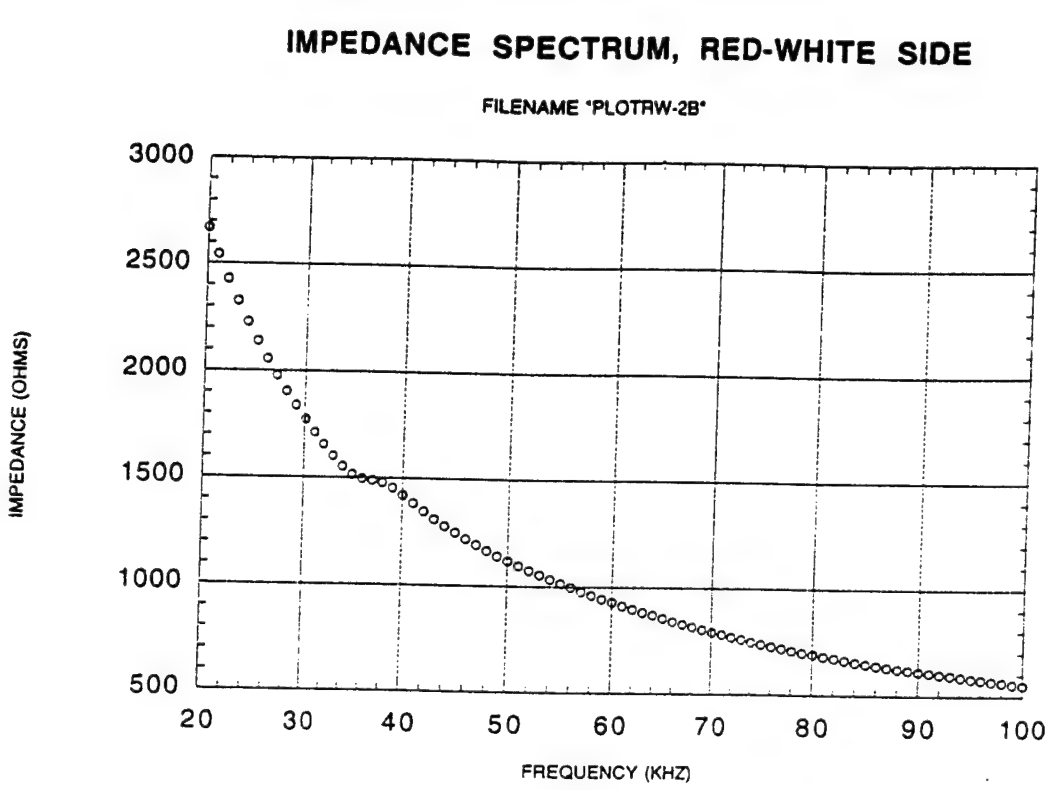

Figure 26c . Electrical impedance of 8 coupons in parallel as a function of frequency. "Red-White" side of Array # 3 (lateral resonance).

Arrays 1, 2, and 3 were tested at Northrup Grumman. The water test chamber at Northrup Grumman is a 50 feet in diameter redwood (high attenuation and low reflections) container. The hydrophone test array and a calibrated Navy transducer were hung 4.6 meters apart, 10 feet deep in the tank, 18 feet from its bottom. Potential reflections from the container walls were eliminated by using an electronic gate, collecting only those signals within the time band that it takes for sound to pass from the projector to the receiver. Fred Geil and John McMaster explained that nonlinearities in the Navy standard hydrophone were normalized.

The testing at Northrup Grumman clearly indicated that lateral resonances (~ 30 kHz) in the composites caused considerable nonlinearity of response in the hydrophones. For example, see Figure 34 of the FFVS of Array # 1 from 10 kHz to 160 kHz.

FFVS (free field voltage spectrum) spectrums at 10 kHz, 20 kHz, 50 kHz, and 100 kHz are shown in Figures 30, 31, 32, and 33 for Array # 1. The Navy standard is driven and the test arrays rotated through 360°. On the FFVS plots, the intensities given in dB to the left are the maximum intensities, usually at 0° dead center in front of the Arrays. Since intensities are given in dB re 1V/μPa, a more negative value represents a lower voltage response. The FFVS spectrums for Array # 2 are shown in Figures 38, 39, 40, 41, and 42 and those for Array # 3 in Figures 50, 51, 52, and 53.

A Broadside FFVS was generated by projecting with the calibrated Navy hydrophone and receiving with the test array perpendicular to the impinging acoustic wave. A lateral resonance around 30 kHz was seen for all three arrays tested. It was noted that the linearity of the response was comparable to that of the calibrated Navy hydrophone except for the 30 kHz region. Figures 34, 43, and 54 correspond to Arrays # 1, # 2, and # 3 respectively.

An "End Fire" test was done where the edge of the array as a receiver is facing the projecting transducer. The array is then rotated 180 and tested again. If the profile (a series of humps and nodes) is the same, then the individual segments of the array are the same. Differences in the capacitance between individual segments would cause these two profiles to be different and was of most concern. Figures 35 and 36 correspond to Array # 1, Figures 44 and 45 for Array # 2, and Figures 55 and 56 for Array # 3. John McMaster at Northrup Grumman pointed out that some of the irregularity of the shapes of certain plots, i.e. Figures 36 and 45, may be due to the cable being out in front of the array.

The relative phase response (Side A compared to Side B on Arrays # 2 and # 3) should be a straight line with no slope when tested broadside. The two halves of the array should have the same phase as was the case for Array # 2 shown in Figures 46, 47, and 48. Array # 1 only had one segment and so was not tested in this manner, nor was Array # 3 tested.

Figures 37 and 48 are the transmit voltage response (TVR) of Arrays 1 and 2, respectively. In this case the test array was used as a transmitter and the Navy hydrophone was the receiver. It is desirable for the response to be linear, though the lateral mode at ~ 30 kHz appears to be an issue here as well.

Fred Geil of Northrup Grumman stated that he would like a hydrostatic voltage coefficient to be over 100 mVm/N. The arrays tested in this study had an average g_h value of 23 mVm/N. Modifications to the epoxy are likely to increase the sensitivity into the 100 mVm/N range.

An attempt to diminish the effects of lateral resonances was undertaken. Microballoons were added to the urethane that went between the coupons for Arrays # 5 and # 6. This made the urethane encapsulation a two step procedure. First the microballoon filled urethane was cast between the coupons. By this time the coupons were already electrically connected by the copper conductive tape and had spacers glued between them to hold them in place. After the microballoon filled urethane was cured, the array was placed in the aluminum mold for final urethane encapsulation. Array # 6 is shown in Figure 26.

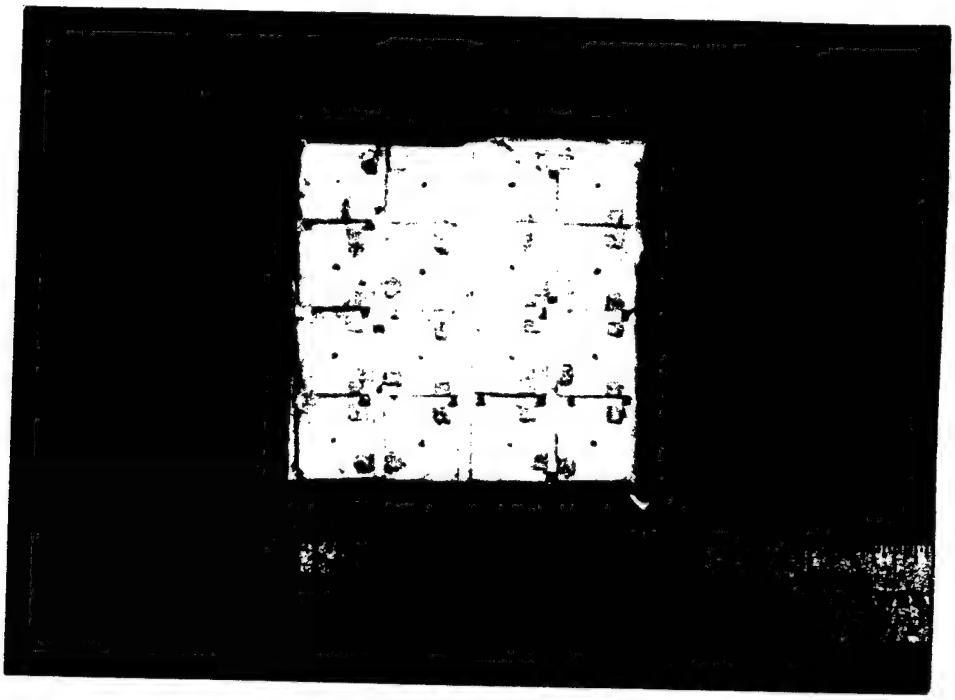

Figure 27 Array # 6 made with microballoons in the urethane between the coupons.

Arrays 5 and 6, with microballoons in the urethane between the coupons, were tested using an HP 3585A Spectrum Analyzer with an internal oscillator as a driver. The lateral resonance around 30 kHz disappeared, but a discernible deflection in the spectrum showed up around 100 kHz for both Array # 5 and # 6. Acoustical testing took place at Northrup Grumman in June on Array # 6 with microballoons in the urethane between the coupons, and the results are shown in Figures 57-65. Figure 61 shows that there still is a fairly significant lateral resonance, in spite of the use of the microballoons.

Figures 57-65 are the results of tank testing at Northrup Grumman on Array # 6. Figures 57, 58, 59, and 60 show the FFVS of Array # 6 at 10 kHz, 20 kHz, 50 kHz, and 100 kHz, respectively. Hollow microspheres were added to the urethane encapsulation applied between the coupons in order to decrease the urethane stiffness while not significantly increasing its Poisson's Ratio. This was done in an attempt to reduce the lateral mode response which was detected in the first three arrays at around 30 kHz during the tank testing. Though testing of arrays 5 and 6 on a spectrum analyzer in

the electro-ceramics lab at Alfred University indicated a reduction in this lateral resonance, tank testing at Northrup Grumman shows only a slight reduction in the resonance as is evident from Figures 61, 62 and 63. It is likely that the signal generator in the spectrum analyzer has too low an output to drive the lateral resonance and/or is not matched electrically to the arrays within the lateral resonance bandwidth. Figure 64 shows the phase vs. frequency of Array # 6 at 45^{o}, and Figure 65 is the FFVS endfire plot for Array # 6.

A table of properties for the six arrays is shown below in Table V. The sensitivity values on the far right of the table were taken from the polar plots at 0 degrees (straight ahead). The sensitivity values increase as expected going from Array # 1 to # 2, but not for Array 3. Possible explanations for this are the nonlinearity caused from harmonics of the lateral resonance and/or from effects of the regular periodicity of the coupon spacing (commonly seen in 1-3 composites, used for medical imaging). The first harmonic of the lateral resonance is approximately 3 times the fundamental, 3 x 33 kHz = 100 kHz. This could explain the hump at 100 kHz on the Broadside FFVS plots, for example, Figures 34, 43, 54, and 61. The higher capacitance of these reticulated composite arrays as compared to 0-3 composites or PVDF may make it easier to match them electrically to the drive/receive circuitry. The dielectric constant for the composite material is shown in Table V to be 226 as compared to about 8 for PVDF.

Table V Comparison of Array Properties.

ARRAY	THICKNESS (mm)	AVE. d_{33}	CAPACITANCE at 10 kHz (pF) (including coax.)	CAPACITANCE at 10 kHz (pF)	FFVS @ 100 kHz max dB re 1 volt/μPa
1	4	202	* 226		-193.8
2	6	209			-190.6
3	6	269		3872	-193.7
4	6	255	5175	3435	
5	6	274	5368	3628	
6	6	321	6097	4357	-191.3

d33 pertains to the average of the 16 coupons for each array.

* this particular value is the average dielectric constant

PHASE III, MANUFACTURING ASSESSMENT

A) Variability and Process Control

For the final three arrays the coupons were selected in order of capacitance and placed into arrays with adjacent coupons of similar capacitance. If properties, e.g. capacitance or d_{33}, were extreme to the high or low side, those coupons were set aside and not used. Once the coupon dimension, 15 ppi, 3:1 cell aspect ratio, and 15 volume percent ceramic was chosen, most of the coupons made after that point were used in making the final arrays. It seems likely that lateral resonances would tend to cause symmetrical perturbations in the TVR plots and that variability in the coupons is responsible for a fair portion of the asymmetry in the TVR plots. Specific examples potentially include variability from coupon to coupon in d_h, capacitance, and beveled edges (out of square from an edge view).

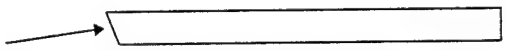

Figure 28 Edge view showing one edge to be beveled (exaggerated) from the cutting process.

A summary of the data taken for individual coupons is shown in Tables III and IV in the last section. Table VI and Table VII below show the variability in that data. The range divided by the mean for the thicknesses and lengths are 8% and 6% respectively; whereas, the range for the capacitances divided by the mean is 12.5 %. Process controls of interest include weight, slurry viscosity, blow off air pressure, size (area and thickness), electrode thickness (control via screen printing), poling voltage, poling temperature, poling time, cure time and temperature for the electrode paste, polymer cure times and temperatures for the epoxy and urethanes, and evacuation times and temperatures for removing air bubbles from the epoxy and urethane. The d_h values for six coupons that were simultaneously processed, are shown in Table VIII along with their statistical analysis. At 1000 psi the range divided by the median is 35 %. Being a strain coefficient, it seems likely that this variability is too extreme and would, as an example, cause perturbations in the wavefront as a transmitter.

Table VI Statistical Analysis of Coupon Dimensions from Table III.

	THICKNESS (mm)	LENGTH (mm)
Mean	6.04	22.25
Standard Error	0.03	0.06
Median	6.05	22.30
Standard Deviation	0.14	0.34
Sample Variance	0.02	0.12
Range	0.49	1.40
Minimum	5.73	21.36
Maximum	6.22	22.76
Count	31	31

Table VII Statistical Analysis of Coupon Capacitances from Table IV.

ARRAY # 4		
Mean	**210**	
Median	212	
Standard Deviation	8	
Sample Variance	64	
Range	**30**	range/mean => 14.3 %
Minimum	193	
Maximum	223	
ARRAY # 5		
Mean	**232**	
Median	231	
Standard Deviation	7	
Sample Variance	46	
Range	**26**	range/mean => 11.2 %
Minimum	223	
Maximum	249	
ARRAY # 6		
Mean	**268**	
Median	266	
Standard Deviation	12	
Sample Variance	156	
Range	**32**	range/mean => 11.9 %
Minimum	253	
Maximum	285	

TABLE VIII Hydrostatic Charge Coefficient, d_h, vs. Pressure.

SAMPLE	d_h 250 psi pC/N	d_h 500 psi	d_h 750 psi	d_h 1000 psi	THICK	CAP nF	g_h 10-3 Vm/N	$d_h g_h$ 10-15 m2/N
44	53.1	52.6	51.3	52.3	5.67	0.252	19.4	1030
45	57	56.5	56.7	56.4	5.84	0.283	17.8	1013
46	62.4	62.5	62.9	63.2	5.364	0.347	16.6	1035
47	61.5	61.9	61.9	68.4	5.75	0.335	16.4	1006
48	49.1	49	48.9	48.5	5.82	0.22	19.8	971
49	49.8	49.7	49.8	49.7	5.49	0.226	20.6	1028

d_h at 250 psi		*d_h at 1000 psi*	
Mean	**55.48**	**Mean**	**56.42**
Standard Error	2.35	Standard Error	3.24
Median	55.05	Median	54.35
Standard Deviation	5.75	Standard Deviation	7.93
Sample Variance	33.01	Sample Variance	62.87
Range	13.3	Range	19.9
Minimum	**49.1**	**Minimum**	**48.5**
Maximum	**62.4**	**Maximum**	**68.4**
Count	6	Count	6

As can be seen in Table VIII, there appears to be no significant change in the hydrostatic charge coefficient with pressure changes ranging from 250 psi on up to 1000 psi. Since g_h is proportional to d_h, this implies that the hydrophones show little variation in voltage sensitivity in water from just below the surface down to depths of about one-half mile.

From these tables it can be seen that there is substantial variation in the properties, several of which directly effect the acoustical properties or indirectly via the electrical impedance. Though tighter processing controls will bring the variability between coupons quite close, another idea is to make the coupons, measure the properties, reject those coupons with extreme values, and modify the remaining ones to limit the variance. This process could with developments, reduce the variability in those properties that would significantly effect the performance of the arrays. Feedback variations include modifying the capacitance by removing electroding and thus decreasing the area, sanding to reduce the overall size, and repoling for higher d_{33}'s. For example, when sample # 63 was repoled the average d_{33} went from 254 to 273. Individual coupon electrical tuning schemes could be considered.

Any major changes in design have to be dealt with in a manufacturing assessment. In this initial work no consideration was given to shielding, such as using copper circuit board cladding. A shielding step would change the process significantly and bring up new issues to resolve. Some potential improvements in the electrical impedance matching of the array to the amplifier or receiver might come about due to the added capacitance of the cladding.

C) Scale-up

In order to assess scale-up, a production rate of 100 square feet per month (composite in the form of arrays) was arbitrary chosen. Design modifications as discussed in the final section of this report, "Conclusions and Future Actions", need to be included. The Manufacturing report also includes a section on scale-up.

If possible a larger coupon size might be considered. Larger coupon sizes, due to decreased handling, make it easier to make larger areas of composite faster. On the other hand, higher volume production volumes have the potential to decrease variability and increase productivity. For example, a great deal of set-up time is avoided when large quantities of foam are cut at one time. Once the cutting machines are set, a very large quantity of foam can be processed in a short time. It is estimated that one thousand square feet of foam can be cut to coupon size in a couple days.

For increased production volumes, additional foam stretch machines would be needed. With only one foam stretch machine, production is limited to about six 4" x 4" arrays per day, stretching on two shifts. Modifications to the machine design could greatly increase the output without taking up as much space as adding a large number of stretch machines. Other scale-up considerations include more room to process the ceramics and more ovens for drying more parts. About 100 silicone molds for epoxy impregnation and additional vacuum pumps and bell jars would be needed. A high quality surface grinder is expected to

keep pace with 100 square feet per month. A high speed precision diamond cut off saw would greatly decrease the variability in sizes and keep the coupons faces square with one another. Additional poling equipment would increase the number of parts that could be poled for large scale production rates. Sixteen encapsulation molds of the present size would be required to produce 100 square feet per month. The molds may be redesigned to accommodate changes discussed in the final section and specific applications.

The Hydrostatic Charge Coefficient test rig in the Electroceramics Division of the New York State College of Ceramics in Alfred, NY is being modified to handle larger area parts. Presently, the test rig is fairly slow and so only selected parts representative of the group were chosen. Future modifications to the rig may include computer data collection. It is expected, however, that the d_{33} values are representative of the d_h values.

Acoustical testing would have to be performed at a facility, such as Northrup-Grumman, as with this project. Some of the parts would be sent out for long term repetitive high hydraulic pressure cycling and explosive shock testing to spot potential problems. An airbox apparatus has been suggested and could be built fairly inexpensively to do in-house acoustical analysis of the arrays.

The costs/square inch vary considerably depending on the manufacturing scale. A certain amount of equipment has been purchased, related to processing of the six prototypes. Proper cutting and grinding equipment and tooling are necessary to produce higher quality, tighter tolerance arrays as well as increased production volumes. Several additional personnel would be needed to produce 100 square feet per month. At 100 square feet per month the following cost estimates have been compiled (Table IX and Table X). Some of the costs would be reduced by purchasing used equipment, renting, or other cost saving measures.

Table IX Equipment Costs for Scale-up.

EQUIPMENT	DOLLARS
foam stretch machines	10000
jar mill and media	300
dryer	1500
furnace, controller, recorder	35000
shipping, installation	4000
150 RTV silicone molds (20 ea.)	3000
table	100
2 vacuum pumps	700
2 vacuum jars	180
rotary surface grinder	80000
poling power supply	20000
poling tank	300
poling heater	500
Chanel d33 meter	1800
Hewlett-Packard 4192A, impedance analyzer	22000
EQUIPMENT TOTAL	179380

Table X Operating Expenses for Scale-up.

EXPENSE	
Direct Labor	458518
Fringe Benefits (38.5%)	176529
Fixed Plant Overhead (58.4%)	267775
Direct Materials	238030
Other Direct Costs:	
Outside Testing	12000
Travel	4000
consultant fees	10000
hazardous waste removal	10000
other	5000
Subtotal	1181852
General and Administrative (12%)	141822
Total Costs	1323674
Fixed Fee Earned (12%)	158841
Total Amounts	$ 1482515

CONCLUSIONS AND FUTURE ACTIONS

This project has shown conclusively that reticulated ceramic processing is adaptable to the production of piezoelectric composites for hydrophone and transmitter applications. A wide range of shapes are readily fabricated (squares, rectangles, discs, donuts, cylinders, and tubes). Reticulated piezoelectric ceramic composites have potential because of their low cost, high capacitance, and ruggedness. In order to enhance the hydrostatic coefficient, the polyurethane precursor foam is stretched at high temperature and cooled in place. The final material is a distorted 3-3 reticulated piezoelectric ceramic composite. An average value for d_h is 46 pC/N and for g_h is 23 mVm/N. The acoustical impedance was calculated to be 4.2 MRayl for the composite, ignoring the effect of the urethane encapsulate. The g_{33} coefficient was calculated to be 97 mVm/N, five times that of the pure PZT material. Unlike the 1-3 piezoelectric composites, the ceramic portion of the distorted 3-3 composites are interconnected, causing lateral resonances.

The assembly of composite coupons into flexible, conformable arrays has been demonstrated. Though the sensitivities are modest, -192 dB re 1 Volt / μPa (-188 dB subtracting out the cables), the composite material is highly robust and shock resistant. The hydrophones did have a lateral resonance (~33 kHz) related to the lateral resonant mode of the coupons. At the lower frequencies, 10 kHz to 30 kHz, the acoustical plots are very uniform and symmetrical, indicating that this composite could be used, as is, for low frequency narrow bandwidth hydrophones and projectors. Distorted 65 ppi reticulated piezoelectric ceramic has been sent to an ultrasonic transducer manufacturer to be used in the prototyping of 1 MHz nondestructive testing transducers.

Shock testing, high hydrostatic pressure cycle testing, butadiene encapsulation, and shielding are areas that need work, in order to utilize the composite for hydrophone applications.

Different shaped coupons have been suggested to reduce the lateral mode. One suggestion is to utilize a rectangular shape where the length and width are not equal so that there are two distinct lateral resonances, instead of one pronounced lateral resonance. Perhaps a better suggestion is to use triangular shapes, since they have no defined lateral distance which supports a lateral resonance. In order to go to triangular coupons, the foam cutting, epoxy impregnation mold, and mold for urethane encapsulation would have to be changed. None of these issues are of major concern. Another benefit to using the triangular shape is an increase in flexibility as shown in Figure 29.

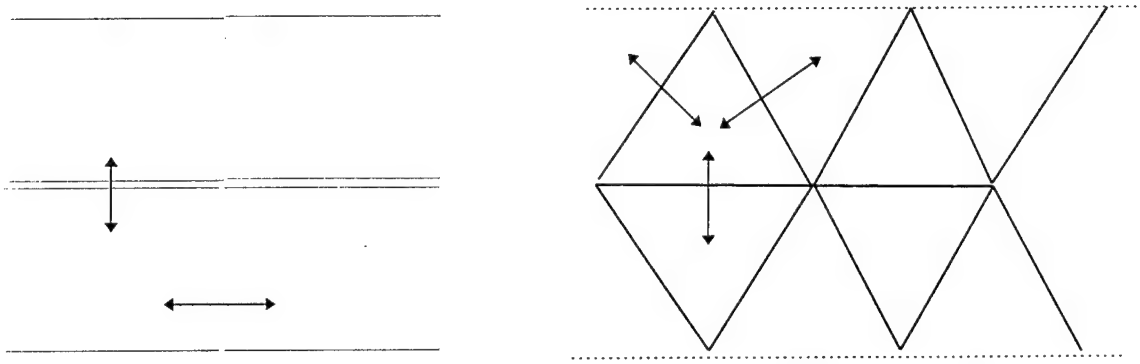

Figure 29 The left diagram shows rectangular coupons with two degrees of freedom and two well defined lateral resonances. The right diagram shows triangular coupons with three degrees of freedom and thus increased flexibility. The triangular shape has no specific pronounced lateral resonance frequency (dimension).

Rather than modify the shape of the coupons or in conjunction with modifying the shape are some other ideas to increase the sensitivity while alleviating the lateral resonances. Since the epoxy filler was too stiff, only about one-tenth of the acoustic pressure was being felt by the active ceramic (Ref. # 1, p 132). Finite element modeling indicated that dropping the

elastic modulus of the epoxy and reducing the Poisson's ratio at the same time will result in much higher sensitivity with a diminished d_{31} (lateral resonance) and thus improved acoustics (Ref. # 1, p 132). Dr. Walter A. Schulze of the NYS College of Ceramics in Alfred, NY received funding in August of 1997 from the Center for Advanced Ceramic Technology to sponsor a Ph. D. student, David Williams, to develop an improved reticulated piezoelectric ceramic composite. It is believed that a highly sensitive composite with a linear acoustic response and output can be realized with only minor modifications.

Some modifications underway include modifying the present polymer by adding microballoons, using a alternate polymer with a negative Poisson's ratio, and modifications to the foam preparation procedure. So far the results appear promising. Some alternate polymers have been identified. Also, a new process for preparing the precursor foam has resulted in foam with a negative Poisson's ratio.

An issue of concern is the variability between the properties of the individual coupons used in the arrays, in particular the capacitance and dissipation. Within this project, the variability in d_h appears to be too great. It is felt that a high degree of consistency can be expected by large scale production, the addition of certain processing equipment, and the implementation of tighter production tolerances.

As the lateral modes of the individual coupons are diminished the benefits of reticulated piezoelectric composite processing flourish. Some potential applications include broadband hydrophones and projectors, fish finders, ultrasonic imaging, and therapeutic ultrasound.

REFERENCES

1. Reticulated Ceramic PZT/Polymer Piezoelectric Composites for Hydrophone Applications by Matthew Jay Creedon, Ph. D. Thesis, New York State College of Ceramics, Alfred University, November 1996.

APPENDIX

NORHRUP GRUMMAN ACOUSTICAL TEST DATA

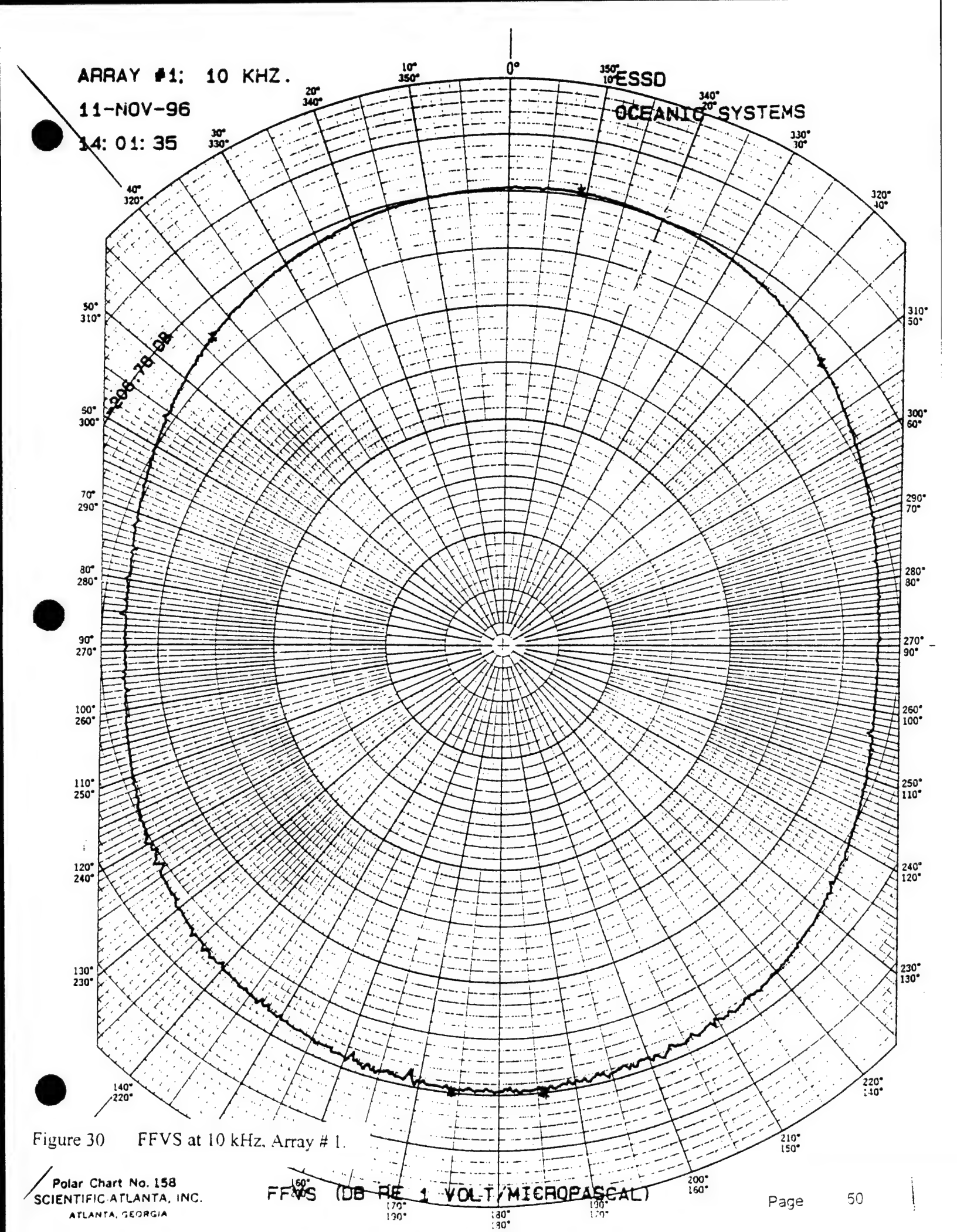

Figure 30 FFVS at 10 kHz, Array # 1.

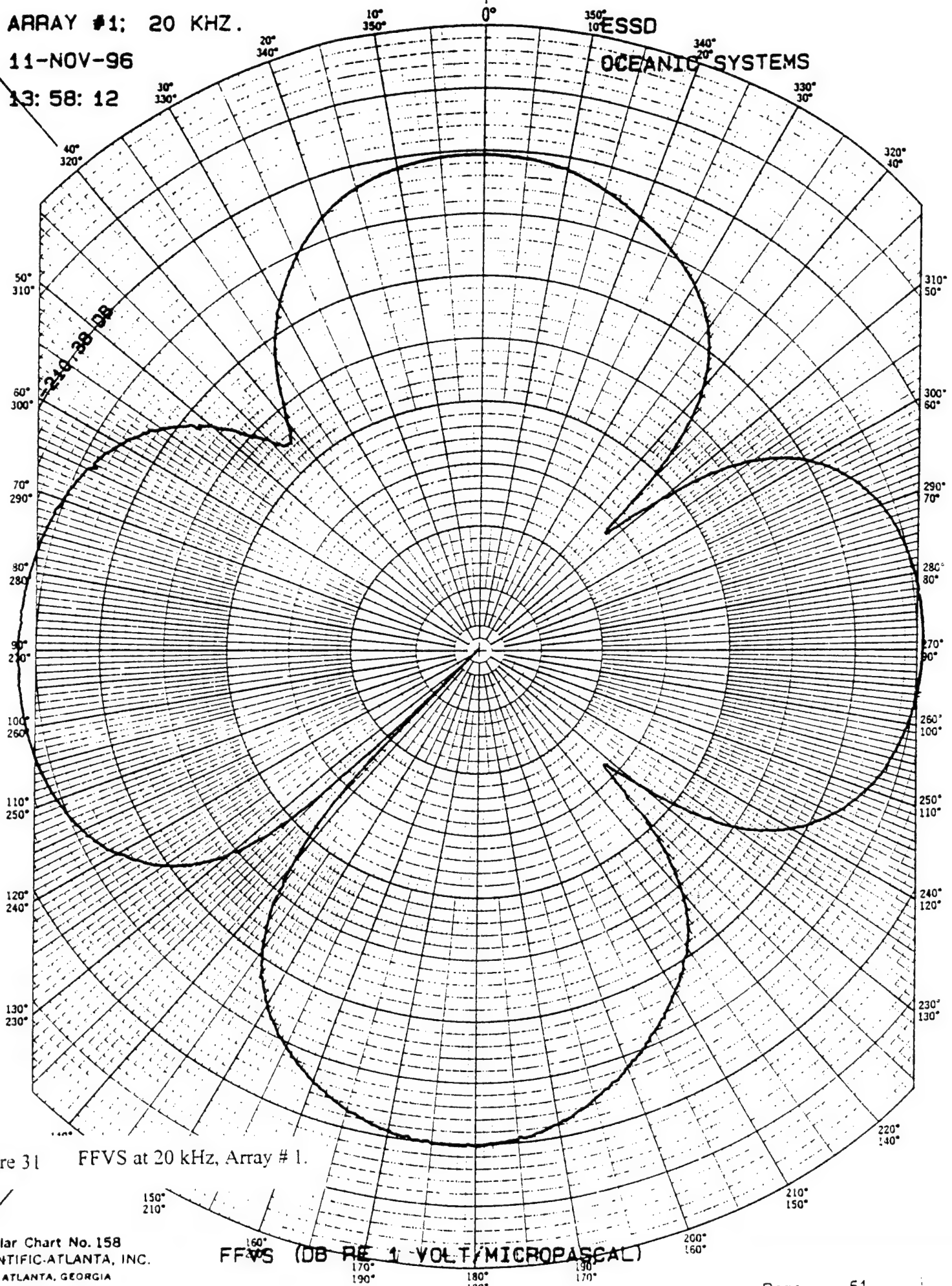

ire 31 FFVS at 20 kHz, Array # 1.

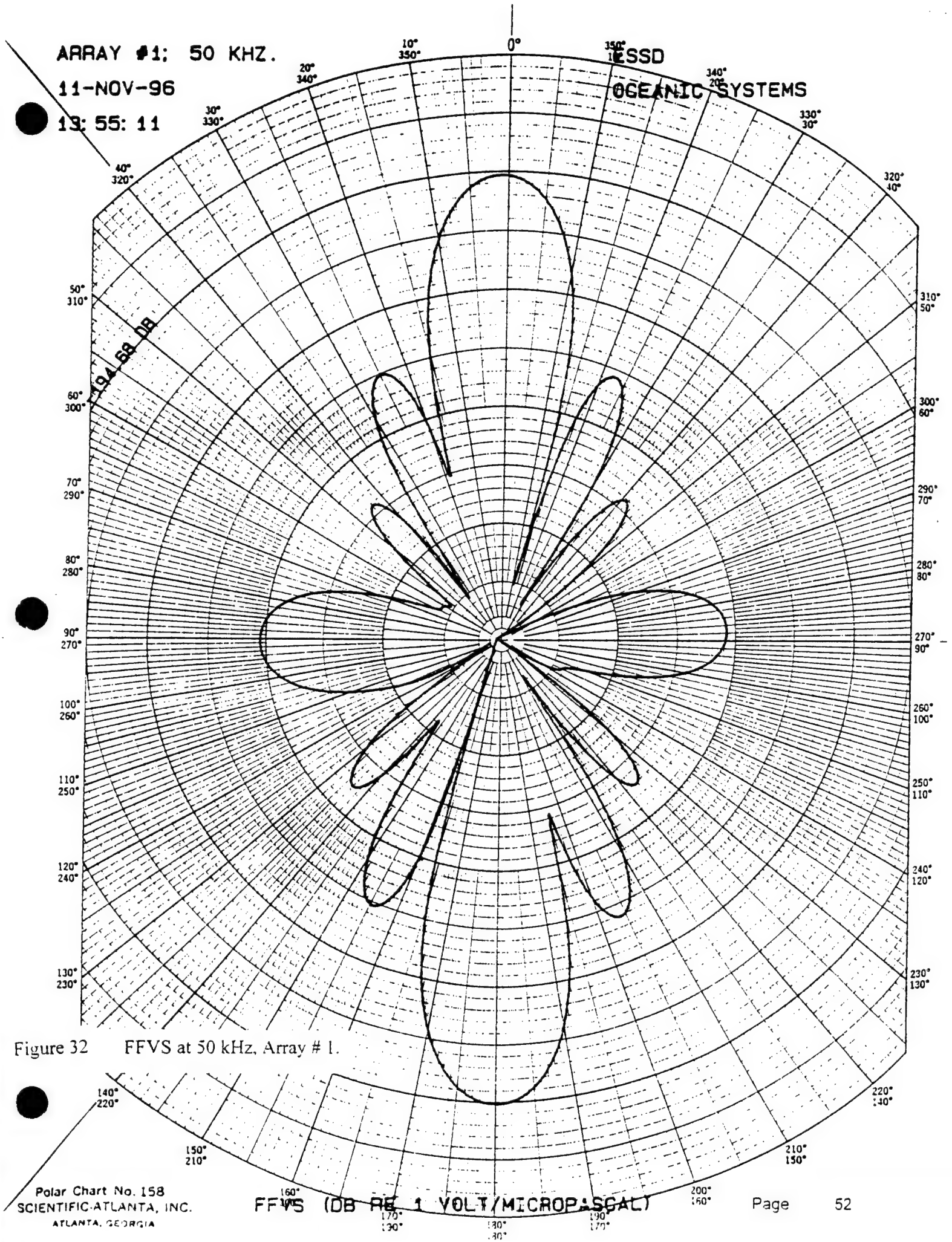

Figure 32 FFVS at 50 kHz, Array # 1.

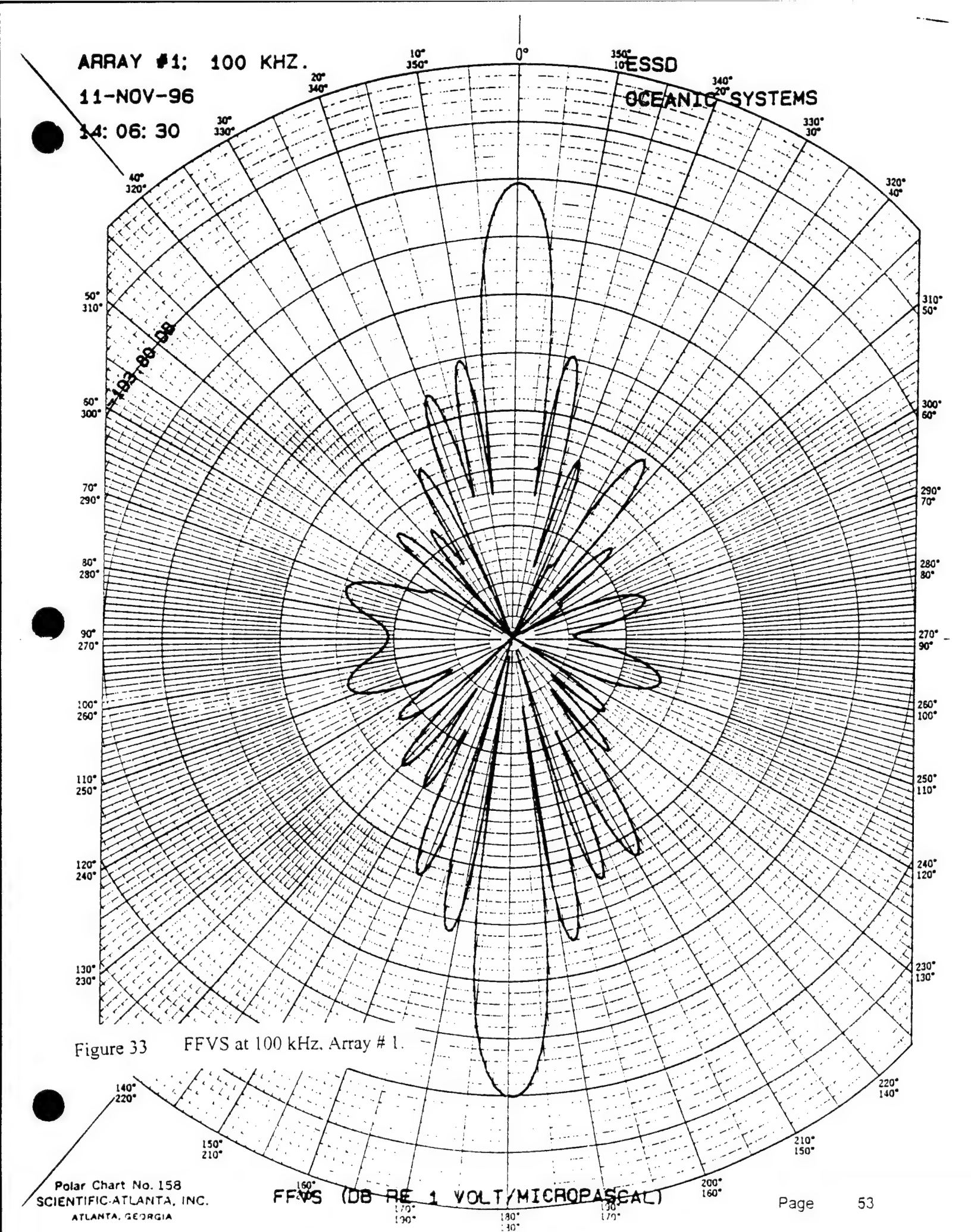

Figure 33 FFVS at 100 kHz. Array # 1.

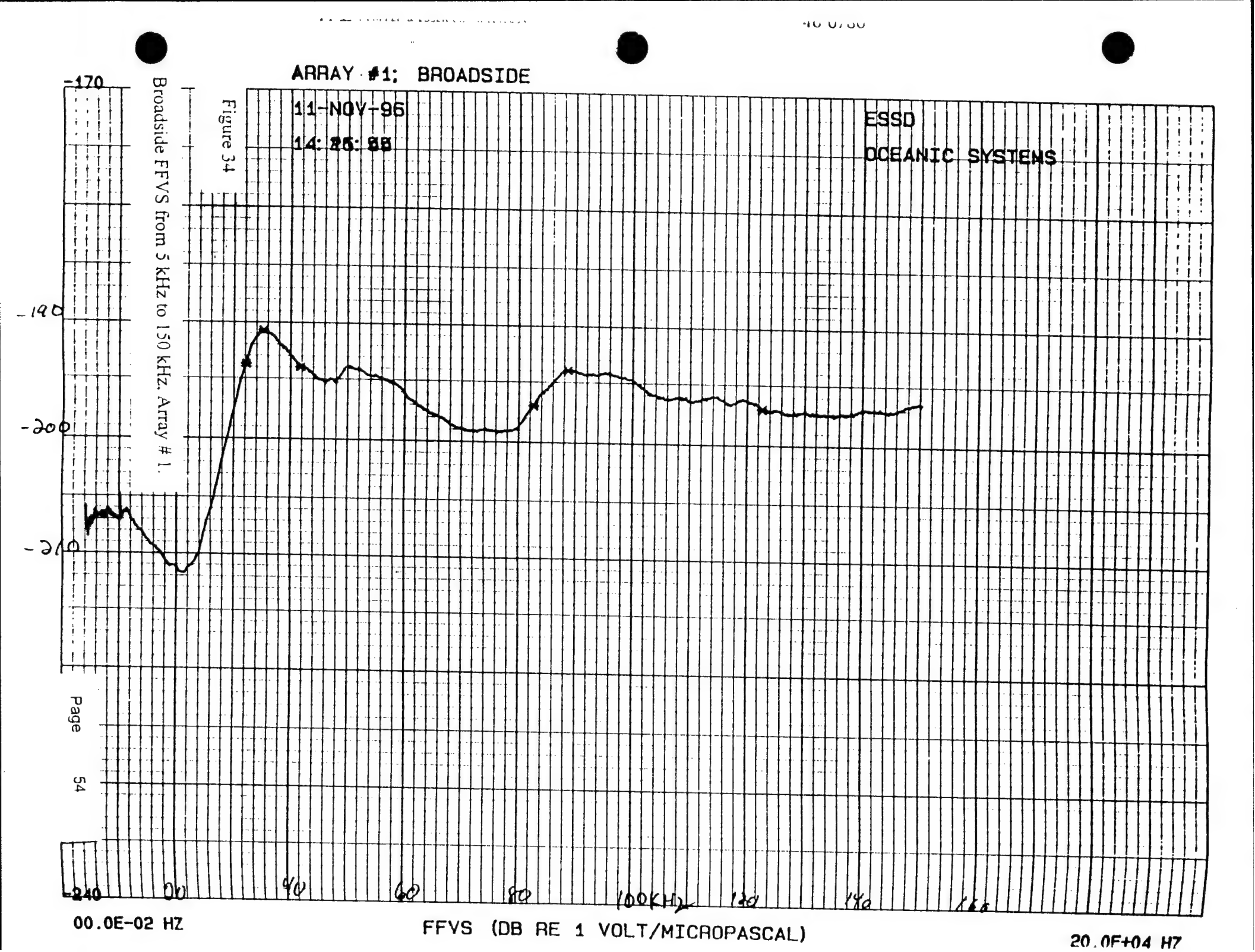

Figure 34

Broadside FFVS from 5 kHz to 150 kHz. Array # 1.

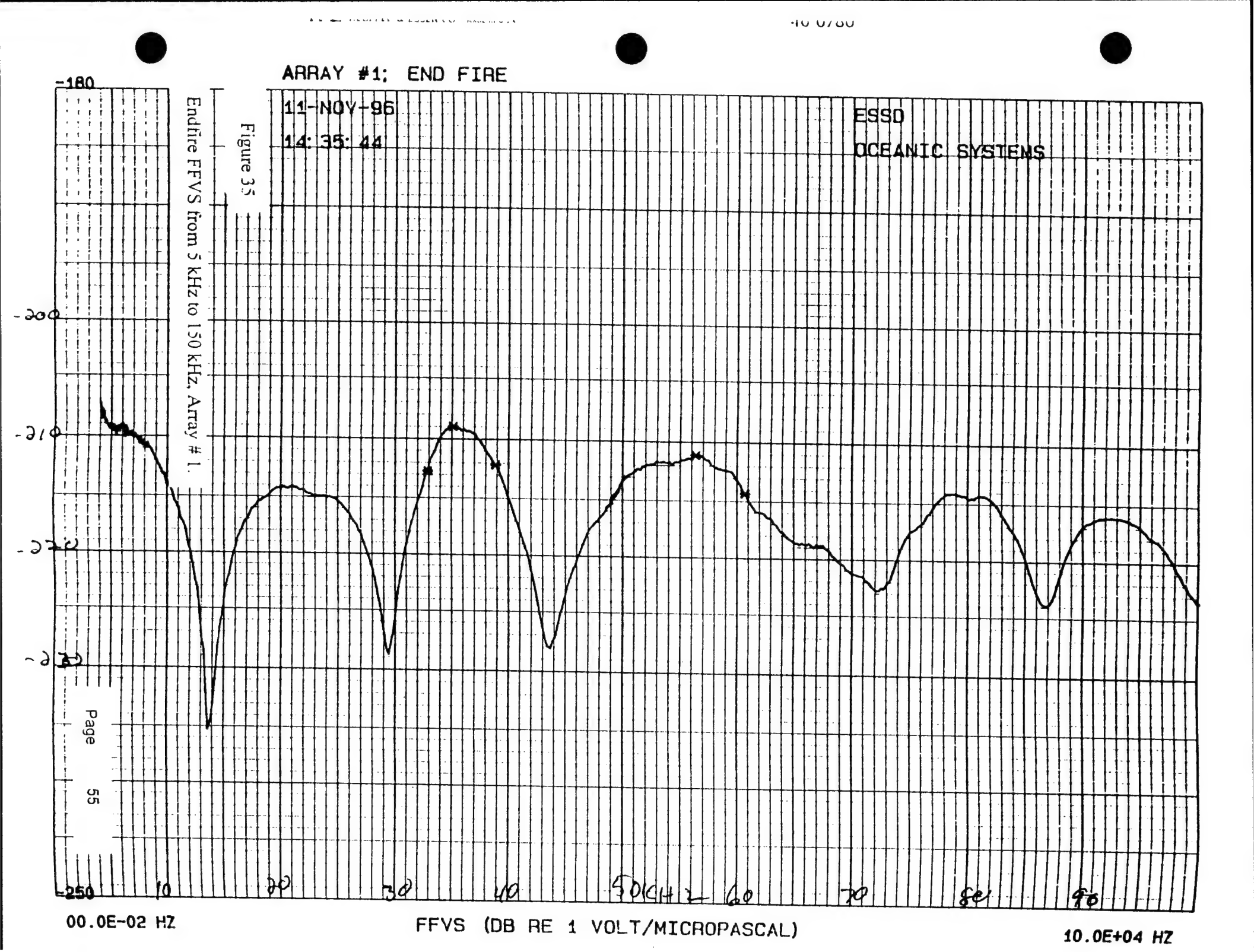

Figure 35

Endfire FFVS from 5 kHz to 150 kHz. Array # 1.

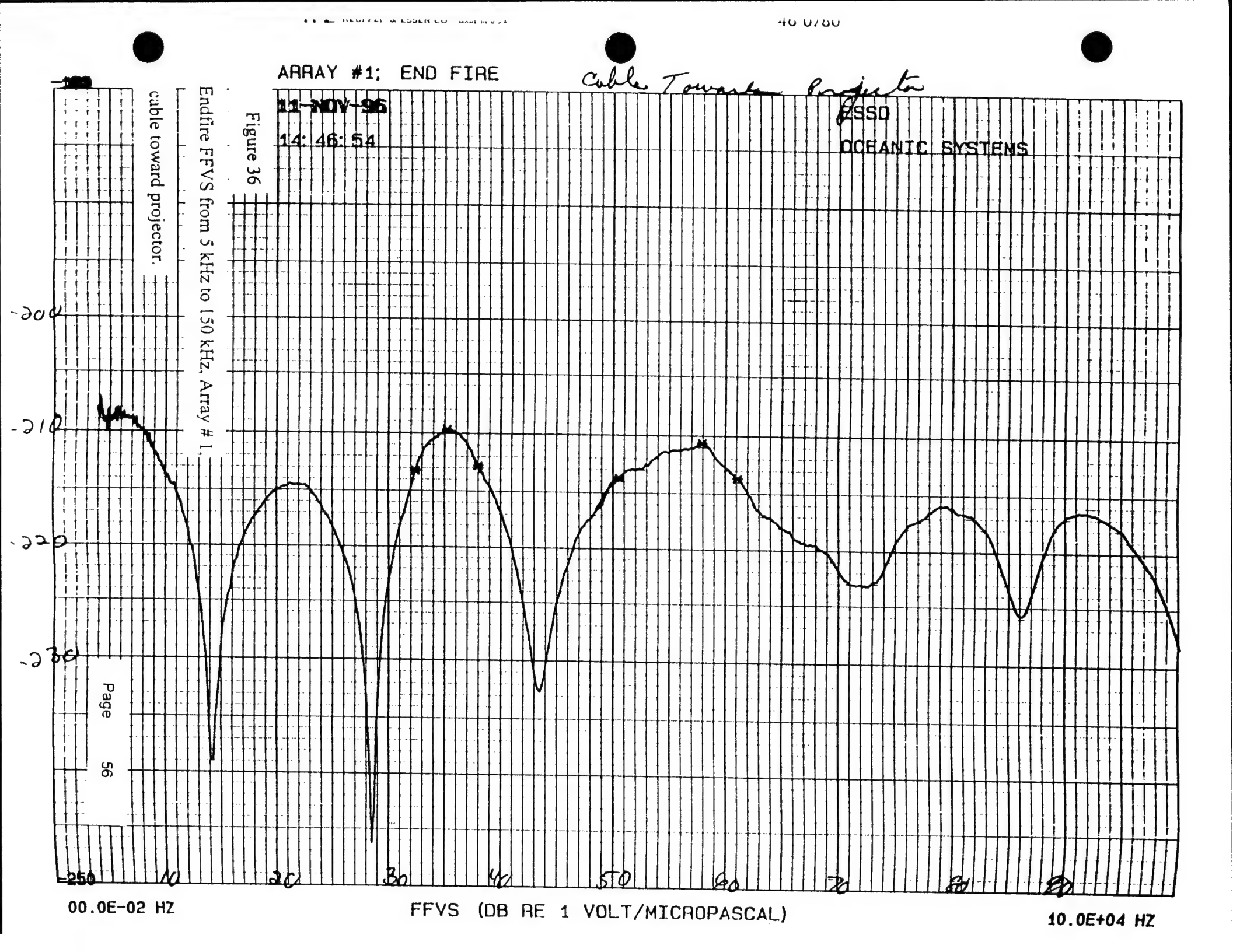

Figure 36

Endfire FFVS from 5 kHz to 150 kHz, Array # 1, cable toward projector.

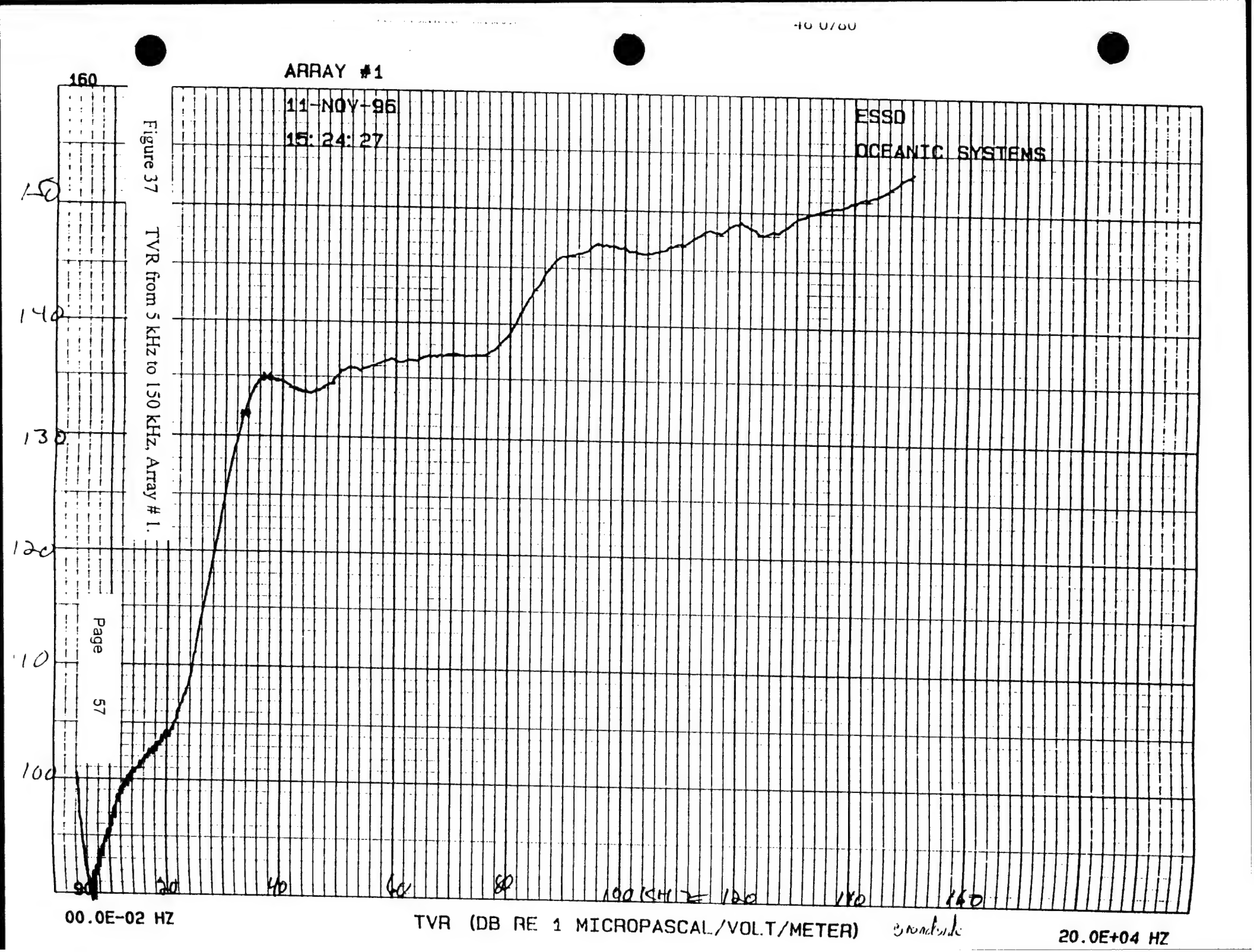

Figure 37 TVR from 5 kHz to 150 kHz, Array # 1.

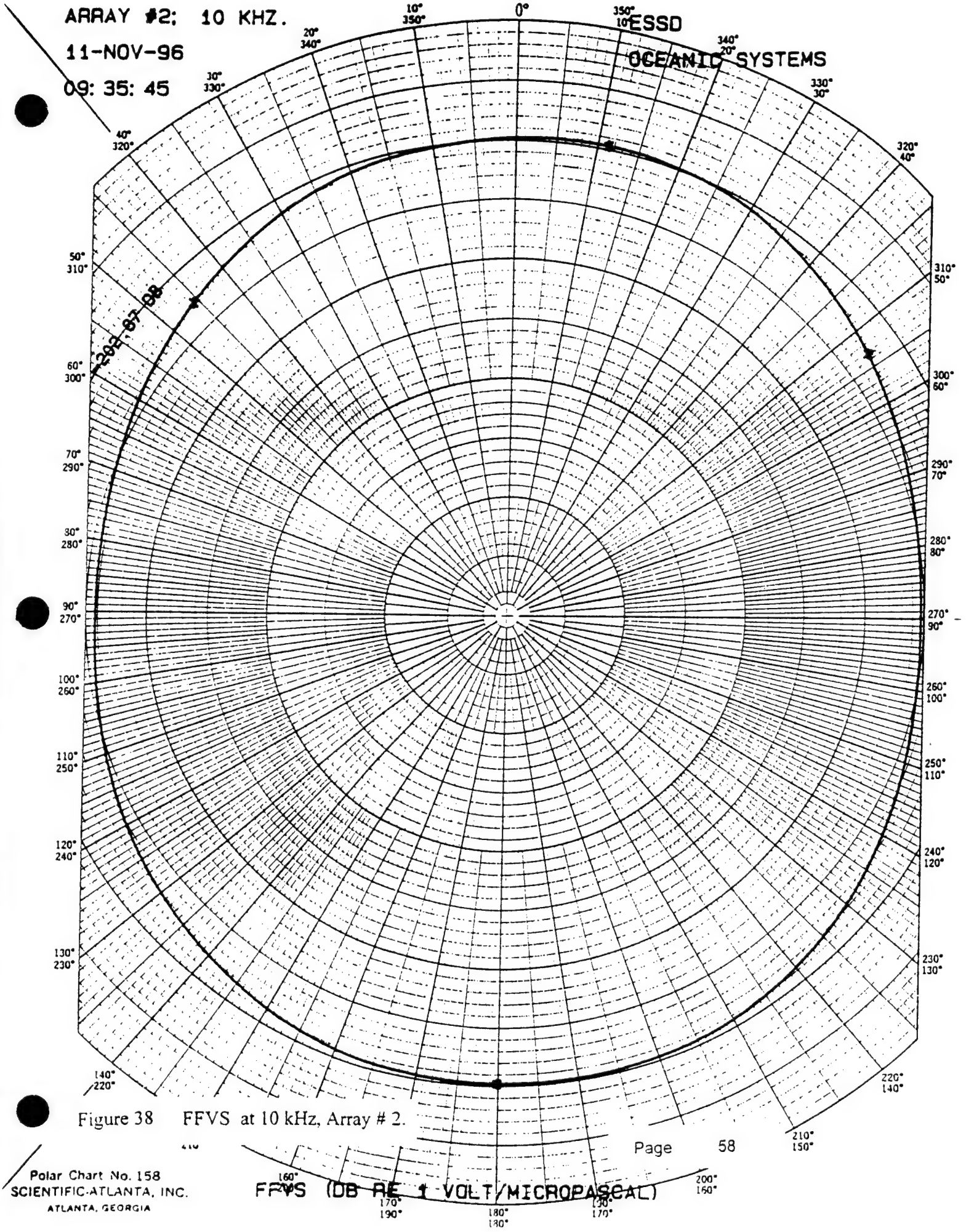

Figure 38 FFVS at 10 kHz, Array # 2.

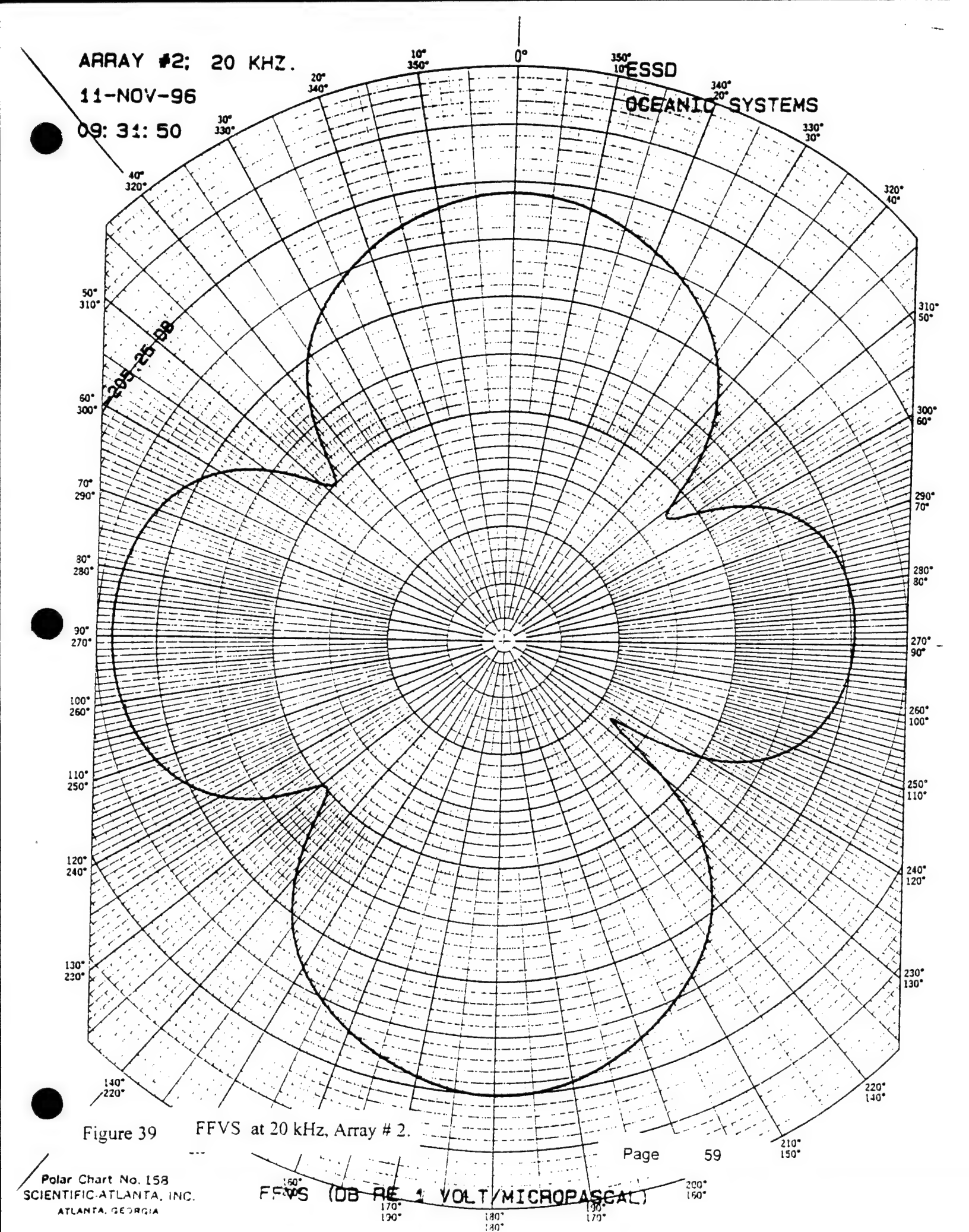

Figure 39 FFVS at 20 kHz, Array # 2.

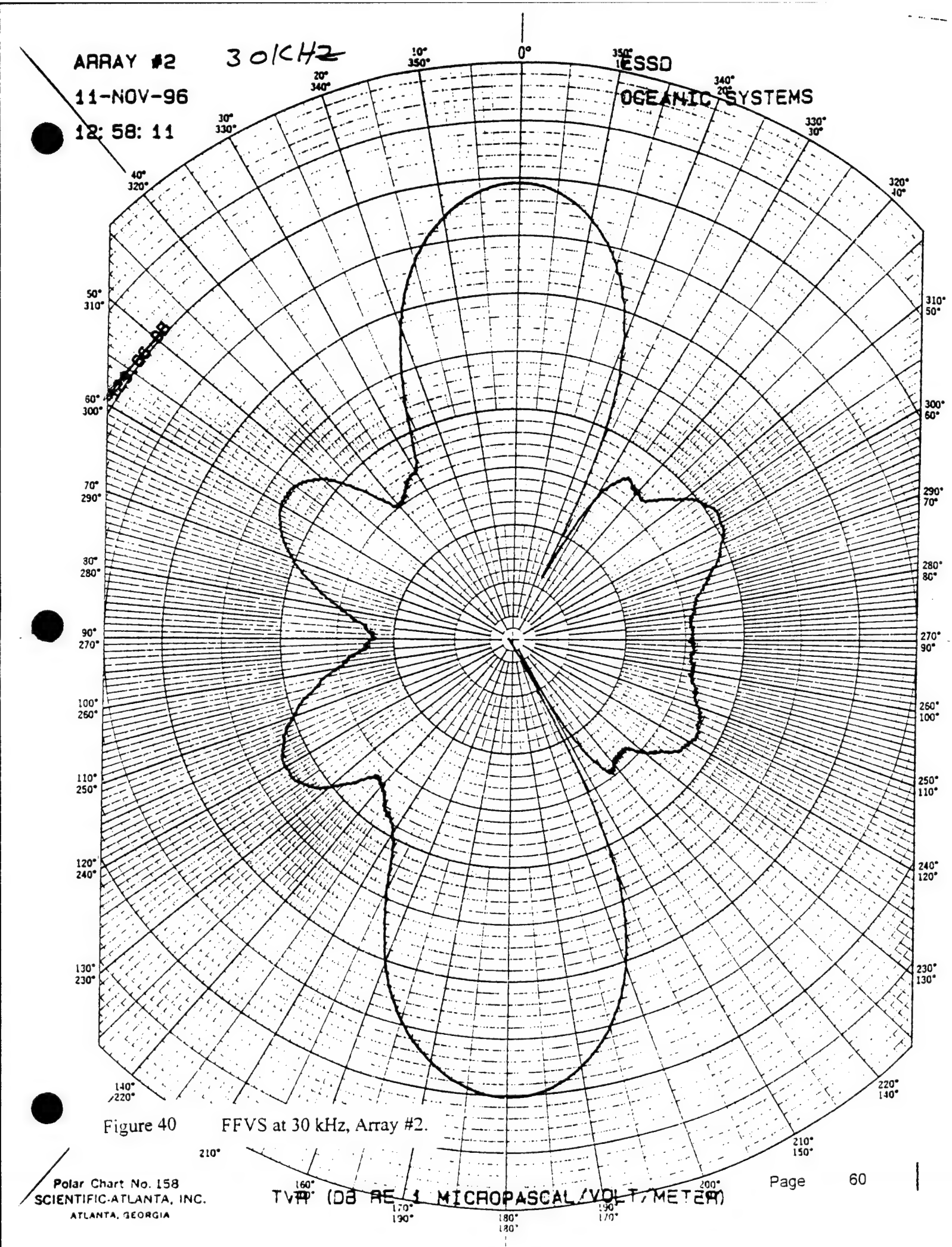

Figure 40 FFVS at 30 kHz, Array #2.

Polar Chart No. 158
SCIENTIFIC-ATLANTA, INC.
ATLANTA, GEORGIA

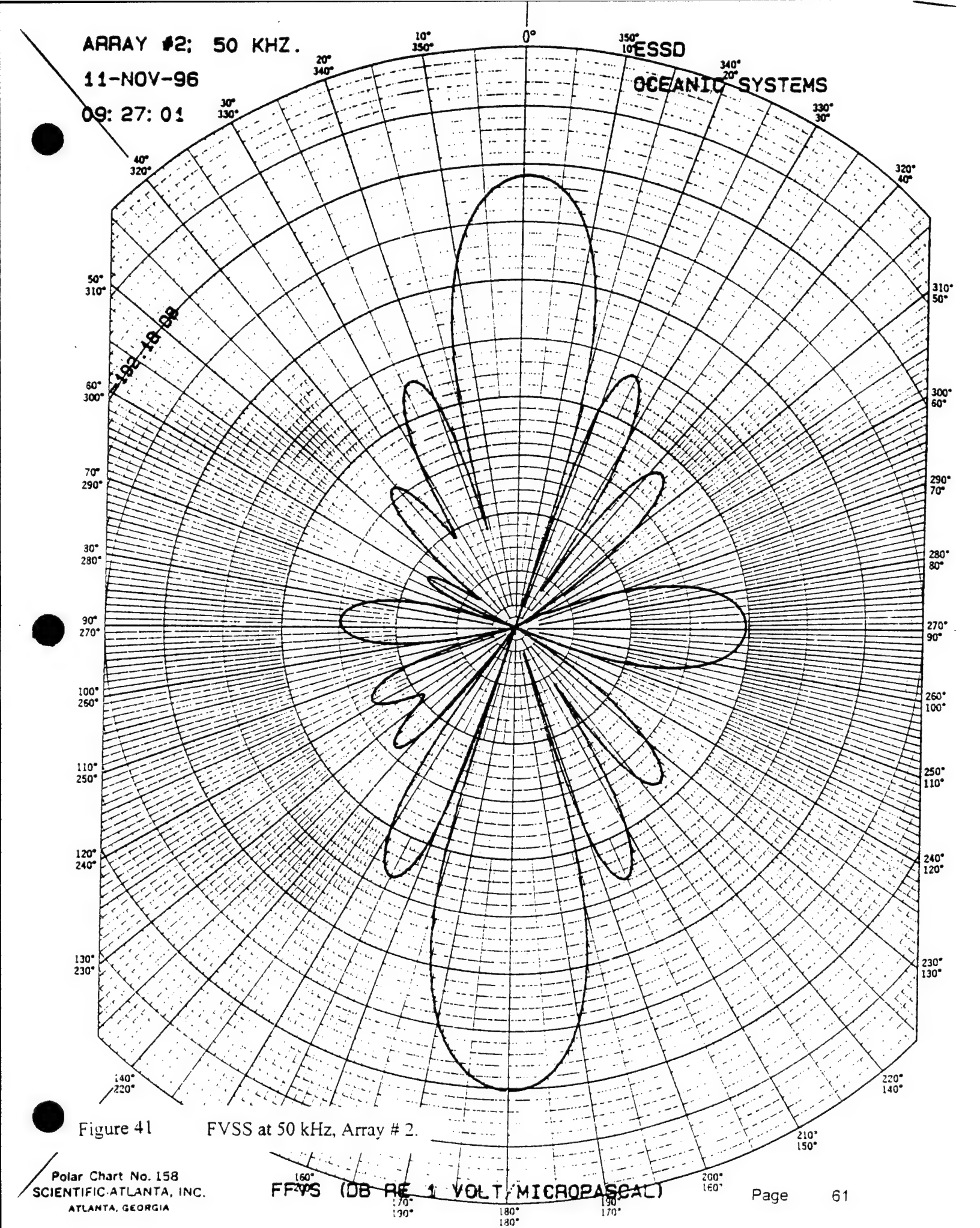

Figure 41 FVSS at 50 kHz, Array # 2.

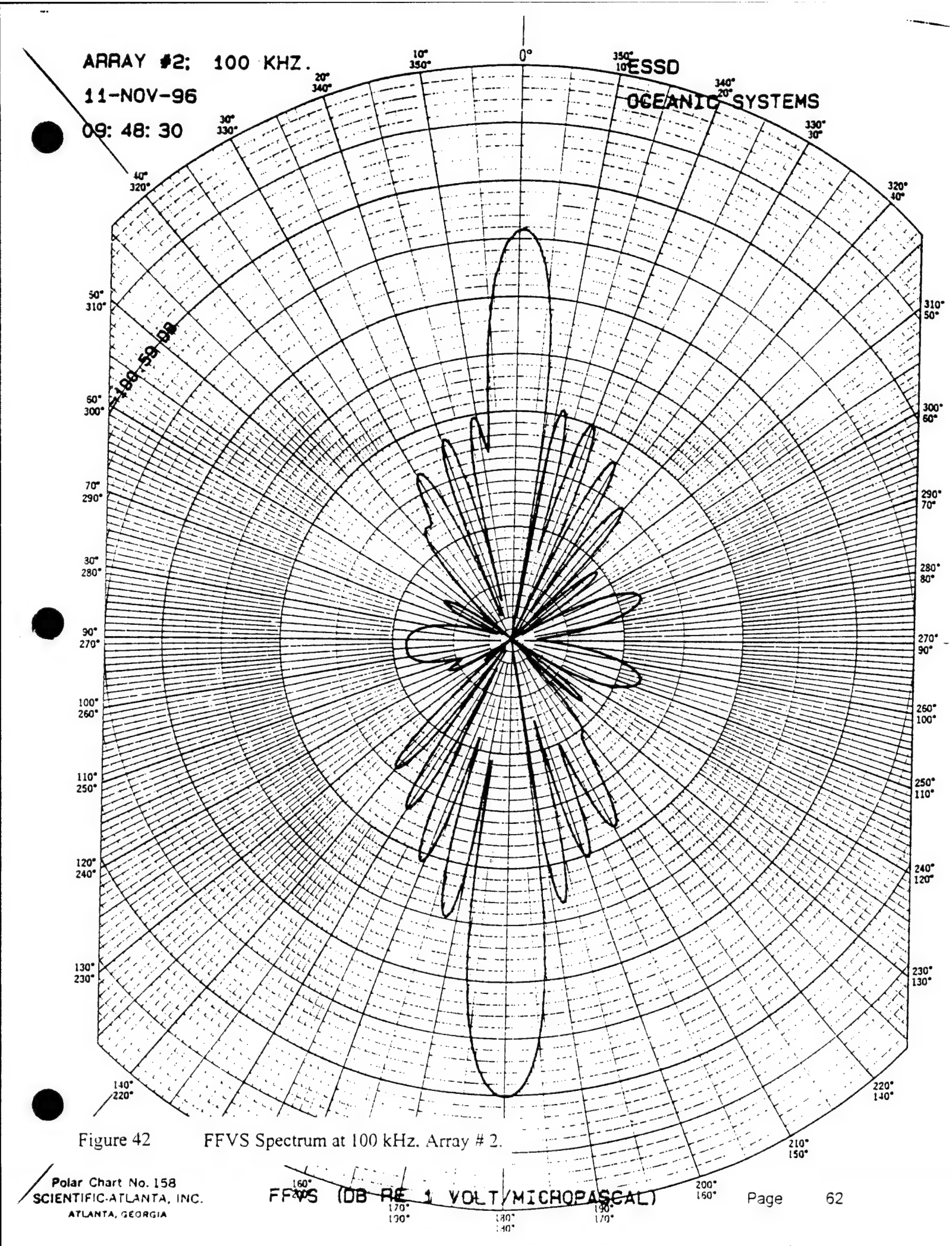

Figure 42 FFVS Spectrum at 100 kHz. Array # 2.

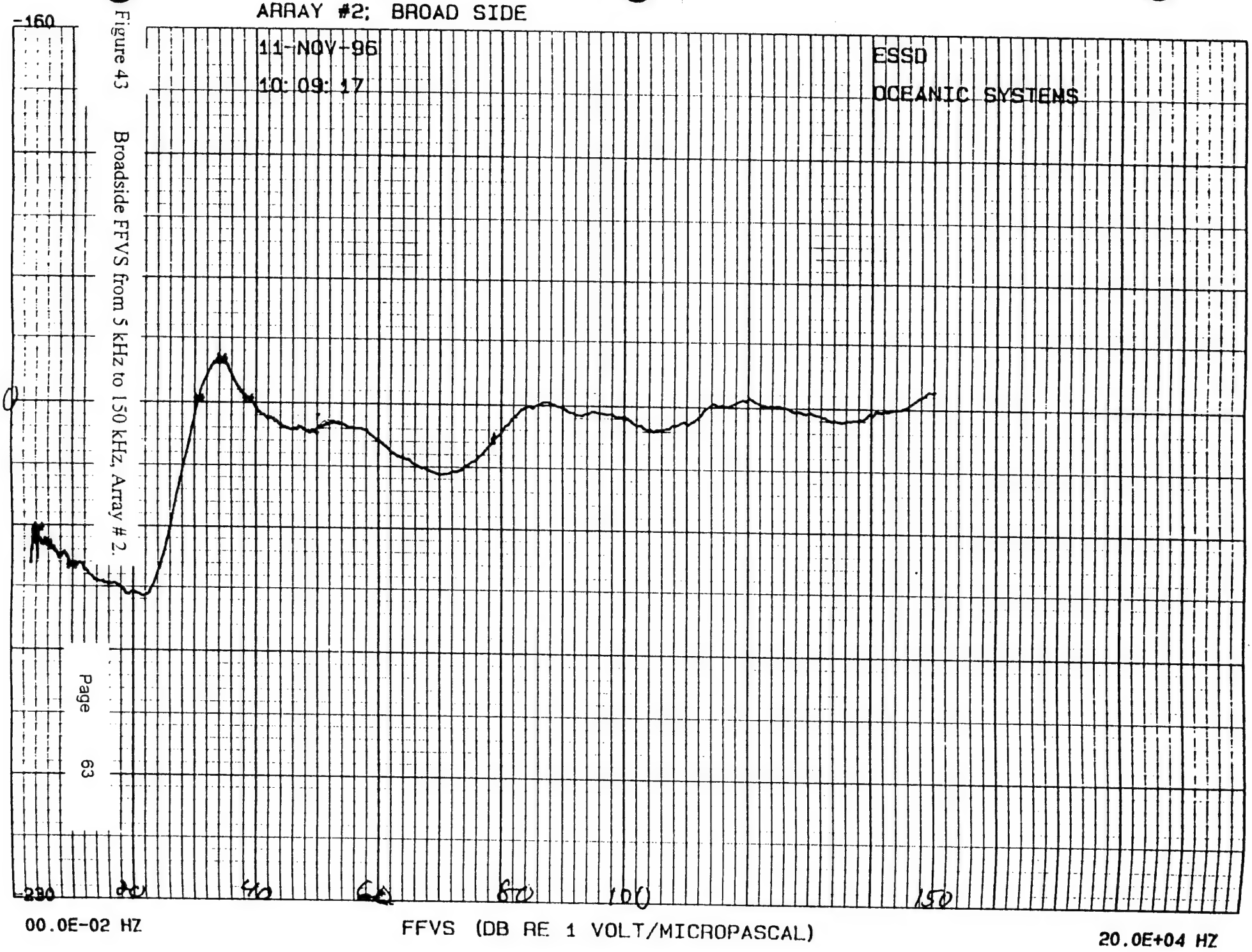

Figure 43 Broadside FFVS from 5 kHz to 150 kHz, Array # 2.

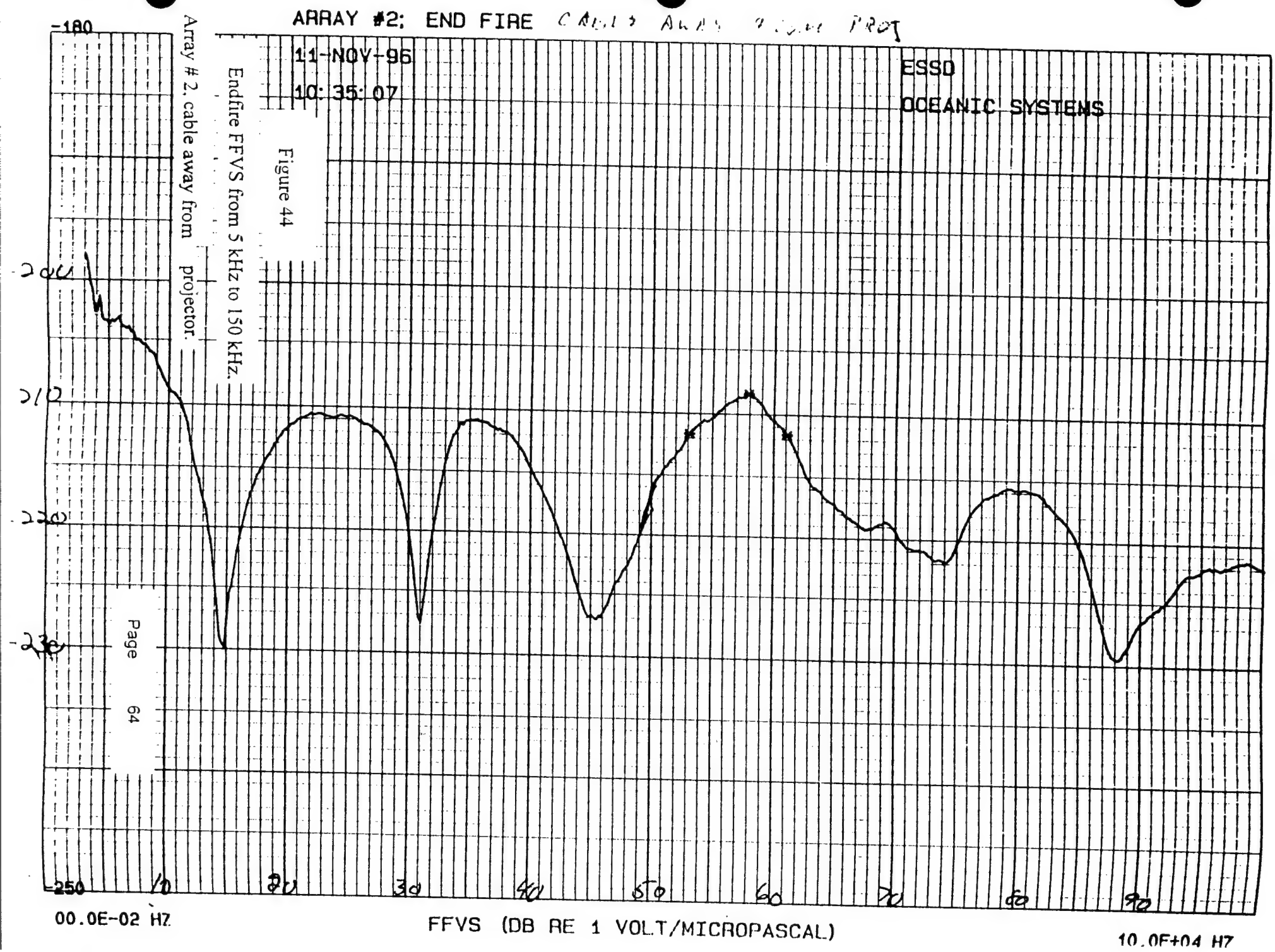

Figure 44

Endfire FFVS from 5 kHz to 150 kHz.

Array # 2, cable away from projector.

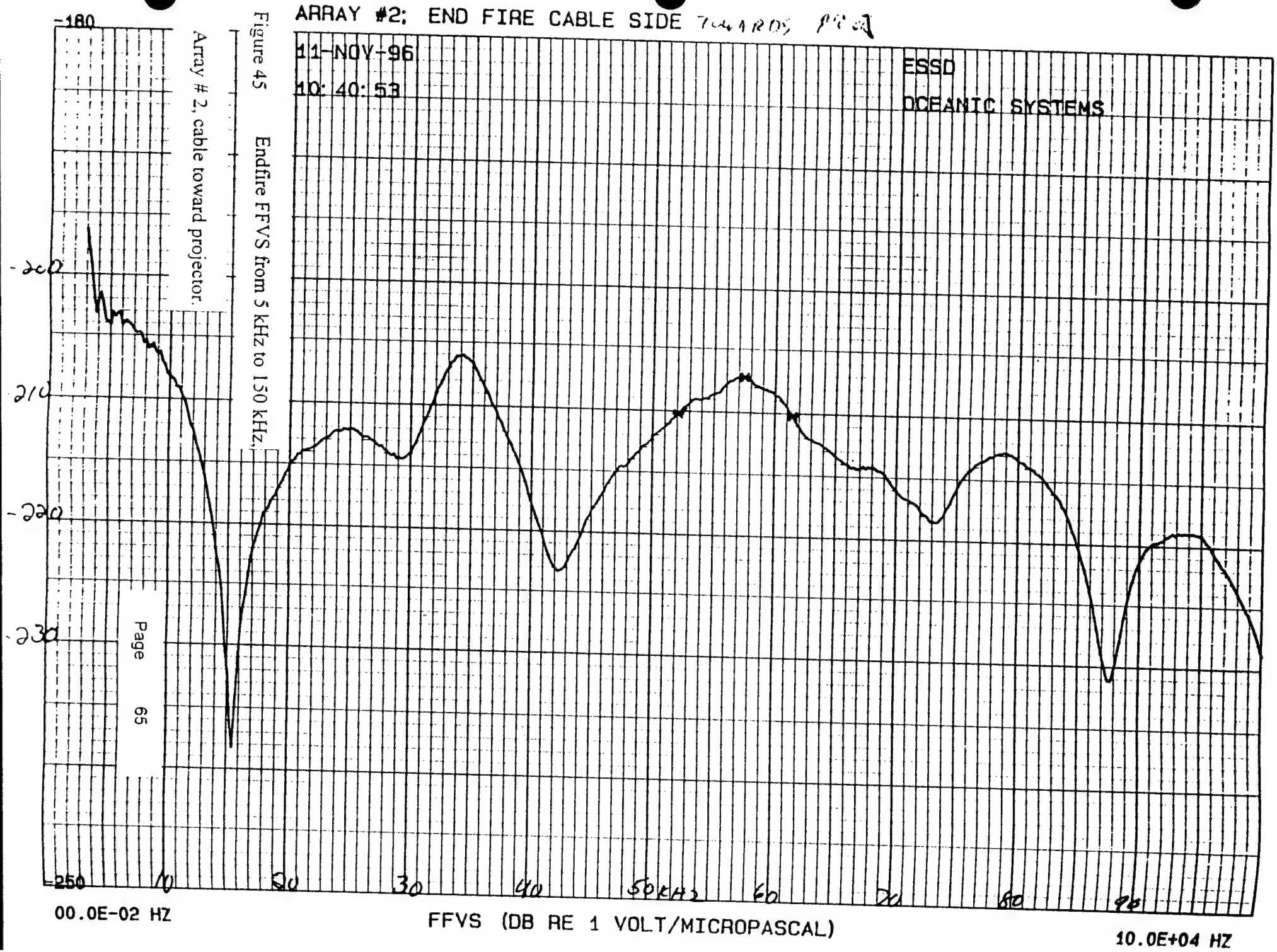

Figure 45 Endfire FFVS from 5 kHz to 150 kHz, Array # 2, cable toward projector.

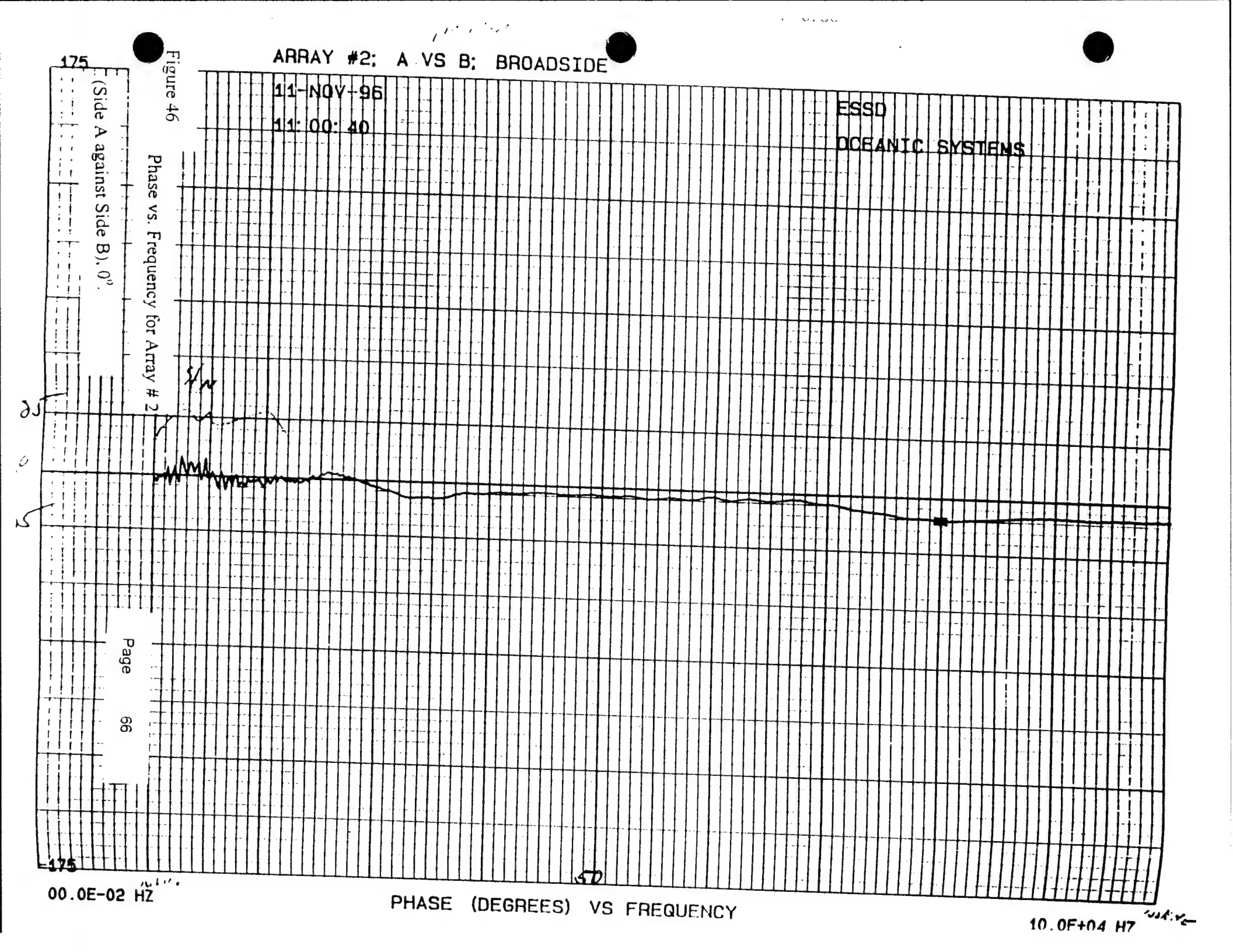
ARRAY #2: A VS B: BROADSIDE
11-NOV-96
11:00:40
ESSD
OCEANIC SYSTEMS
175
(Side A against Side B), 0°.
Phase vs. Frequency for Array # 2
Page 66
-175
00.0E-02 HZ
PHASE (DEGREES) VS FREQUENCY
10.0E+04 HZ

Figure 46

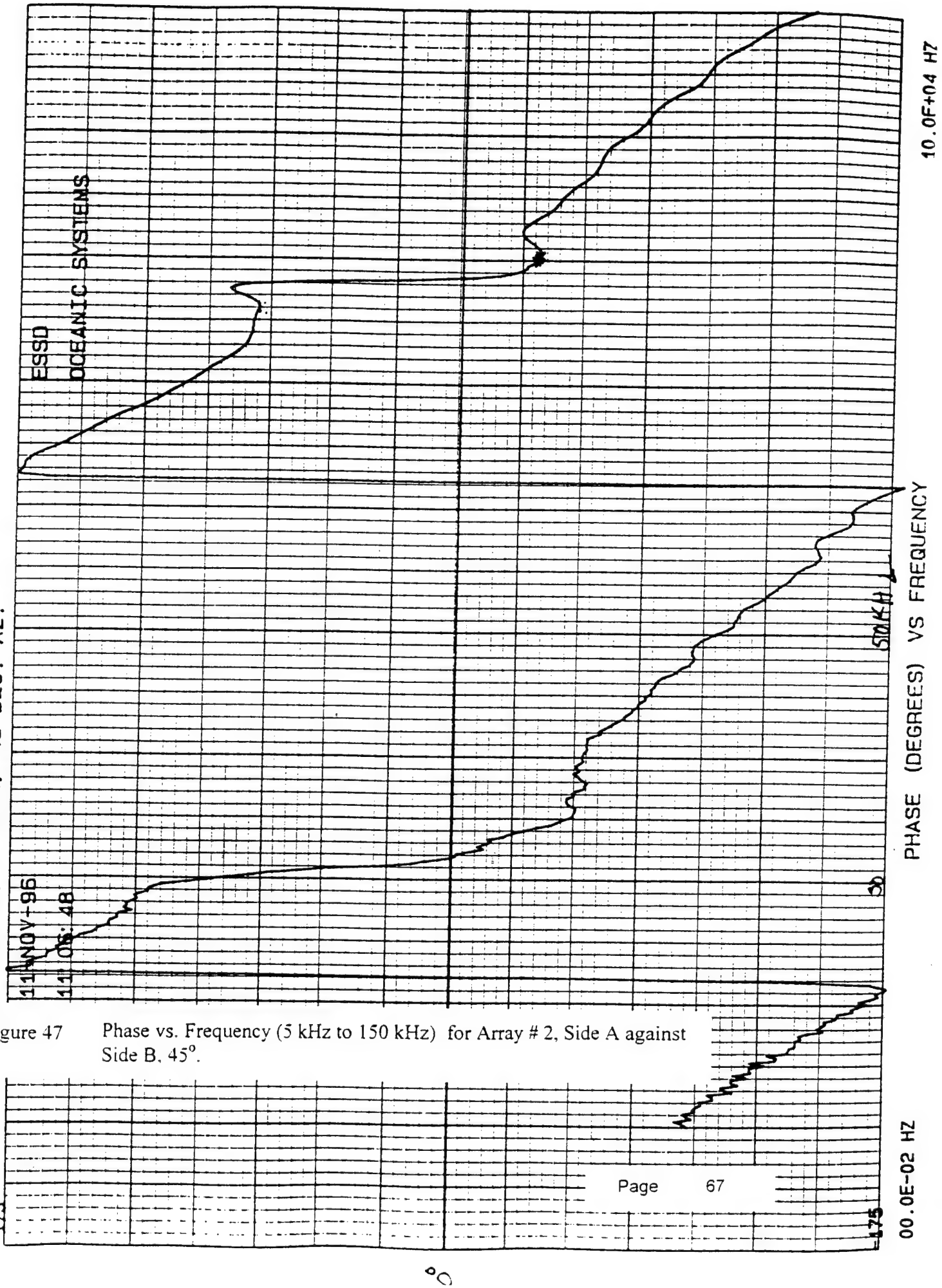

Figure 47 Phase vs. Frequency (5 kHz to 150 kHz) for Array # 2, Side A against Side B, 45°.

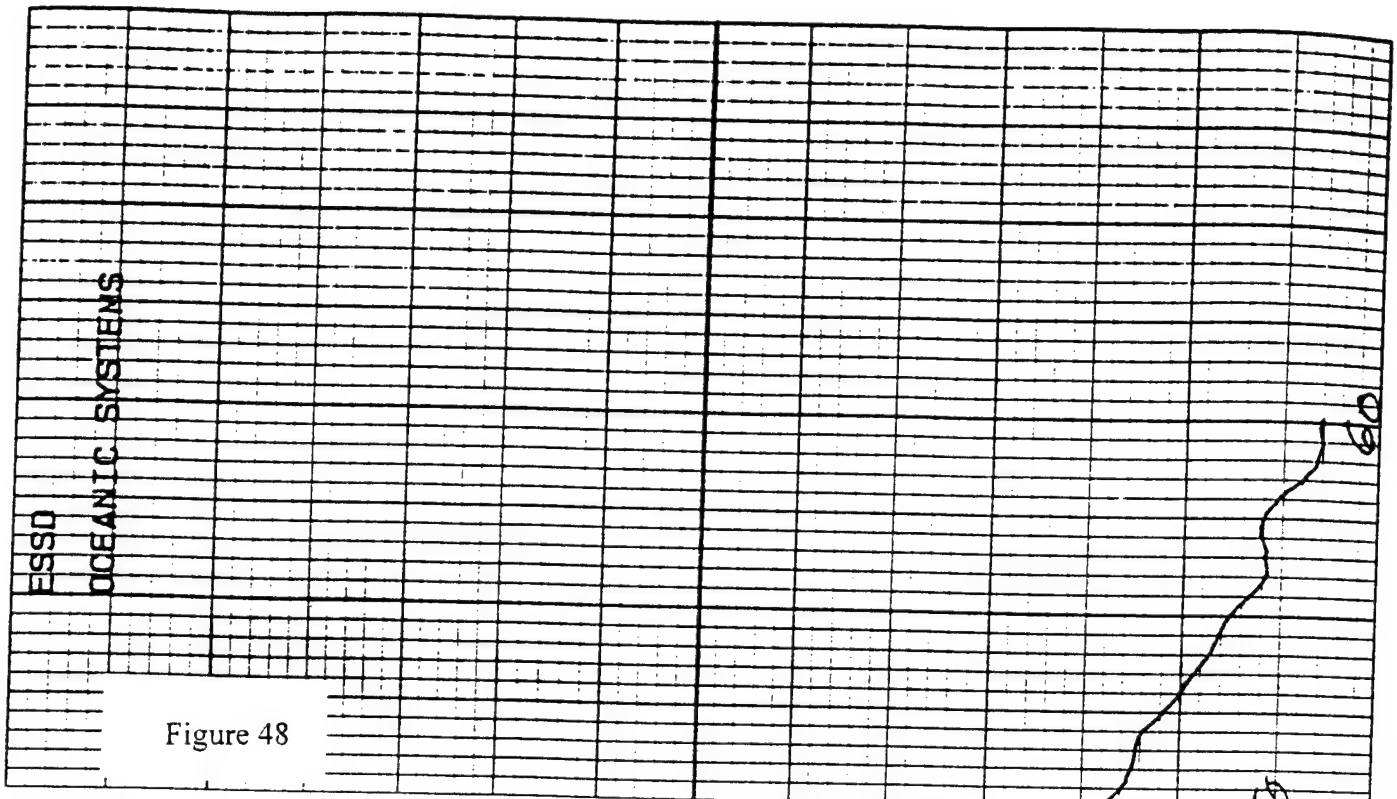

Figure 48

Phase vs. Frequency (20 kHz to 60 kHz) for Array # 2, Side A against Side B), 45°.

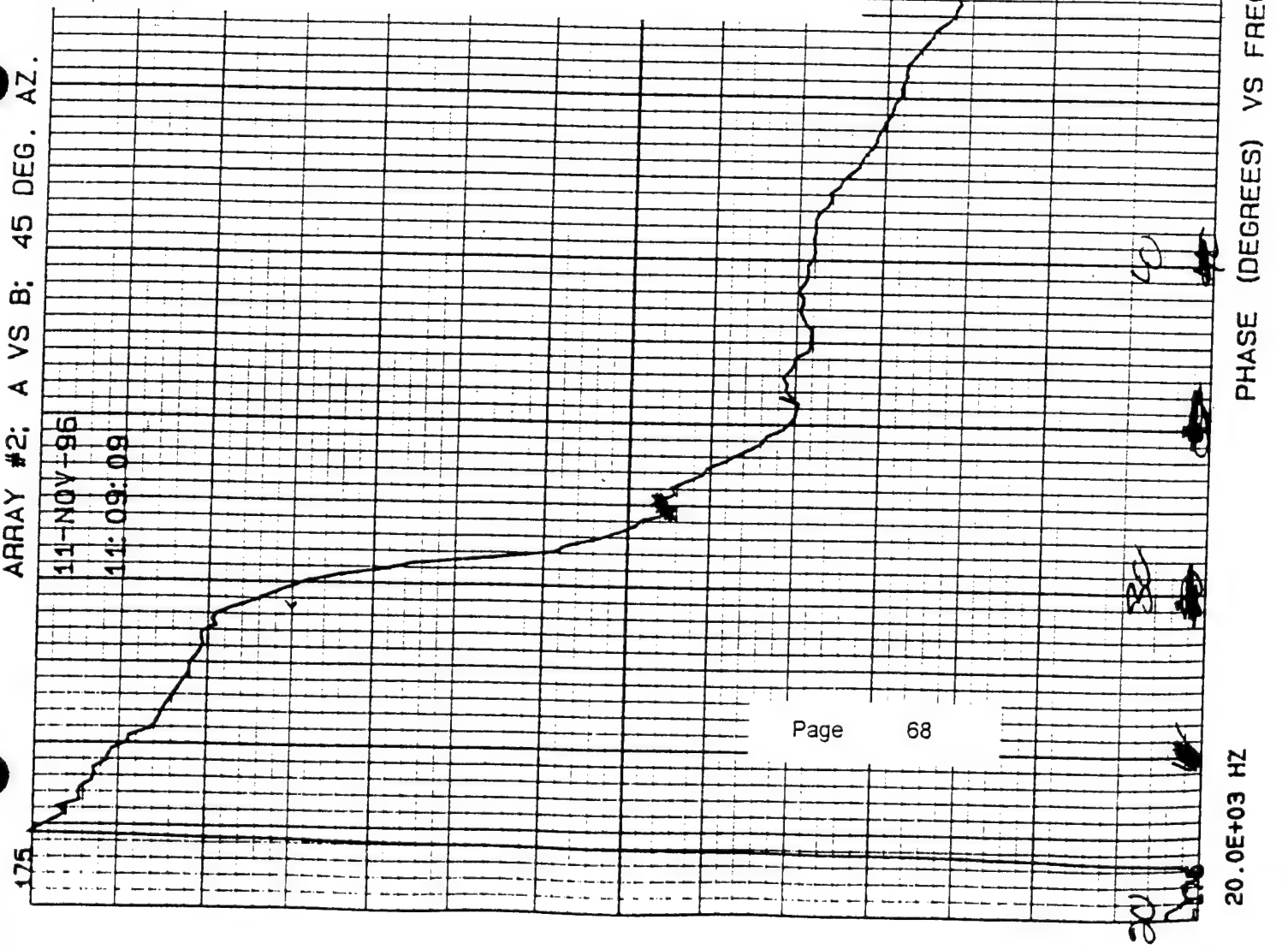

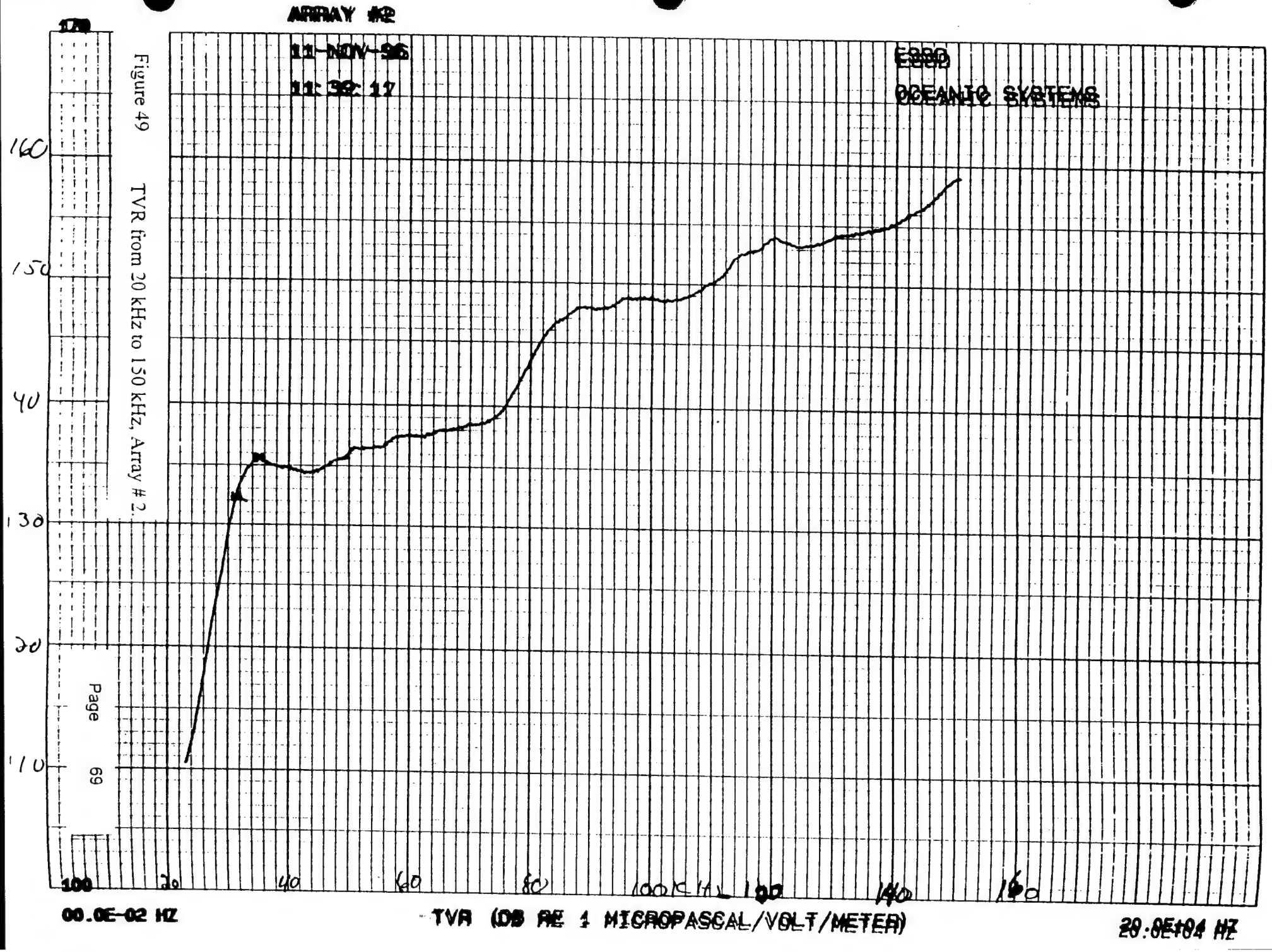

Figure 49 TVR from 20 kHz to 150 kHz, Array # 2.

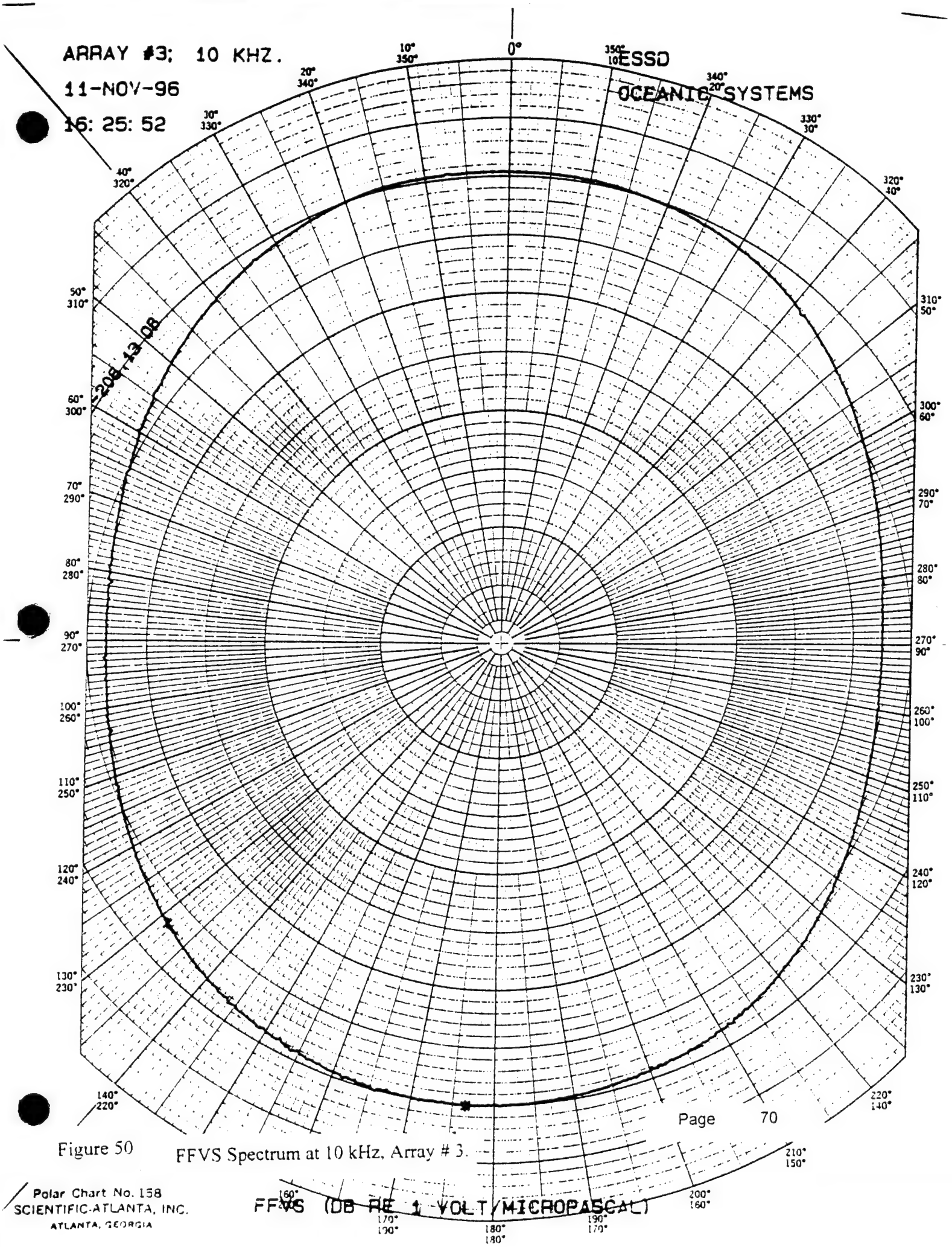

Figure 50 FFVS Spectrum at 10 kHz, Array # 3.

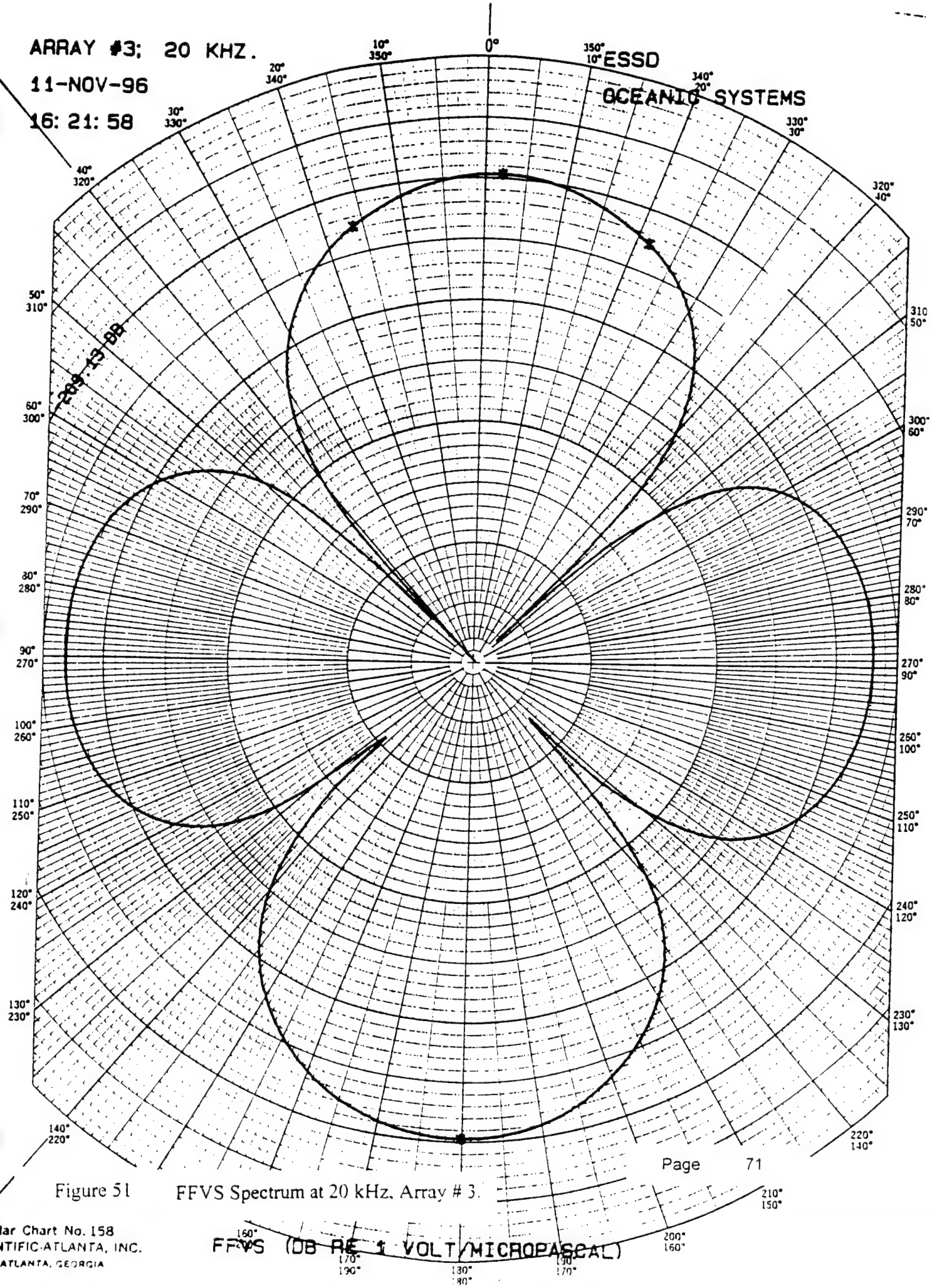

Figure 51 FFVS Spectrum at 20 kHz, Array # 3.

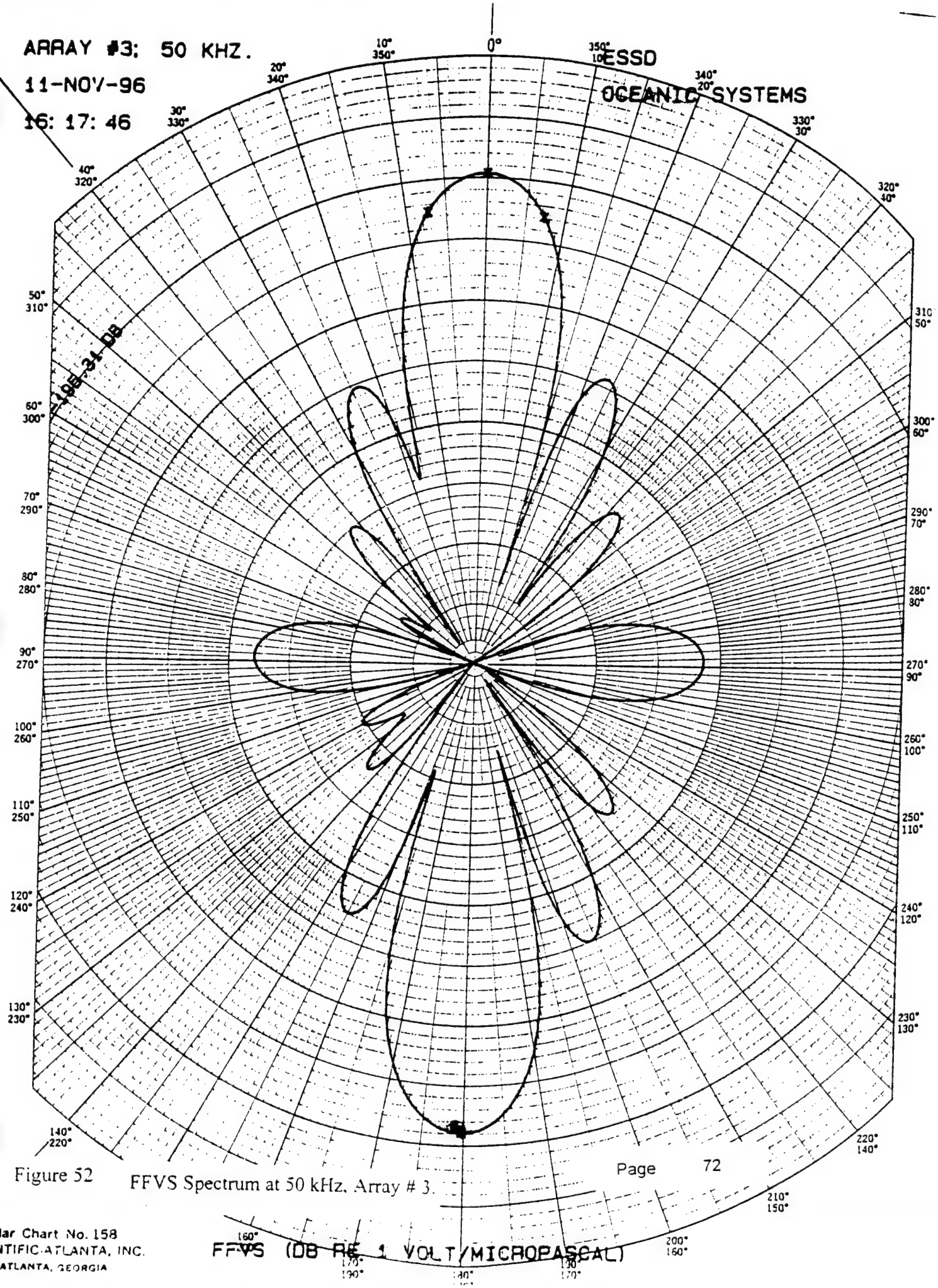

Figure 52 FFVS Spectrum at 50 kHz, Array # 3.

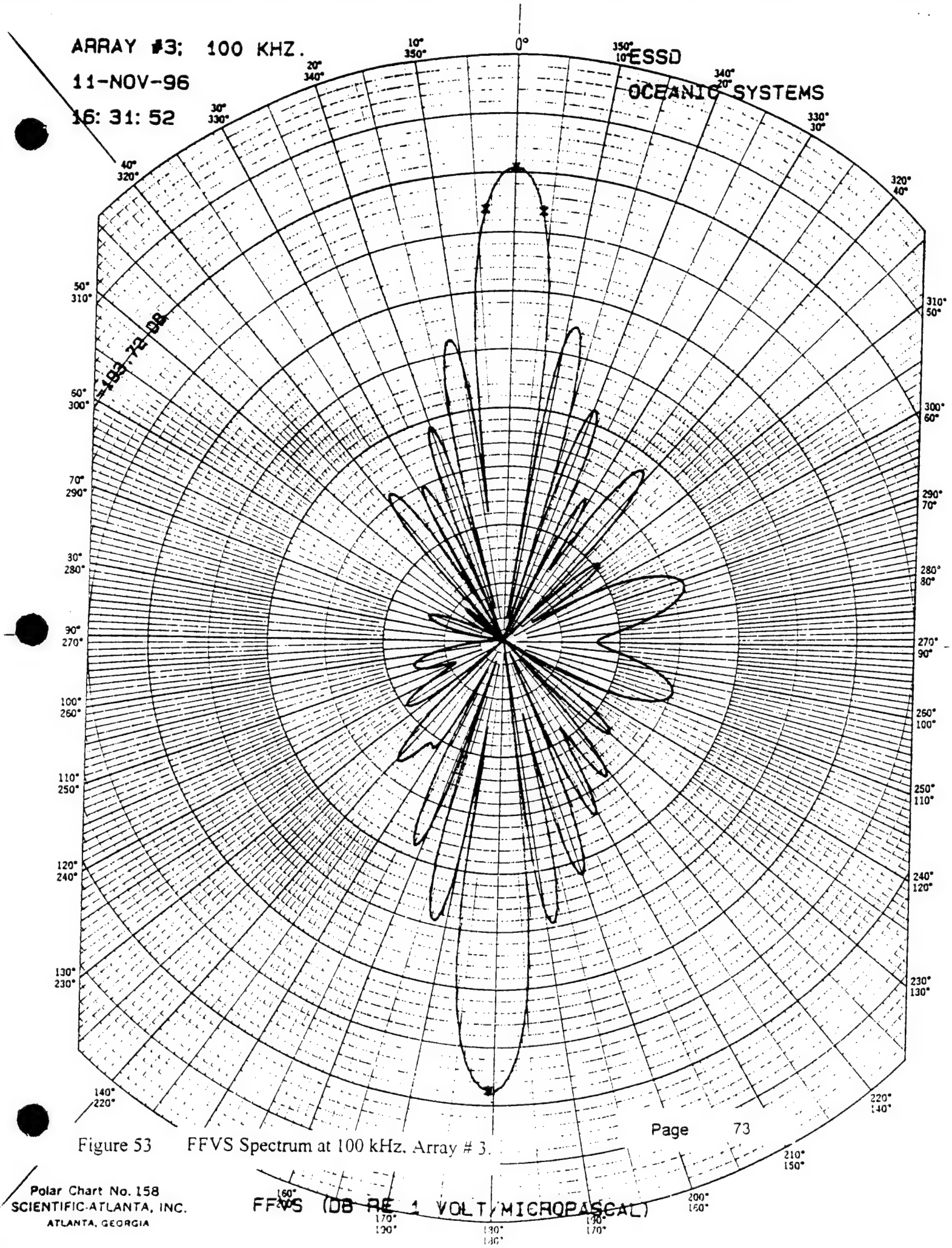

Figure 53 FFVS Spectrum at 100 kHz, Array # 3.

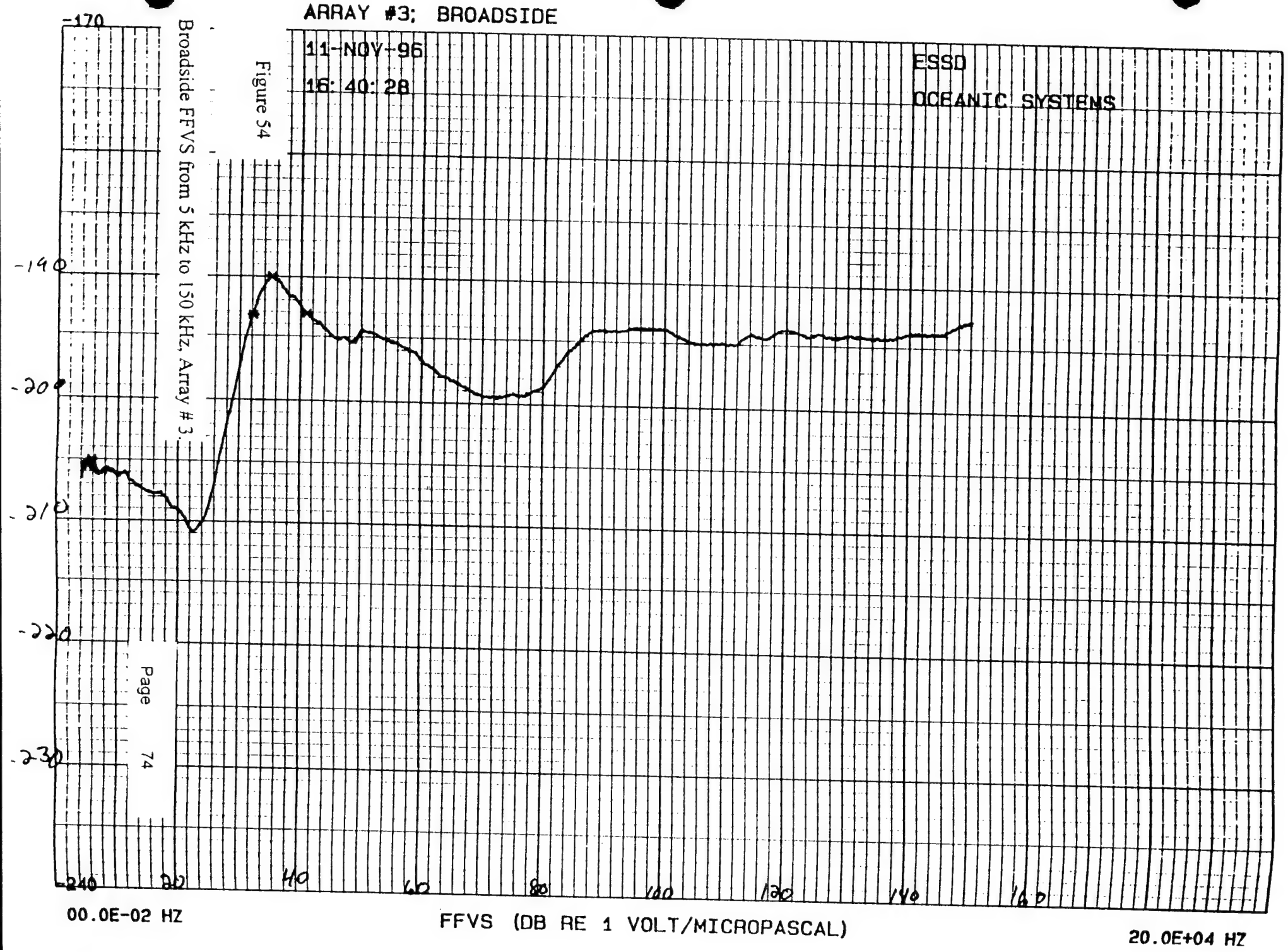

Figure 54

Broadside FFVS from 5 kHz to 150 kHz, Array # 3

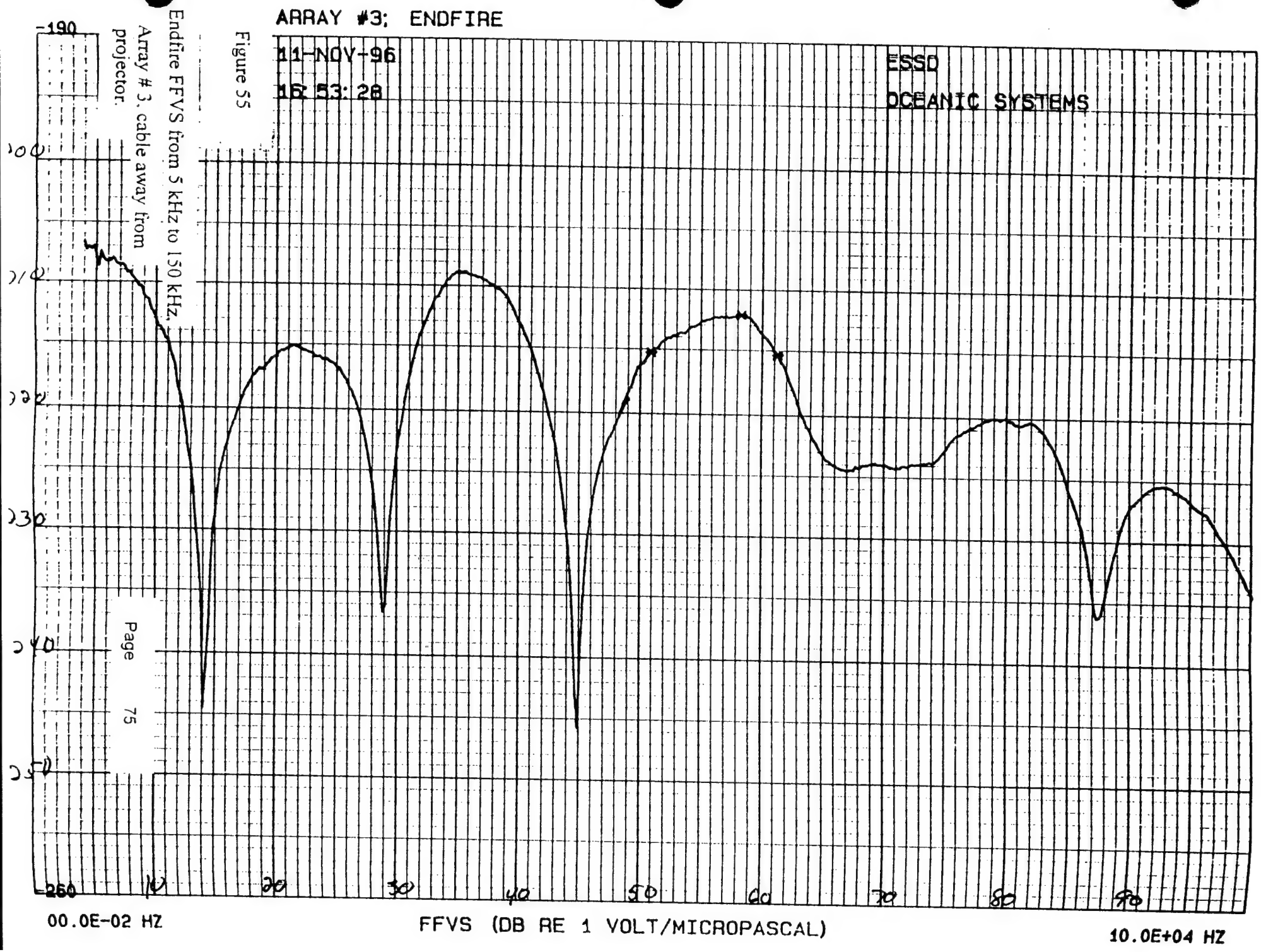

Figure 55 Endfire FFVS from 5 kHz to 150 kHz.

Array # 3, cable away from projector.

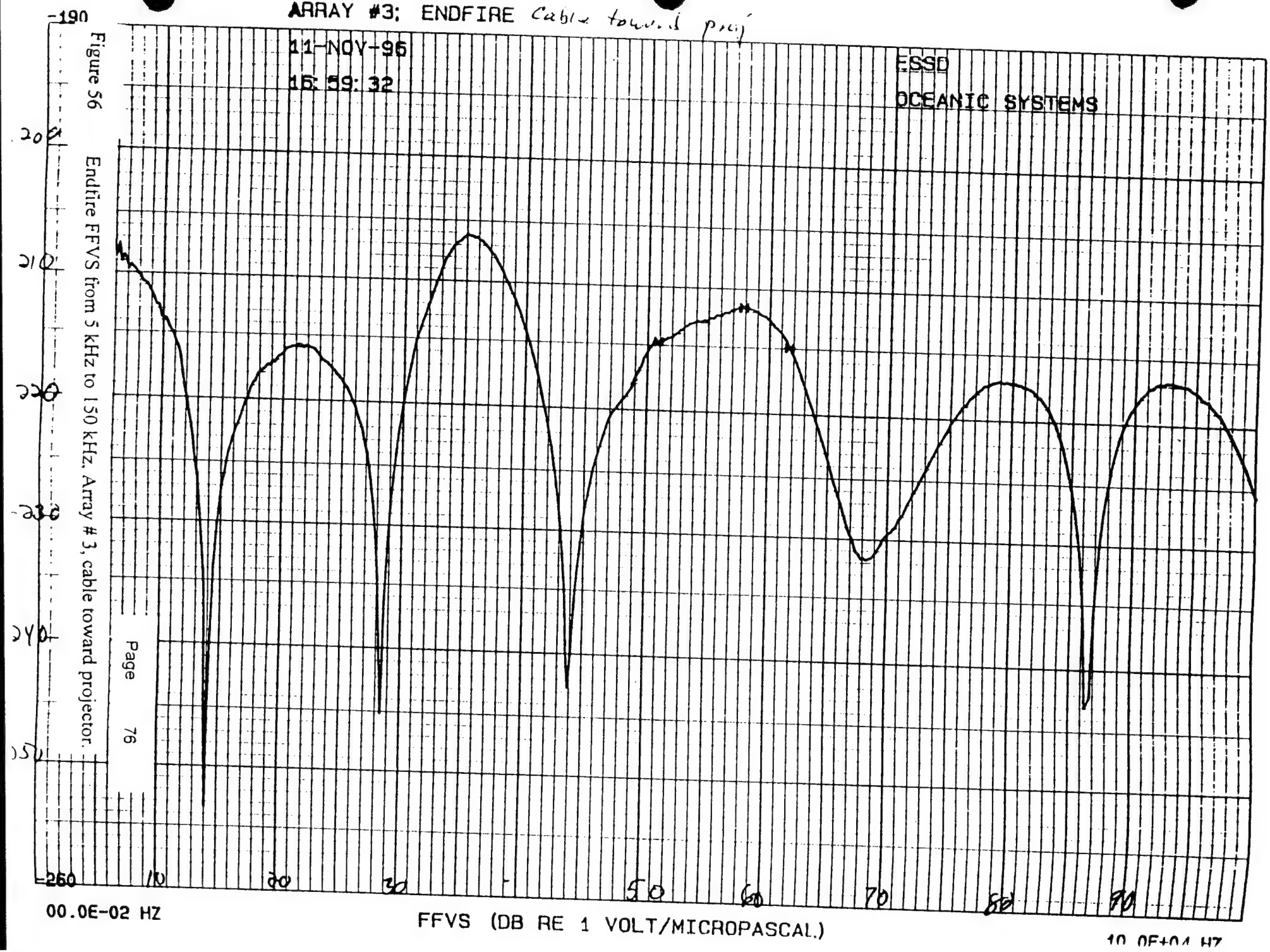

Figure 56 Endfire FFVS from 5 kHz to 150 kHz, Array # 3, cable toward projector.

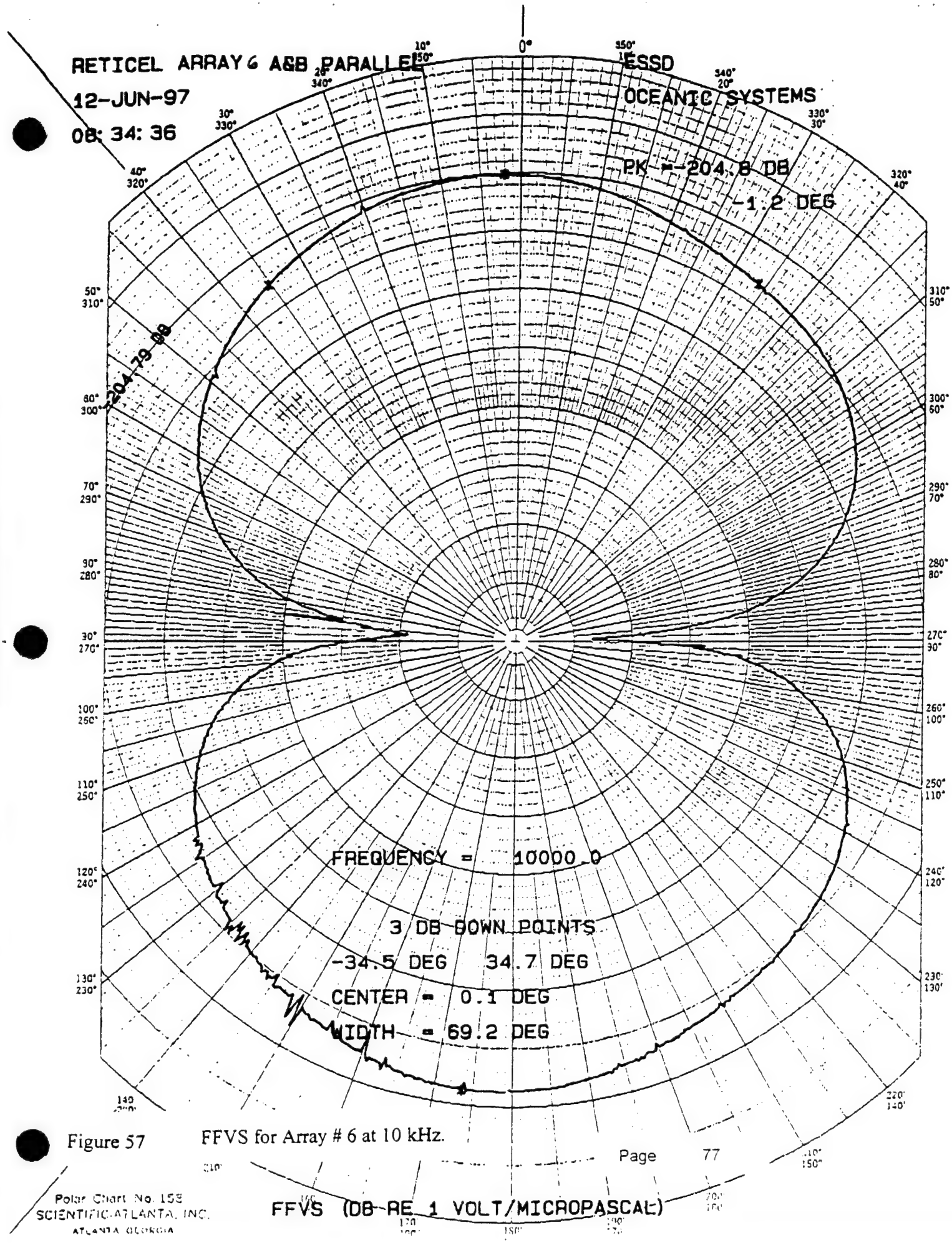

Figure 57 FFVS for Array # 6 at 10 kHz.

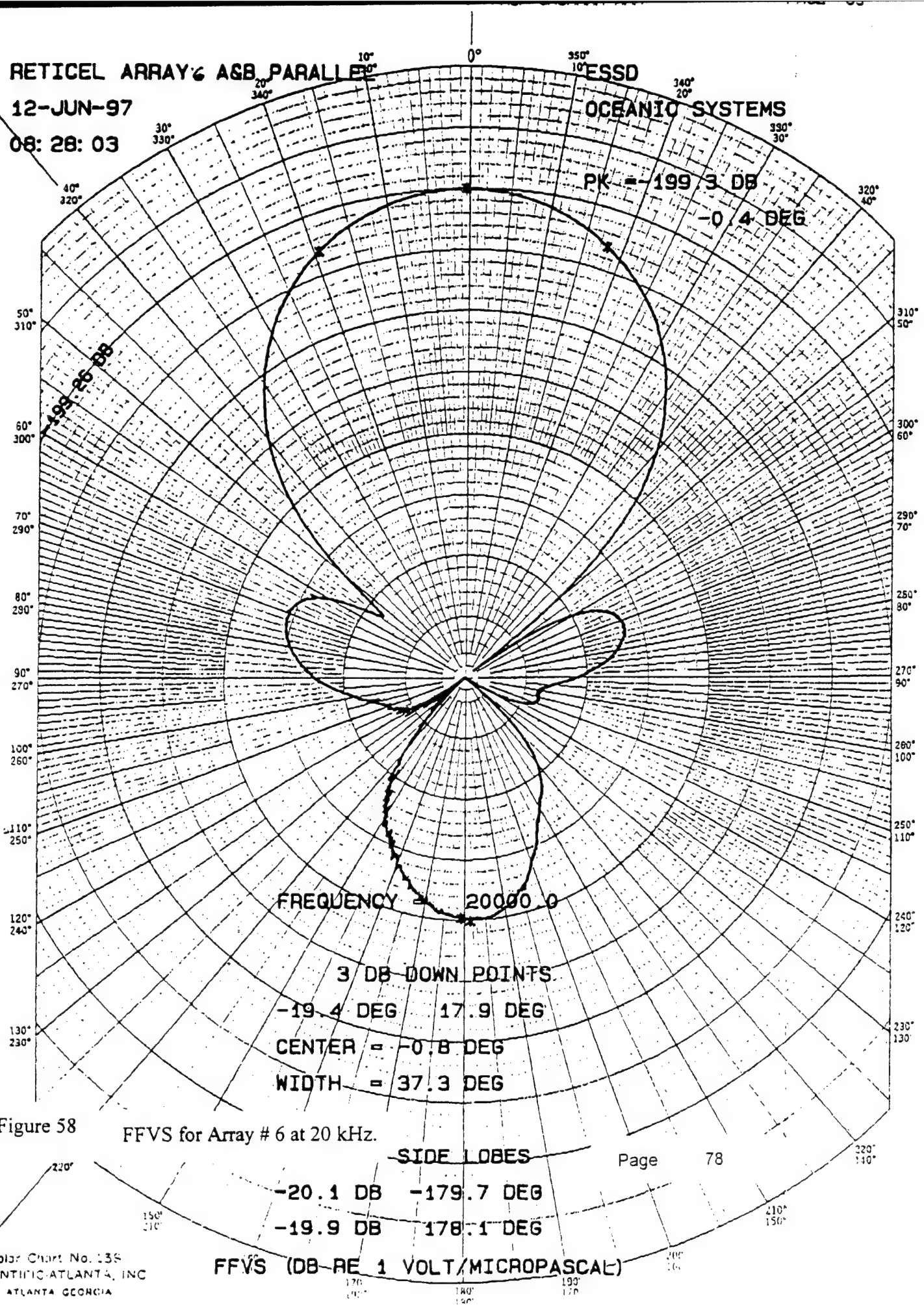

Figure 58 FFVS for Array # 6 at 20 kHz.

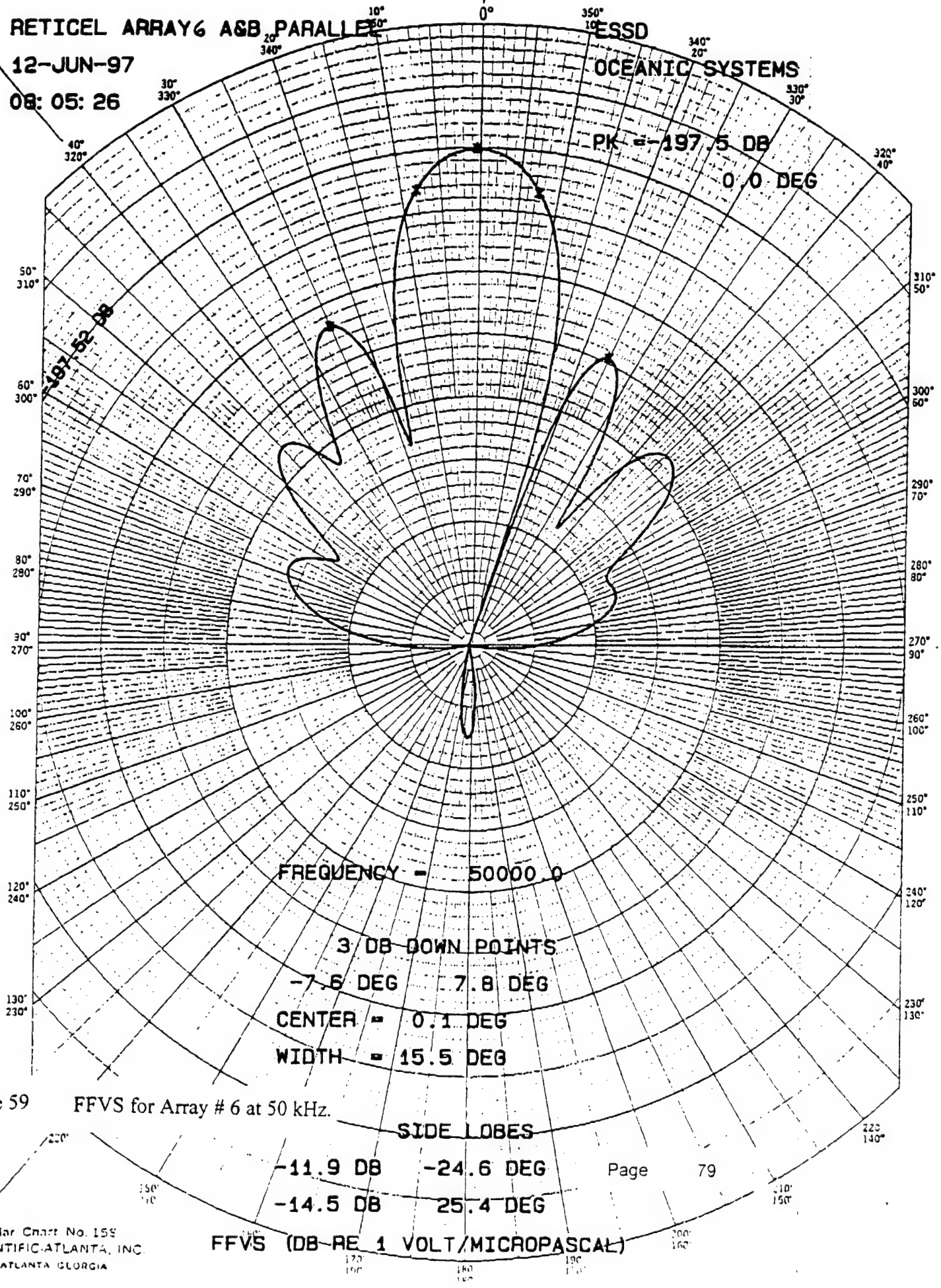

Figure 59 FFVS for Array # 6 at 50 kHz.

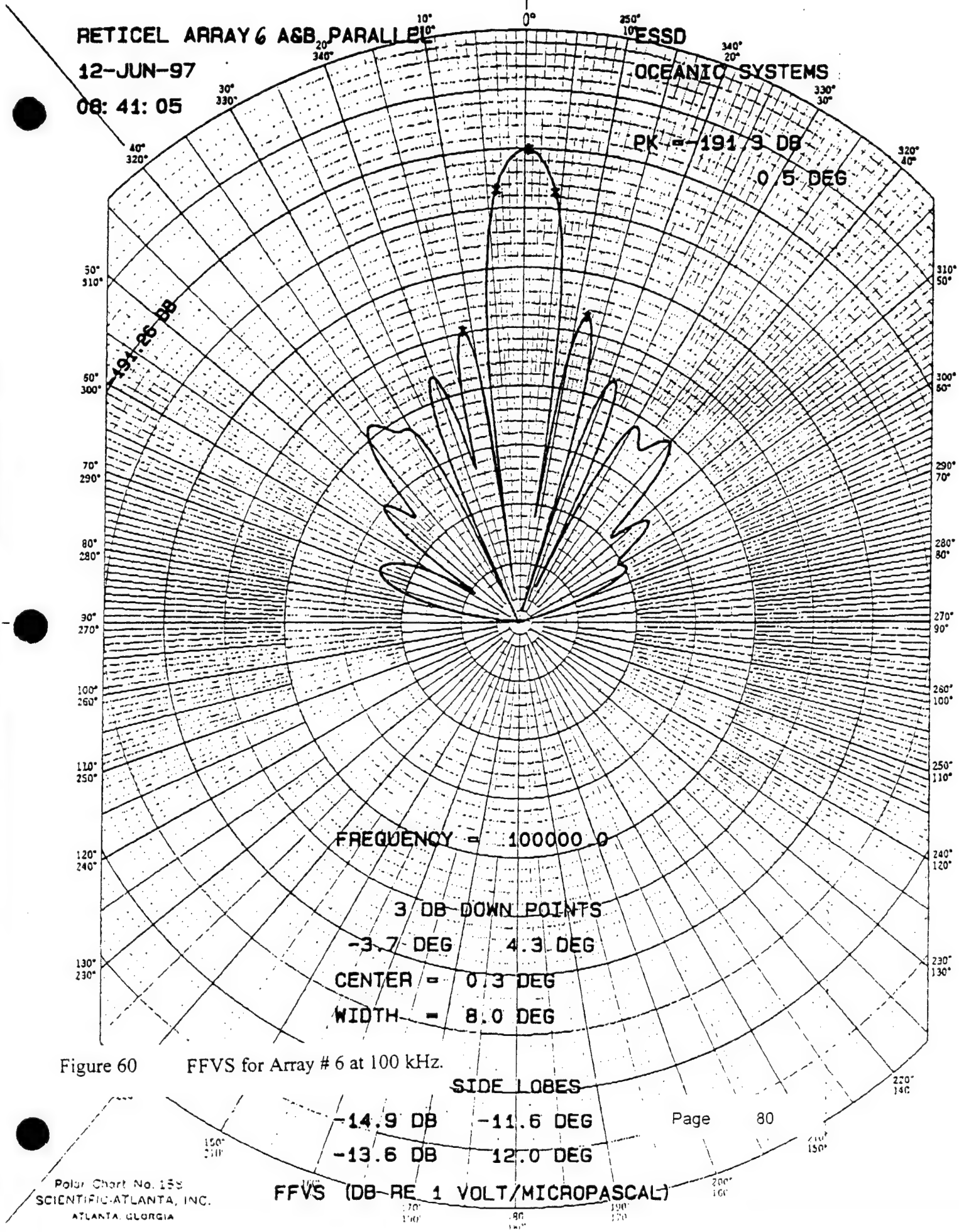

Figure 60 FFVS for Array # 6 at 100 kHz.

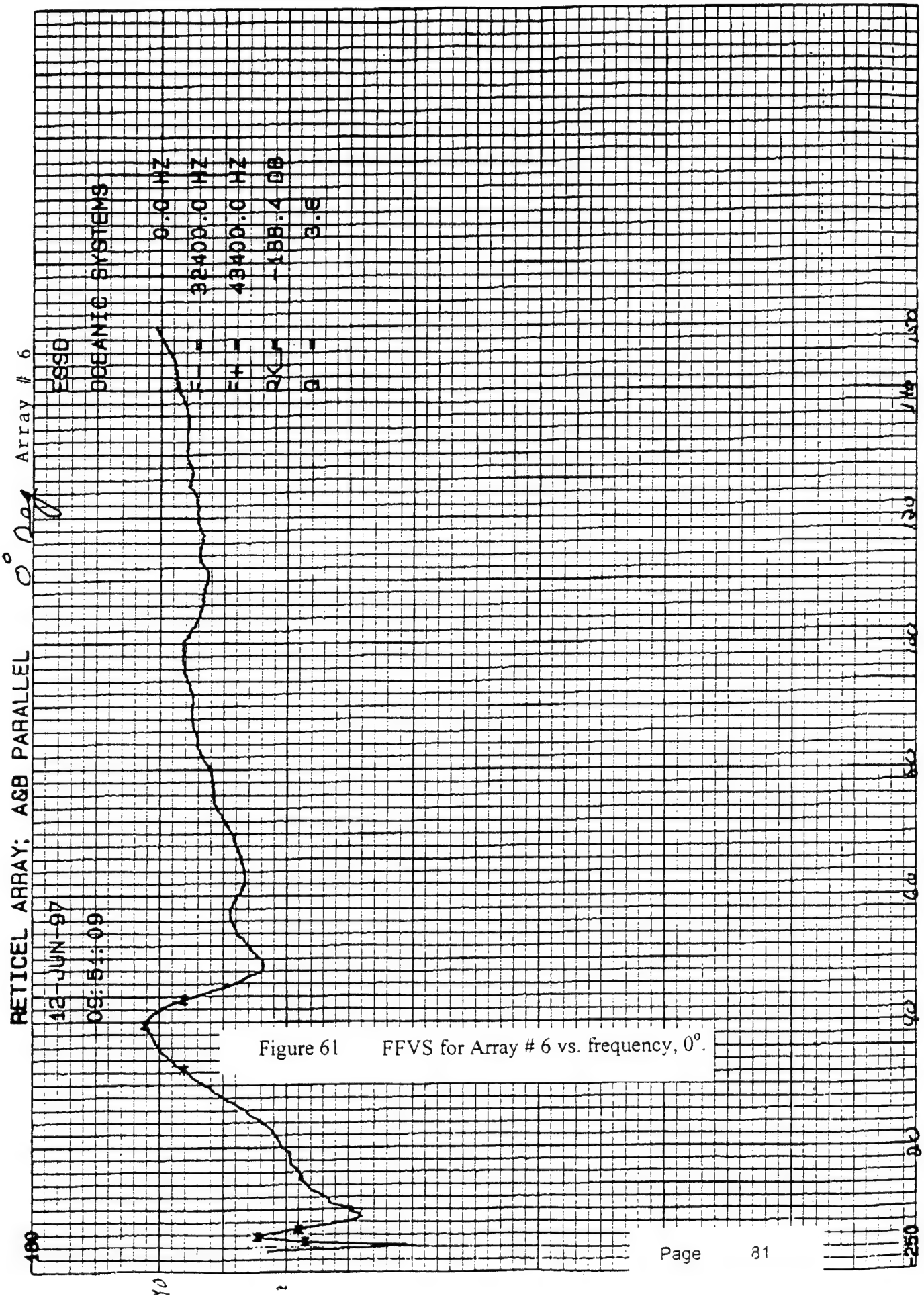

Figure 61 FFVS for Array # 6 vs. frequency, 0°.

Figure 62 TVR for Array # 6, 45°.

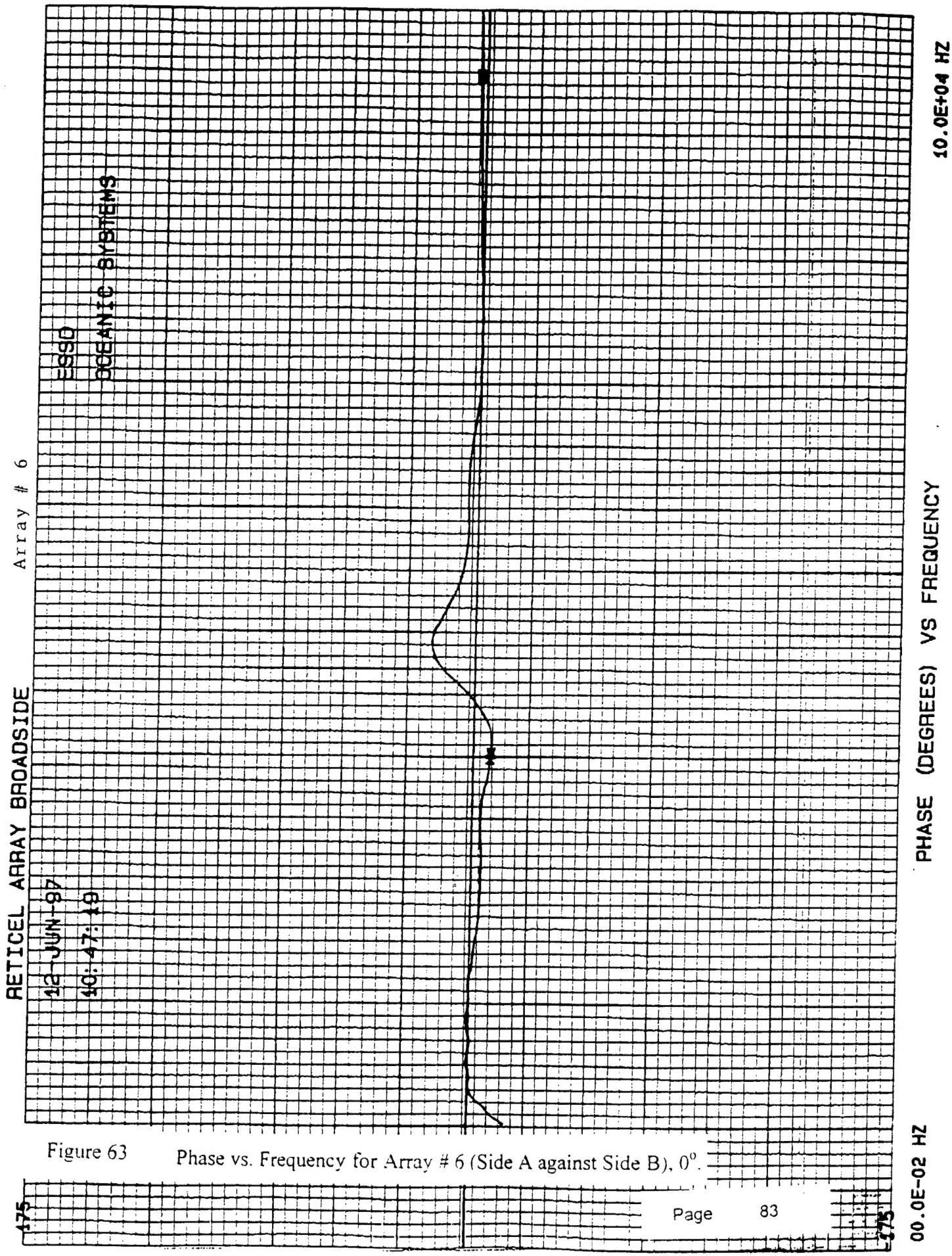

Figure 63 Phase vs. Frequency for Array # 6 (Side A against Side B), 0°.

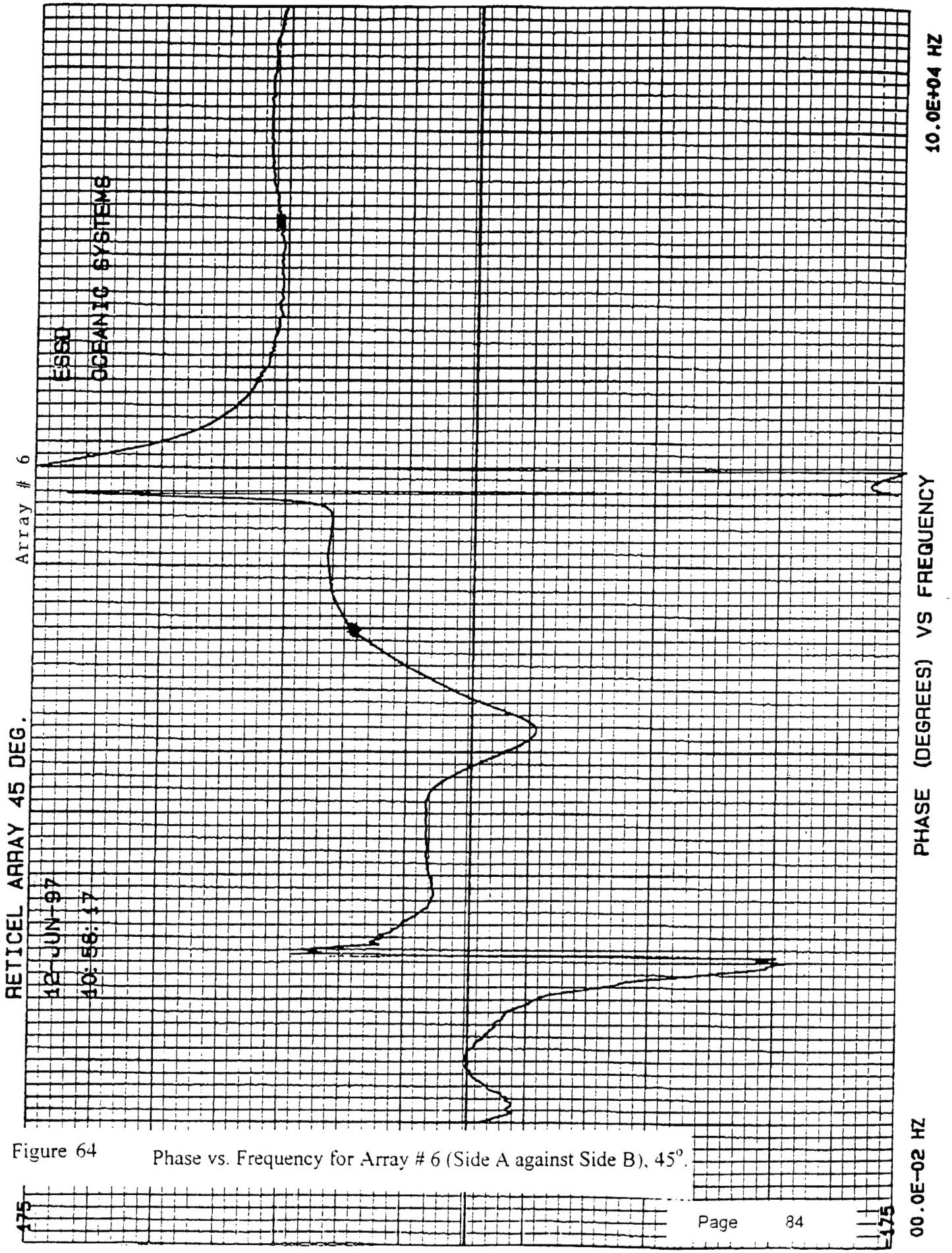

Figure 64 Phase vs. Frequency for Array # 6 (Side A against Side B), 45°.

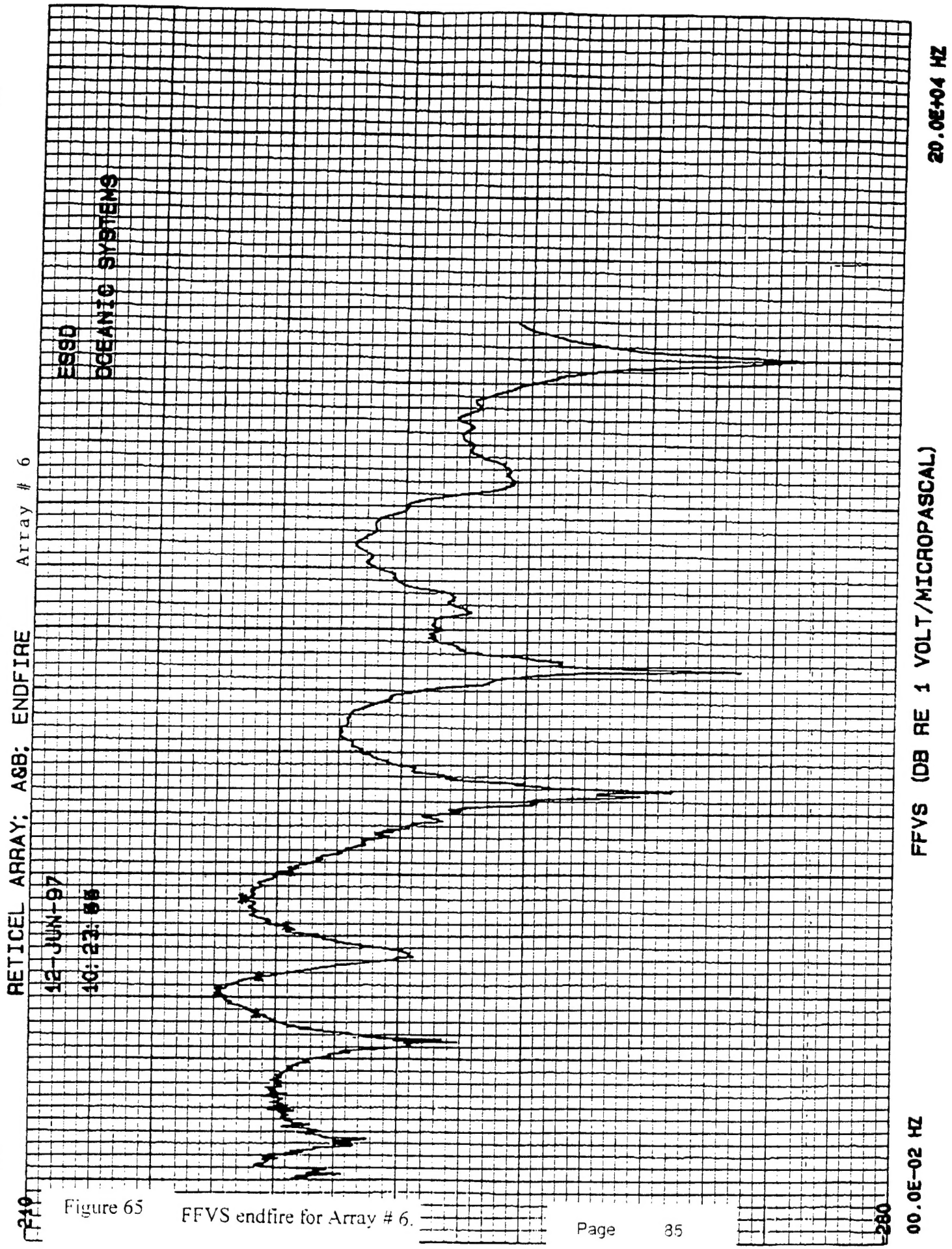

Figure 65 FFVS endfire for Array # 6.